

Magnetoelectric effects in Josephson junctions

I. V. Bobkova,^{1,2,3} A. M. Bobkov,¹ and M.A. Silaev⁴

¹*Institute of Solid State Physics, Chernogolovka, Moscow reg., 142432 Russia*

²*Moscow Institute of Physics and Technology, Dolgoprudny, 141700 Russia*

³*National Research University Higher School of Economics, Moscow, 101000 Russia*

⁴*Independent researcher*

(Dated: July 20, 2022)

The review is devoted to the fundamental aspects and characteristic features of the magnetoelectric effects, reported in the literature on Josephson junctions (JJs). The main focus of the review is on the manifestations of the direct and inverse magnetoelectric effects in various types of Josephson systems. They provide a coupling of the magnetization in superconductor/ferromagnet/superconductor JJs to the Josephson current. The direct magnetoelectric effect is a driving force of spin torques acting on the ferromagnet inside the JJ. Therefore it is of key importance for the electrical control of the magnetization. The inverse magnetoelectric effect accounts for the back action of the magnetization dynamics on the Josephson subsystem, in particular, making the JJ to be in the resistive state in the presence of the magnetization dynamics of any origin. The perspectives of the coupling of the magnetization in JJs with ferromagnetic interlayers to the Josephson current via the magnetoelectric effects are discussed.

CONTENTS

I. Introduction	1	IV. Triplet correlations generated by the moving condensate	22
II. Direct and inverse magnetoelectric effects in Josephson junctions: main properties and physical systems	4	A. Triplets induced by the static Meissner currents	22
A. Anomalous phase shift - a realization of inverse magnetoelectric effect in Josephson junctions with spin-orbit coupling and Zeeman field	4	B. Dynamic triplets induced by alternating electric fields	23
B. Anomalous phase shift in topological insulator-based S/F/S junctions	7	V. Conclusions	25
C. Anomalous phase shift in S/F/S junctions via inhomogeneous ferromagnets	9	Acknowledgments	25
D. Direct magnetoelectric effect in Josephson junctions via spin-orbit materials	10	References	25
E. Direct magnetoelectric effect in S/TI/S junctions	13		
III. Magnetoelectric effects and magnetization dynamics	13		
A. Direct coupling between magnetization and superconducting condensate: basic physics and equations	13		
B. Supercurrent-induced magnetization dynamics in S/F/S junctions via spin-textured ferromagnets	14		
C. Resistive state of the Josephson junctions in the presence of magnetization dynamics	16		
D. Electrical control of magnetization in S/F/S junctions	17		
1. Magnetization dynamics under the applied voltage	17		
2. Electrical control of the magnetization easy axis	18		
3. Magnetization reversal by electric current pulses. Cryogenic memory elements.	20		

I. INTRODUCTION

Since the discovery of the Josephson effect in 1962¹⁻³, there has been a growing interest in the fundamental physics⁴ and applications of this effect. The achievements in Josephson-junction technology enabled the development of sensors for detecting ultralow magnetic fields and weak electromagnetic radiation, ultrafast digital rapid single flux quantum (RSFQ) circuits, the design of large-scale integrated circuits for signal processing and general-purpose computing as well as adiabatic superconducting cells operating as an artificial neuron and synapse⁵⁻⁷.

Theoretical investigations of hybrid structures involving superconductors and ferromagnets and subsequent experimental realization of superconductor/ferromagnet/superconductor Josephson junctions^{4,8,9} have led to the discovery of spin-triplet Cooper pairs, thus giving rise to a synergy between superconductivity and spintronics. The emergent new field was called superconducting spintronics and is being actively developed now^{10,11}. One of the key effects in spintronics is the so-called magnetoelectric effects. In the most general sense the field embrace all the effects

related to the coupling and interconversion of the charge and spin degrees of freedom. The field already went beyond the framework of the fundamental physics only and, in particular, a scalable energy-efficient magnetoelectric spin-orbit logic (MESO) has been proposed¹² thus potentially opening new technology paradigm for improving energy efficiency in beyond-CMOS computing devices.

Here our goal is to review of current understanding of fundamental aspects of magnetoelectric effects in Josephson junctions, which potentially open new perspectives in superconducting spintronics. As an introduction, we discuss the fundamental aspects of the related magnetoelectric effects in nonsuperconducting systems briefly and then their analogues in superconducting materials and structures. The main part of the review is devoted to the magnetoelectric effects in a particular type of superconducting hybrids - Josephson junctions (JJs). In Sec. II we discuss the manifestations of the direct and inverse magnetoelectric effects in different types of JJs, Sec. III is devoted to the role of the magnetoelectric effects in the magnetization dynamics and electrical control of the ferromagnet magnetization in the JJs via ferromagnets. A specific for superconductivity magnetoelectric effect - generation of triplet superconductivity by a moving condensate is discussed in Sec. IV. Sec. V provides a short summary of the current situation in the field. Studies of magnetoelectric effects have a long history¹³⁻¹⁵. The most common view is that the magnetoelectric media are characterized by unconventional equilibrium responses to an electric field \mathbf{E} and a magnetic field \mathbf{B} . While \mathbf{E} induces only an electric polarization in ordinary materials, it also creates a magnetization in magnetoelectric materials. Similarly, the magnetic field \mathbf{B} in magnetoelectric materials generates an electric polarization in addition to a magnetization. Further, the advent of multiferroic materials^{16,17} with their large magnetoelectric couplings has greatly boosted current interest in magnetoelectricity. But we do not touch on this physics in the review. Here we focus on the related phenomena of current-induced spin polarization and the inverse effects. In this field besides the well-established spin Hall effect and inverse spin Hall effect¹⁸⁻³⁰ the direct and inverse magnetoelectric effects are also known. The essence of the direct magnetoelectric effect is creating a stationary spin density S_a along the a direction in spin space in response to an electric field E_k applied in the k direction in the real space:

$$S^a = \sigma_k^a E_k. \quad (1)$$

The effect is known for a wide class of systems. It is theoretically investigated and measured for spin-orbit coupled materials^{23,31-33}, where it is also called the Edelstein effect. In this case the Edelstein conductivity σ_k^a is proportional to the SOC constant of the material. The mutual orientation of the applied electric field and the induced electron spin polarization is determined by the particular form of the SOC. Let's consider the exam-

ples of Rashba and Dresselhaus SOC. These types of SOC were originally discussed for noncentrosymmetric zinc-blende or wurtzite semiconductors by Dresselhaus³⁴, and Rashba³⁵. The Rashba-type SOC also arises due to the structural inversion asymmetry (SIA). SIA typically occurs at the surfaces or interfaces. An important realization of a system with Rashba-type spin-orbit coupling is a 2D electron gas in doped semiconductor heterostructures^{36,37}, that support an electron gas at the interface between two materials. Another possibility to study the Rashba-effect in 2DEG are surfaces that support a surface state, e.g. in Au(111)³⁸: the electrons of the surface state move in a potential gradient that is provided by the surface itself. The hamiltonian term accounting for the Rashba SOC takes the form $\hat{H}_R = \alpha \hat{z}(\boldsymbol{\sigma} \times \mathbf{p})$, where α is the Rashba constant and \hat{z} is the unit vector along the z -axis, chosen along the polar vector of the material, which determines the direction of the broken inversion symmetry. $\boldsymbol{\sigma} = (\sigma_x, \sigma_y, \sigma_z)^T$ is the vector of Pauli matrices in spin space and \mathbf{p} is the electron momentum. For Rashba SOC $\sigma_x^y = -\sigma_y^x$, while the other components of σ_k^a are zero. Therefore, for this case the induced spin polarization lies in the plane perpendicular to the polar vector and is perpendicular to the applied electric field. The simplest form of the Dresselhaus SOC hamiltonian, realized in the presence of strain along the (001) direction is $\hat{H}_D = \beta_D(p_x \sigma_x - p_y \sigma_y)$, where β is the Dresselhaus SOC constant. If the current direction coincides with x or y axes, the induced spin polarization is directed along the current.

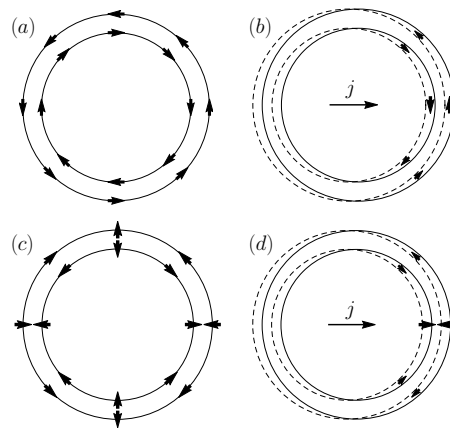


FIG. 1. Spin-split helical Fermi surfaces for (a) Rashba and (c) Dresselhaus spin-orbit coupled materials. (b) and (d) Current-induced shift of the Fermi surface. The original Fermi surface in the absence of the applied current is shown by the dashed lines. The direction of the accumulated spin in each of the subbands is shown by arrows.

The reason for the electrically induced spin polarization and qualitative understanding of its direction with respect to the current in normal quasi-2D systems is clearly seen from Fig. 1, where the helical Fermi surfaces of the Rashba and Dresselhaus materials are demon-

strated. The electric current results in the total shift of all the Fermi surfaces by q along the current direction. This leads to the nonzero average spin polarization of the corresponding electronic states in each of the helical bands. Due to the different spin structure of the helical Fermi surfaces the directions of the resulting electron polarizations in the Rashba and Dresselhaus cases are different. The average polarization is perpendicular to the applied current for the Rashba case and can have different mutual orientations with the current for the Dresselhaus SOC depending on the orientation of the current with respect to the crystal axes. The split helical Fermi surfaces contribute to the polarization in opposite directions, as it is seen from Fig. 1. This leads to a great reduction of the total polarization, the resulting effect is nonzero only due to the difference between the Fermi momenta for the helical subbands. Therefore, the current induced spin polarization is always proportional to the ratio $\Delta_{so}/\varepsilon_F$, where Δ_{so} is the energy splitting of the helical subbands, $\Delta_{so} \sim \alpha(\beta_D)p_F$ for the Rashba (Dresselhaus) case.

The direct magnetoelectric effect has also been predicted and measured in topological insulators^{39–43}, where the mutual orientation of the spin polarization and the current is the same as for the case of Rashba materials. In addition, the direct magnetoelectric effect also exists in spin-textured ferromagnets, where the induced spin polarization takes the form:

$$\mathbf{S}_\perp = -\frac{b_J j}{J_{sd} M^2} \mathbf{M} \times \partial_x \mathbf{M} + \frac{c_J j}{J_{sd} M} \partial_x \mathbf{M}, \quad (2)$$

which results in the well-known spin transfer torque⁴⁴ acting on the magnetization according to

$$\mathbf{T} = J_{sd} \mathbf{M} \times \mathbf{S}_\perp = b_J j \partial_x \mathbf{M} - \frac{c_J j}{M} \mathbf{M} \times \partial_x \mathbf{M}, \quad (3)$$

where M is the saturation magnetization in the ferromagnet, J_{sd} is the coupling constant of the exchange interaction between the s -band conduction electrons and d -band localized electrons responsible for the magnetism. \mathbf{S}_\perp means the component of the current-induced spin polarization, perpendicular to the magnetization direction, because it is this component that leads to a torque on the magnetization.

There is also an inverse magnetoelectric effect (it is also called by the spin-galvanic effect), which consists of generating a charge current j_k by a steady spin imbalance, which can be induced, for example, by a time-dependent magnetic field via the paramagnetic effect⁴⁵:

$$j_k = \sigma_k^a (g \mu_B \dot{B}^a), \quad (4)$$

where g is the Lande factor, μ_B is the Bohr magneton, and \dot{B}^a is the time derivative of the magnetic field component along the a axis. The inverse magnetoelectric effect has been observed in experiments with spin-orbit coupled materials^{46,47} and topological insulators^{48,49}.

The inverse magnetoelectric effect also takes place in spin-textured metallic ferromagnets. In this case, it man-

ifests itself as the so-called electromotive force (emf) induced by the magnetization dynamics^{50–60}

$$F_i = \frac{\hbar}{2} \left[\mathbf{m}(\partial_t \mathbf{m} \times \nabla_i \mathbf{m}) + \beta(\partial_t \mathbf{m} \nabla_i \mathbf{m}) \right], \quad (5)$$

where $\mathbf{m}(\mathbf{r}, t)$ is the unit vector in the direction of the magnetization and β is a phenomenological parameter. Due to the existence of the electromotive force the magnetization dynamics leads to appearance of an additional voltage drop. This voltage can vary in the range from nV to μV ⁵⁹ and in special situations can be used for electrical detection of the presence of magnetization dynamics⁶¹.

Conceptually the same magnetoelectric effects also take place in superconducting systems. However, here the physical situation is somewhat different because of the presence of the superconducting condensate. In contrast to the normal case, in a superconductor an equilibrium electric supercurrent can flow in the absence of an external electric field and is directly related to the gauge invariant superconducting condensate phase $\mathbf{j} \propto \mathbf{v}_s \propto \nabla \varphi - (2e/c)\mathbf{A}$, where v_s is the condensate velocity, φ is the phase of the superconducting order parameter and \mathbf{A} is the vector potential. That leads to two consequences: (i) a supercurrent can generate an equilibrium spin polarization in the presence of intrinsic SOC^{62–65}, extrinsic impurity-induced SOC^{66,67}, in topological insulator-based superconducting heterostructures^{68,69} and in superconductor/ferromagnet hybrids with spin-textured ferromagnets^{70,71} and (ii) in contrast to the normal case, in superconductors a static Zeeman field B can induce a supercurrent j_k :

$$j_k = \chi_k^a h^a. \quad (6)$$

where $h^a = (1/2)g\mu_B B^a$. This effect has been obtained for a case of a 2D superconductor with Rashba SOC⁷². It was also discussed for heterostructures consisting of the superconducting and ferromagnetic layers with SOC^{73–77} or for a ferromagnet/superconducting TI hybrid structures⁷⁸, when the exchange field is not induced by the externally applied magnetic field, but is generated by the proximity to the ferromagnet. In the case of heterostructures with thick enough superconducting layer (the thickness should be much larger than the superconducting coherence length)^{73,76} such a state with a spontaneous supercurrent flowing along the S/F interface and decaying into the depth of the superconductor can be a true ground state of the system. The same is valid if the exchange field is spatially inhomogeneous^{74,75} and even a topologically nontrivial vortex states can appear under the appropriate conditions^{77,78}.

But for the case of the superconductors with an intrinsic SOC in the homogeneous Zeeman field the state carrying homogeneous nonzero supercurrent is not the true ground state. In the true ground state the superconducting phase gradient is developed in order to compensate the supercurrent. The resulting state is characterized by the zero supercurrent and *nonzero* superconducting phase gradient. It is called by the helical state

and is a specific for superconducting systems manifestation of the inverse magnetoelectric effect. There is an important difference between the helical state and the well-known inhomogeneous FFLO state^{79–82}. While in the phase-modulated FFLO state the direction of the superconducting phase gradient does not depend on the direction of the exchange field, in the helical phase they are directly related. This fact results in strong coupling between the magnetization and the condensate phase. Therefore, it leads to the possibilities of the electrical control of the magnetization dynamics, which look perspective from the point of view of spintronics applications. The helical state has been predicted for superconductors with intrinsic Rashba SOC under the applied Zeeman field^{83–88} and superconducting hybrids with spin-textured ferromagnets^{70,71}, where the magnetic inhomogeneity plays a role of the effective SOC.

The helical state is a kind of inverse magnetoelectric effect, which is realized in the simply connected superconducting systems. Similar effects occur also in an S-X-S Josephson junction, between two superconductors and a normal or ferromagnetic interlayer X with an intrinsic SOC or if the interlayer is a spin-textured ferromagnet. In a Josephson junction the supercurrent depends on the phase difference φ between the superconducting electrodes. Similar to the simply connected superconductors a Zeeman field may induce a supercurrent through the junction at zero phase difference between the superconductors according to Eq. (6). In the ground state of the junction this "anomalous supercurrent", generated by the inverse magnetoelectric effect, is compensated by the phase shift $\varphi_0 \neq 0, \pi$. It is called by the anomalous ground state phase shift and the Josephson junctions manifesting this effect are called φ_0 -junctions.

The φ_0 -junctions have been predicted in a wide class of systems including S/F/S junctions with intrinsic SOC, S/N/S junctions with intrinsic SOC under applied Zeeman field^{89–100}, S/topological insulator/S junctions under the applied Zeeman field or if the Zeeman field in the topological insulator surface states is induced by the proximity to a ferromagnet (S/TI-F/S junctions)^{101–105} and also in S/F/S junctions with spin-textured interlayers^{71,106–118}. Below we will discuss all the mentioned classes of systems in more details. The anomalous phase shift has been observed experimentally for Al/InAs/Al Josephson junctions (JJ)¹¹⁹, in JJs via nanowire quantum dots¹²⁰, in Bi_2Se_3 JJs¹²¹ and in JJs via bismuth nanowires¹²² under the applied magnetic field. The magnetoelectric nature of the anomalous phase shift has been unveiled in Ref. 98. It has also been reported very recently that the anomalous phase shift is a key ingredient of the mechanism providing an extremely long-range interaction of magnetic moments in a coupled system of JJs with magnetic interlayers¹²³. There is also a recent review¹²⁴, specially devoted to the physics of the anomalous phase shift.

Naturally, the equilibrium direct magnetoelectric effect discussed above can also occur in Josephson junctions.

Indeed, it has been predicted for JJs via normal interlayers with Rashba SOC in diffusive¹²⁵ and ballistic¹²⁶ systems and via TI interlayers⁶⁸. The effect plays a key role in the electrical control of magnetization in S/F/S Josephson junctions, which is also discussed in detail below.

For completeness, we briefly mention other reported effects in superconducting hybrids, which can also be viewed as magnetoelectric ones but are not discussed in detail in this review. One group of effects is related to different types of quasiparticle nonequilibrium in the system. Among them are spin-charge conversion effects in superconducting hybrids. They involve a nonequilibrium spin polarization and spin current pumped into a superconducting system by some external source. It has been shown that for the Rashba SOC and SOC caused by spin-orbit impurities such a nonequilibrium spin distribution can generate the electric current and electric potential in superconductors^{127–129}. This nonequilibrium situation resembles much the analogous inverse magnetoelectric and spin Hall effects in normal systems.

II. DIRECT AND INVERSE MAGNETOELECTRIC EFFECTS IN JOSEPHSON JUNCTIONS: MAIN PROPERTIES AND PHYSICAL SYSTEMS

A. Anomalous phase shift - a realization of inverse magnetoelectric effect in Josephson junctions with spin-orbit coupling and Zeeman field

The minimal form of the current-phase relation (CPR) characterizing the dc Josephson effect is given by $j(\varphi) = j_c \sin \varphi$. Here j is the total superconducting current flowing across the junction, $|j_c|$ is the critical current and φ is the phase difference between superconducting electrodes^{3,4}. The ordinary Josephson junctions have $j_c > 0$ yielding the zero phase difference ground state $\varphi = 0$. In certain cases $j_c < 0$ leading to the ground state $\varphi = \pi$. Such π -junctions are realized in S/F/S JJs^{8,130–132}, non-equilibrium S/N/S JJs¹³³, non-equilibrium S/F/S systems¹³⁴, d -wave superconductors^{135,136}, semiconductor nanowires¹³⁷, gated carbon nanotubes¹³⁸ or multi-terminal Josephson systems¹³⁹. The π -junctions can be used in scalable superconducting logic and quantum computers^{140–143}.

Even more exotic situation occurs in systems with magnetoelectric effects where the φ_0 -junctions are realized. They are described by the CPR⁹²

$$j(\varphi) = j_c \sin(\varphi + \varphi_0). \quad (7)$$

with *anomalous (spontaneous) phase shift* $\varphi_0 \neq 0, \pi$. In this case there is a finite supercurrent at zero phase difference $j_{an} = j_c \sin \varphi_0$ called the *anomalous (spontaneous) current*.

The Josephson energy $E_J = j_c [1 - \cos(\varphi + \varphi_0)]$ yields the ground state with non-trivial phase difference $\varphi =$

$-\varphi_0$ and zero current $j(\varphi_0) = 0$. Such a phase-shifted ground state is analogous to the helical state in the homogeneous superconductor discussed above. The general symmetry requirements for obtaining the φ_0 -Josephson junctions are the same as for having magnetoelectric coupling in the homogeneous superconductor. That is, we need to combine the two symmetry breaking mechanism. First, the time-reversal symmetry is to be broken by the Zeeman field \mathbf{h} inside the Josephson junction. Second, the orbital and spin degrees of freedom should be coupled so that it is impossible to invert the magnetic moment by spin rotation independently from the orbital coordinates. By analogy with spontaneous current (6) one can construct the phenomenological expression for the anomalous phase shift $\varphi_0 \propto \chi_x^a h^a$, where \mathbf{x} is the axis across Josephson junction. This type of symmetry breaking is enabled e.g. by Rashba-type SOC $\chi_c^a \propto \varepsilon_{cba} n_b$ with anisotropy vector \mathbf{n} . In this case the spontaneous current is $\mathbf{j} \propto \mathbf{n} \times \mathbf{h}$ and the anomalous phase shift is $\varphi_0 \propto \mathbf{x} \cdot (\mathbf{n} \times \mathbf{h})$.

Theoretical description of the φ_0 -junctions is significantly more challenging than that of the 0 and π -junctions. To obtain the anomalous phase shift one has to include the magnetoelectric coupling which is beyond the standard quasiclassical approximation^{64,66,68,71,96,98,116,118,126,144–152}. For Rashba-type SOC described by the hamiltonian $H_R = \alpha[\mathbf{p} \times \mathbf{n}]\boldsymbol{\sigma}$ in the ballistic regime and for large Rashba constant α , the anomalous phase shift is given by⁹²

$$\varphi_{0b} = \frac{4\hbar\alpha d}{(\hbar v_F)^2}, \quad (8)$$

where d is the length of the Josephson junction interlayer and v_F is the Fermi velocity of the electrons in the interlayer. In the diffusive regime for weak α , highly transparent interfaces and neglecting spin-relaxation, the predicted result for the anomalous phase shift is

$$\varphi_{0d} = \frac{\tau m^* h (\alpha d)^3}{3\hbar^6 D}, \quad (9)$$

where τ is the elastic scattering time, m^* is the effective electron mass and D is the diffusion constant⁹⁶.

The anomalous Josephson effect based on the systems with SOC has been found in recent experiments. Anomalous phase junctions were demonstrated in *Bi*-nanowires¹²², *InSb* nanowires in a quantum dot geometry¹²⁰, in JJ using *Bi₂Se₃*¹²¹, in heterostructures formed by *InAs* and epitaxial superconducting *Al*¹¹⁹ and also in JJs via *InAs* nanowires¹⁵³. In the quantum dot realization¹²⁰ and in Ref. 119 the gate-tunable phase has been achieved. The JJs of Ref. 120 support a few modes and consequently exhibit small critical currents, and the structures investigated in Ref. 119 have high interface transparency and large critical currents. In *Bi₂Se₃*, which is a topological insulator, large planar φ_0 -junction are possible¹²¹, however, they are not gate-tunable. In all the experimental works, the exchange field inside the

interlayer of the JJ, which is required for the generation of the anomalous phase shift, has been created by the externally applied in-plane magnetic field via the Zeeman effect $\mathbf{h} = (1/2)g\mu_B \mathbf{B}_y$, where g -is the electron g -factor for the corresponding material and \mathbf{B}_y is the magnetic field component, perpendicular to the anisotropy vector \mathbf{n} (along z , see Fig. 2) and to the Josephson current direction.

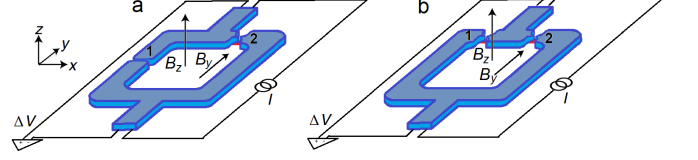


FIG. 2. Sketches of experimentally used SQUID-based setups for the anomalous phase shift measurements. (a) Asymmetric SQUID. The critical current of the reference JJ 1, without an anomalous phase shift, is much higher than the critical current of the φ_0 -JJ 2. (b) Symmetric SQUID. Both JJs 1 and 2 have the same critical currents. The anomalous phase shifts for these junctions are opposite due to the current flowing in the opposite directions.

The anomalous phase shift has been observed directly through measurements of the current-phase relationship in a Josephson interferometer. A typical current-biased measurement of a single JJ shows no measurable signature. Under the applied current, the phase difference across the JJ changes to maximise the critical current. This means that any phase shift applied to such a system will be invisible. Therefore, the experimental works use SQUID geometry, whose primary property is phase sensitivity.

One scheme of measurements, which was realized in Refs. 120–122, is based on the asymmetric SQUID configuration. The SQUID consists of two junctions in parallel with very different critical currents $I_{c1} \gg I_{c2}$, where I_{c1} is the critical current of the reference JJ and I_{c2} is the critical current of the investigated JJ. The sketch of the asymmetric SQUID is presented in Fig. 2(a). The phase differences φ_1 and φ_2 for the two junctions are linked by the relation $\varphi_1 - \varphi_2 = 2\pi\Phi/\Phi_0$, where $\Phi = B_z S$ is the magnetic flux enclosed in the SQUID of surface S , B_z is a magnetic field component perpendicular to the sample, i.e. along \mathbf{e}_z , and Φ_0 is the flux quantum. As the critical current I_{c1} is much higher than I_{c2} , then $\varphi_1 = \pi/2$ and $I_c = I_{c1} + I_{c2} \cos[2\pi\Phi/\Phi_0 - \varphi_0]$. Thus, a measurement of the critical current I_c as function of B_z provides a measure of the current I_2 as function of φ_2 , i.e. the CPR. In the experiments the Zeeman field \mathbf{h} has been induced by the externally applied in-plane magnetic field $\mathbf{h} = (1/2)g\mu_B \mathbf{B}_y$, where $B_y = B \cos \theta$ is the in-plane component of the applied magnetic field, see Fig. 3(b). Then the anomalous phase results in the increased oscillation frequency of the critical current as a function of the applied magnetic field¹²¹ $2\pi\Phi/\Phi_0 - \varphi_0 = \omega B$, where $\omega = 2\pi S \sin \theta / \Phi_0 - \varphi_0 / B$. The corresponding experi-

mental results adopted from Ref. 121 are presented in Fig. 3(a).

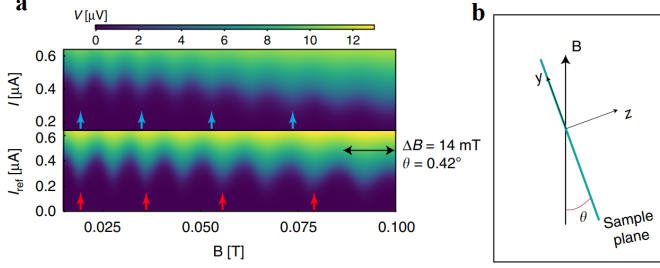


FIG. 3. (a) Voltage map showing the critical current oscillations of the anomalous device (upper picture) and of the reference device (bottom picture) as a function of magnetic field B . The critical current of both devices oscillates due to the perpendicular component of the magnetic field $B_z = B \sin \theta$, as it is sketched in panel (b). Due to the anomalous phase shift, the frequency of the anomalous device is larger than the reference one. The oscillation frequency can be changed by mechanically tilting the sample, i.e by changing the angle Θ between the plane containing the superconducting loop and the magnetic field B . The colored arrows guide the eyes to help visualise the increased phase shift in the anomalous device. Adopted from Ref. 121.

The other measurement scheme is to consider the symmetric SQUID, where the JJs has the same critical currents $I_{c1} = I_{c2} = I_c$ ¹⁵³. In this case the total supercurrent through the interferometer is

$$I_s = 2I_c \sin \delta_0 \cos \left[\frac{1}{2} \left(2\pi \frac{\Phi}{\Phi_0} + \varphi_{tot} \right) \right], \quad (10)$$

where $\delta_0 = (\varphi_0^{(1)} + \varphi_0^{(2)})/2 - (\varphi_1 + \varphi_2)/2$ and $\varphi_{tot} = \varphi_0^{(1)} - \varphi_0^{(2)}$ is the total anomalous phase built in the interferometer. With the geometry realized in Ref. 153 and shown in Fig. 2(b), the two junctions experience the same in-plane magnetic field orientation but the supercurrents flow in opposite directions resulting in $\varphi_0^{(1)} = -\varphi_0^{(2)}$ and $\varphi_{tot} = 2\varphi_0$. The stable state configuration of the SQUID is achieved by minimizing the total Josephson free energy obtained at $\delta_0 = \pi/2$. Therefore, the maximum supercurrent, which can be sustained by the system, is

$$I_S(\Phi) = 2I_c \left| \cos \left[\pi \frac{\Phi}{\Phi_0} + \frac{1}{2} \varphi_{tot} \right] \right|. \quad (11)$$

Therefore, the dependence $I_S(\Phi)$ contains the anomalous phase shift. Notably, there is a replica of the $I_S(\Phi)$ oscillations in the voltage drop $\Delta V(\Phi)$ when $I > I_S$, and the SQUID operates in the dissipative regime, as conventionally realized with strongly overdamped JJs. This replica is used in Ref. 153 for measurements of the anomalous phase shift. The results, adopted from Ref. 153, are represented in Fig. 4. Fig. 4(a) demonstrates evolution of $\Delta V(\Phi)$ at constant current bias as a function of the applied in-plane magnetic field.

Fig. 4(b) shows the resulting anomalous phase shift extracted from the data in Fig. 4(a) according to the resistively shunted junction (RSJ) model relation $\Delta V = (R/2) \sqrt{I^2 - 4I_c^2 \cos(\pi\Phi/\Phi_0 + \varphi_{tot}/2)^2}$.

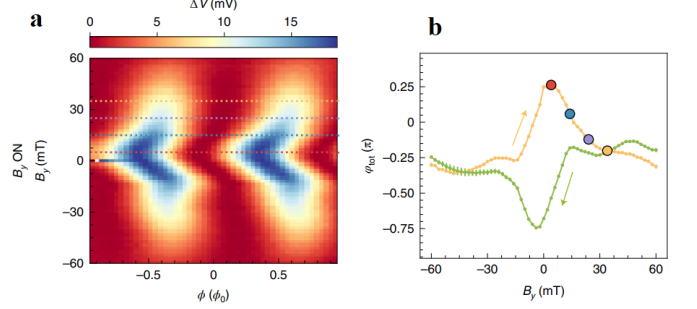


FIG. 4. (a) Voltage drop $\Delta V(\Phi)$ at constant current bias $I = 1 \mu A$ versus in-plane magnetic field B_y applied orthogonal to the nanowire axis. (b) Phase shift φ_{tot} extracted from the data (a) with back (blue) and forth (red) sweeps in B_y . The colored points in panel (b) correspond to the field values marked by the dashed lines of the same color in panel (a). Figure is adopted from Ref. 153.

Experimental data provide rather large values of the anomalous phase shift of the order of π . For example, in Ref. 121 $\varphi_0 \approx 0.9\pi$ was measured at $B_y \approx 100 mT$. It was compared to the theoretical predictions for the ballistic Eq. (8) $\varphi_{0b} \approx 0.01\pi$ and diffusive Eq. (9) $\varphi_{0d} \approx 0.94\pi$. The authors concluded that their JJs agree with the theory developed in Ref. 96. In Ref. 153 it was also reported that their data could be fitted by the diffusive theory⁹⁶. Rather high values of $\varphi_0 \sim \pi/2$ at $B_y \approx 400 mT$ (the particular value of φ_0 depends on the gate voltage) have also been observed in Ref. 119. The authors compare their results to the theoretical predictions expressed by Eqs. (8) and (9) and concluded that both results return values of φ_0 which are much smaller than the observed ones. A possible explanation is that the investigated JJs were in the short junction limit with a fully developed proximity effect inside the interlayer, which is not described by those theoretical results.

As it was mentioned earlier, in all the discussed experiments, the exchange field generating φ_0 has been created by the externally applied field. Refs. 121 and 119 report the linear dependence of the anomalous phase shift on the in-plane magnetic field, as it is predicted by Eqs. (8) and (9). The experimental results reported in Ref. 153 are more complicated. The nonmonotonic dependence of the anomalous phase shift on the applied in-plane field with a maximum shift at $B_y \approx 5 mT$ and saturation for $|B_y| > 30 mT$ has been observed, see Fig. 4(b). The authors suggest that this behavior is due to magnetic Kondo impurities in the nanowire. Due to the antiferromagnetic nature of the Kondo interaction, the effective exchange field created by these unpaired spins is opposite to the Zeeman field generated by B_y so that the two contributions are competing in the

anomalous phase with a partial cancellation. The total anomalous phase shift is divided into two contributions $\varphi_0(B_y) = \varphi_{int}(B_y) + \varphi_{ext}(B_y)$, where $\varphi_{int}(B_y)$ is an intrinsic phase shift, which is present even in the absence of the in-plane magnetic field if a finite B_y has been previously applied. Since it stems from a ferromagnetic ordering, φ_{int} depends only on the history of B_y and shows a hysteresis in the back and forth sweep direction. The extrinsic contribution to the phase shift, φ_{ext} stems directly from the external magnetic field. The dependence $\varphi_{ext}(B_y)$ is characterized by a linear increase at low magnetic fields up to a maximum phase shift of $\pm\pi/2$. Based on the diffusive theory⁹⁶ the authors of Ref. 153 developed a model explaining the observed behavior of φ_{ext} . It leads to $\varphi_{ext} \approx C\alpha^3 B_y + O(B^3)$. This model provides a reasonable explanation of the obtained data and predicts a nonuniversal saturation of the anomalous phase shift at large fields with the saturation value depending on the spin-orbit strength.

The measurement of the intrinsic anomalous phase shift generated by the magnetic impurities reported in Ref. 153 is an important step to the development of a new generation of anomalous phase shift JJs based on magnetic materials. It will open a great perspective for experimental investigation of exciting physics related to the coupling between the condensate phase and the magnetization of the magnet and their interplay. Several examples of the corresponding theoretical predictions are discussed below in this review.

B. Anomalous phase shift in topological insulator-based S/F/S junctions

Here we consider the Josephson junction through topological insulators where the SOC is so strong that only one helical band is present. In such systems, one can expect the strongest possible spontaneous phase shift effect. At the same time, having only one helical band allows for the significant simplification of the theoretical description using the generalized quasiclassical theory. More particular, we consider the anomalous phase shift in superconductor/ferromagnet/superconductor (S/F/S) Josephson junctions designed on a three dimensional topological insulator (3D TI) surface. At present, great progress has been made in the experimental implementation of F/TI hybrid structures. In particular, a structure was successfully implemented experimentally, in which a sufficiently strong exchange field was induced in the surface states of the TI due to the proximity effect with a high- T_c ferromagnetic insulator^{154–157}.

The 3D TI surface states host Dirac quasiparticles, exhibiting full spin-momentum locking: an electron spin always makes a right angle with its momentum. The sketch of the system under consideration and the Fermi surface of the conducting electrons in the 3D TI surface states are demonstrated in Fig. 5. The spin-momentum locking gives rise to a very strong dependence of the CPR

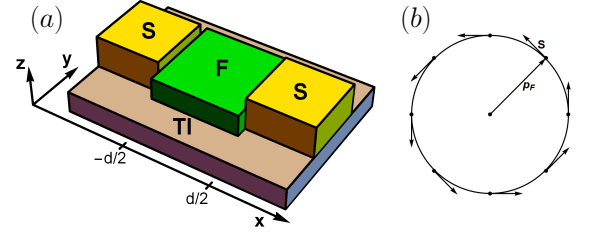


FIG. 5. (a) Sketch of the superconductor/ferromagnet/superconductor (S/F/S) Josephson junction on top of the 3-dimensional topological insulator (3D TI). The length of the interlayer d is assumed to be of the order of the normal state coherence length ξ_N of the 3D TI conductive surface layer. (b) Helical Fermi surface of the conductive surface states of the 3D TI. For a given momentum direction the electron spin \mathbf{s} makes a right angle with the momentum direction. The opposite spin direction is not allowed.

on the magnetization direction^{101,102,104,148}. In particular, the anomalous ground state phase shift proportional to the in-plane magnetization component perpendicular to the supercurrent direction was reported.

It is assumed that the magnetization $\mathbf{M}(\mathbf{r})$ of the ferromagnet induces an effective exchange field $\mathbf{h}(\mathbf{r}) \sim \mathbf{M}(\mathbf{r})$ in the underlying conductive surface layer. The discussed theory is also applicable if the Zeeman term in the hamiltonian of the TI surface states is induced by the applied magnetic field. The hamiltonian that describes the TI surface states in the presence of an in-plane exchange field $\mathbf{h}(\mathbf{r})$ reads:

$$\hat{H} = \int d^2\mathbf{r}' \hat{\Psi}^\dagger(\mathbf{r}') \hat{H}(\mathbf{r}') \hat{\Psi}(\mathbf{r}'), \quad (12)$$

$$\hat{H}(\mathbf{r}) = -iv_F(\nabla \times \mathbf{e}_z)\hat{\sigma} + \mathbf{h}(\mathbf{r})\hat{\sigma} - \mu, \quad (13)$$

where $\hat{\Psi} = (\Psi_\uparrow, \Psi_\downarrow)^T$, v_F is the Fermi velocity, \mathbf{e}_z is a unit vector normal to the surface of TI, μ is the chemical potential, and $\hat{\sigma} = (\sigma_x, \sigma_y, \sigma_z)^T$ is a vector of Pauli matrices in the spin space. It was shown^{68,104} that in the quasiclassical approximation ($\hbar, \varepsilon, \Delta$) $\ll \mu$ the Green's function has the following spin structure: $\hat{g}(\mathbf{n}_F, \mathbf{r}, \varepsilon) = \hat{g}(\mathbf{n}_F, \mathbf{r}, \varepsilon)(1 + \mathbf{n}_\perp \hat{\sigma})/2$, where $\mathbf{n}_\perp = (n_{F,y}, -n_{F,x}, 0)$ is the unit vector perpendicular to the direction of the quasiparticle trajectory $\mathbf{n}_F = \mathbf{p}_F/p_F$ and \hat{g} is the *spinless* 4×4 matrix in the particle-hole and Keldysh spaces containing normal and anomalous quasiclassical Green's functions. The spin structure above reflects the fact that the spin and momentum of a quasiparticle at the surface of the 3D TI are strictly locked and make a right angle. It was demonstrated^{68,104,158} that the spinless retarded Green's function $\hat{g}(\mathbf{n}_F, \mathbf{r}, \varepsilon)$ obeys the following transport equations in the ballistic limit:

$$-iv_F \mathbf{n}_F \hat{\nabla} \hat{g} = \left[\varepsilon \tau_z - \hat{\Delta}, \hat{g} \right]_\otimes, \quad (14)$$

where $[A, B]_\otimes = A \otimes B - B \otimes A$ and $A \otimes B = \exp[(i/2)(\partial_{\varepsilon_1} \partial_{t_2} -$

$\partial_{\varepsilon_2} \partial_{t_1})]A(\varepsilon_1, t_1)B(\varepsilon_2, t_2)|_{\varepsilon_1=\varepsilon_2=\varepsilon; t_1=t_2=t}$. $\tau_{x,y,z}$ are Pauli matrices in particle-hole space with $\tau_{\pm} = (\tau_x \pm i\tau_y)/2$. $\hat{\Delta} = \Delta(x)\tau_+ - \Delta^*(x)\tau_-$ is the matrix structure of the superconducting order parameter $\Delta(x)$ in the particle-hole space. We assume $\Delta(x) = \Delta e^{-i\chi/2}\Theta(-x - d/2) + \Delta e^{i\chi/2}\Theta(x - d/2)$. The spin-momentum locking allows for including \mathbf{h} into the gauge-covariant gradient $\hat{\nabla}\hat{A} = \nabla\hat{A} + (i/v_F)[(h_x\mathbf{e}_y - h_y\mathbf{e}_x)\tau_z, \hat{A}]_{\otimes}$. Eq. (14) should be supplemented by the normalization condition $\hat{g} \otimes \hat{g} = 1$ and the boundary conditions at $x = \mp d/2$. It is assumed that the JJ is formed at the surface of the TI, the superconducting order parameter Δ and \mathbf{h} are effective quantities induced in the surface states of TI by proximity to the superconductors and a ferromagnet. In this case, there are no reasons to assume the existence of potential barriers at the $x = \mp d/2$ interfaces and, therefore, these interfaces are considered as fully transparent. In this case, the boundary conditions are reduced to continuity of \hat{g} for a given quasiparticle trajectory at the interfaces.

Our derivation closely follows Ref. 148. To obtain the simplest sinusoidal form of the current-phase relation we linearize Eq. (14) with respect to the anomalous Green's function. In this case the retarded component of the Green's function $\hat{g}^R = \tau_z + f^R\tau_+ + \tilde{f}^R\tau_-$. The solution of the linearized Eilenberger equation satisfying asymptotic conditions $f^R \rightarrow (\Delta/\varepsilon)e^{\pm i\chi/2}$ at $x \rightarrow \pm\infty$ and continuity conditions at $x = \mp d/2$ takes the form:

$$\begin{aligned} f_{\pm}^R &= \frac{\Delta e^{\mp i\chi/2}}{\varepsilon} \exp\left[\frac{\mp 2i(\mathbf{h}\mathbf{n}_{\perp} - \varepsilon)(d/2 \pm x)}{v_x}\right], \\ \tilde{f}_{\pm}^R &= -\frac{\Delta e^{\mp i\chi/2}}{\varepsilon} \exp\left[\frac{\mp 2i(\mathbf{h}\mathbf{n}_{\perp} - \varepsilon)(d/2 \mp x)}{v_x}\right], \end{aligned} \quad (15)$$

where the subscript \pm corresponds to the trajectories $\text{sgn } v_x = \pm 1$.

The density of electric current along the x -axis is

$$\begin{aligned} j_x &= -\frac{eN_F v_F}{4} \int_{-\infty}^{\infty} d\varepsilon \int_{-\pi/2}^{\pi/2} \frac{d\phi}{2\pi} \cos \phi \times \\ &\quad \left[(g_+^R \otimes \varphi_+ - \varphi_+ \otimes g_+^A) - (g_-^R \otimes \varphi_- - \varphi_- \otimes g_-^A) \right], \end{aligned} \quad (16)$$

where ϕ is the angle, which the quasiparticle trajectory makes with the x -axis. φ_{\pm} is the distribution function corresponding to the trajectories $\text{sgn } v_x = \pm 1$. In equilibrium $\varphi_{\pm} = \tanh[\varepsilon/2T]$. Exploiting the normalization condition one can obtain $g_{\pm}^R \approx 1 - f_{\pm}^R \tilde{f}_{\pm}^R/2$. Taking into account that $g_{\pm}^A = -g_{\pm}^{R*}$ the following final expression

for the Josephson current has been obtained:

$$j_s = j_c \sin(\chi - \chi_0), \quad (17)$$

$$\begin{aligned} j_c &= ev_F N_F T \sum_{\varepsilon_n > 0} \int_{-\pi/2}^{\pi/2} d\phi \cos \phi \frac{\Delta^2}{\varepsilon_n^2} \times \\ &\quad \exp\left[-\frac{2\varepsilon_n d}{v_F \cos \phi}\right] \cos\left[\frac{2h_x d \tan \phi}{v_F}\right], \end{aligned} \quad (18)$$

$$\chi_0 = 2h_y d/v_F, \quad (19)$$

where $\varepsilon_n = \pi T(2n+1)$. It is seen that the CPR Eq. (17) contains the anomalous phase shift χ_0 . At high temperatures $T \approx T_c \gg \Delta$ the main contribution to the current comes from the lowest Matsubara frequency and Eq. (18) can be simplified further

$$\begin{aligned} j_c &= j_b \int_{-\pi/2}^{\pi/2} d\phi \cos \phi \times \\ &\quad \exp\left[-\frac{2\pi T d}{v_F \cos \phi}\right] \cos\left[\frac{2h_x d \tan \phi}{v_F}\right], \end{aligned} \quad (20)$$

where $j_b = ev_F N_F \Delta^2/(\pi^2 T)$. Similar expression has also been obtained for Dirac materials¹⁵⁸.

Eqs. (19) and (20) demonstrate that the dependence of the Josephson current on the exchange field (and, consequently, the magnetization direction in S/F-TI/S junctions) is highly nontrivial. In contrast to the well-known S/F/S junctions via ordinary ferromagnets, where the critical current is suppressed by exchange field and *does not depend on its direction*, here the critical Josephson current is only suppressed by the x -component of the exchange field. The y -component of the field does not lead to the suppression. Instead, it gives rise to the anomalous phase shift. This statement is also valid for the diffusive case. The Josephson current in 3D TI-based diffusive Josephson junction has been considered in Ref. 104, and exactly the same expression for the anomalous phase shift χ_0 has been obtained. The result for the critical current is different in the diffusive case, but it still only depends on the x -component of the exchange field. Below we explain the qualitative physics of this effect.

Let us consider a pair travelling in the TI surface states in the interlayer region of the JJ and carrying the Josephson current. The pair consists of electrons with opposite momenta and opposite spin directions. At first, we assume that the exchange field is along the y -axis, that is $\mathbf{h} = h\mathbf{e}_y$. Because the spin of an electron is strictly perpendicular to its momentum, each of the electrons forming the pair "sees" its own effective exchange field, which is equal to the projection of \mathbf{h} onto its spin direction. If the electron momentum makes an angle ϕ with the x -axis, the effective field seen by the electron is $h \cos \phi$, see Fig. 6(a). After passing the distance x along the x -axis the electron acquires a phase $\Phi \approx p_{F,x}x + (h \cos \phi/v_{F,x})x$. The second electron from the pair with the opposite values of the momentum and spin sees the opposite effective

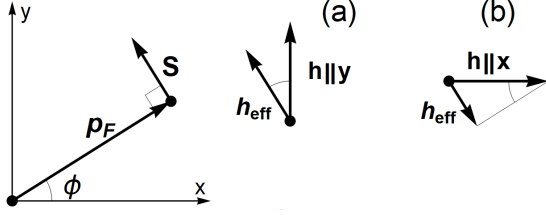


FIG. 6. Illustration of the effective exchange field seen by an electron in the conductive surface states of the 3D TI. \mathbf{p}_F is the electron momentum and \mathbf{S} is its spin. (a) Exchange field \mathbf{h} induced by the proximity to a ferromagnet is along the y -axis. (b) \mathbf{h} is along the x -axis, that is aligned with the Josephson current direction. In both cases the electron only feels effective exchange field \mathbf{h}_{eff} , which is along its spin direction.

exchange field and, therefore, acquires the same phase. The total phase gained by the pair is $(2h \cos \phi / v_{F,x})x$ in agreement with Eq. (15). Taking into account that $v_{F,x} = v_F \cos \phi$ we see that for the given exchange field direction the phase acquired by the pair does not depend on the trajectory direction. Therefore, the contributions from the different trajectories to the Josephson current do not cancel each other due to the momentum averaging. As a result, the critical current is not suppressed by the exchange field, and the influence of the field only appears via the overall phase $\pm 2h_y d / v_F$ acquired by all the pairs travelling through the interlayer to the right (left). Because of the independence of the phase gain on the momentum direction between two scattering events, the consideration is also applicable to the diffusive case resulting in the same answer. Interestingly that the same phase factors can result in the electric current oscillations through the Andreev interferometer¹⁵⁹.

Now let us compare the previous consideration to the case of the exchange field along the x -axis, that is $\mathbf{h} = h\mathbf{e}_x$. In this case the effective exchange field which is seen by the electron is $-h \sin \phi$ and the same reasoning results in the phase acquired by the pair $\Phi = -(2h \tan \phi / v_F)x$. The phase depends on the trajectory direction and, therefore, the Josephson current carried by all the pairs is greatly reduced due the averaging of these acquired phases. It has also been reported that due to the finite width of the junction along the y -direction, the decay of the critical current upon the increase of the x -component of the exchange field is accompanied by the Fraunhofer-like oscillations¹⁶⁰.

In summary, we can see that the Josephson current via the 3D TI-based S/F/S junction depends strongly on the exchange field direction. The physical reason for this dependence is the spin-momentum locking. In particular, the Josephson current exhibits the anomalous phase shift $\chi_0 = 2h_y d / V_F$. It is determined by the exchange field component perpendicular to the current direction analogously to the case of Rashba materials, described above. However, the anomalous phase shift in TI-based

Josephson junctions is much larger than in the materials with Rashba SOC because it does not contain the reducing factor $\Delta_{so} / \varepsilon_F \sim \alpha p_F / \varepsilon_F$. It is directly connected to the fact that the 3D TI has only one helical Fermi surface [see Fig. 5(b)] in contrast to the Fermi surface of a Rashba material, which consists of two helical bands with opposite helicity [see Fig. 1(a)].

C. Anomalous phase shift in S/F/S junctions via inhomogeneous ferromagnets

The interaction of conduction electron spin with a magnetic texture can be described using an artificial spin-orbital coupling potential. In general the local transformation $\hat{U}(\mathbf{r}) = e^{i\hat{\sigma}\boldsymbol{\theta}(\mathbf{r})/2}$ rotates spin axes to the local frame where $\mathbf{h} \parallel \mathbf{z}$. It is parametrized by the spin vector $\boldsymbol{\theta} = \theta\mathbf{n}$ defined by the spatial texture of the exchange field distribution $\mathbf{h}(\mathbf{r}) = \hat{R}(\boldsymbol{\theta}(\mathbf{r}))\mathbf{h}$, where \hat{R} is the spatially-dependent rotation matrix and we choose $\mathbf{h} = h\mathbf{z}$. This transformation generates the spin-dependent potential $\hat{\sigma}_a \{M_k^a, \hat{p}_k\} / 2$ with pure gauge SU(2) field $M_k^a = -i\text{Tr}(\hat{\sigma}_a \hat{U}^\dagger \nabla_k \hat{U}) / 2m$. This artificial SOC leads to the spontaneous current¹⁴⁶ in the form (6) with $\chi_k^a \propto M_k^a$ so that $\mathbf{j} \propto h\chi_k^z$. This spontaneous current is nonzero provided that $M_k^z \neq 0$ which physically means that the magnetic texture is non-coplanar. On the qualitative level, the non-coplanarity is needed to obtain the different orbital states of conduction electrons in magnetic textures $\pm\mathbf{h}(\mathbf{r})$ connected by the time-reversal transformation $\mathbf{h} \rightarrow -\mathbf{h}$. In the non-coplanar case it is not possible to compensate this sign change by the global, that is coordinate-independent spin rotation. The minimal non-coplanar texture consists of three magnetic moments $\mathbf{m}_{1,2,3}$ with nonzero scalar spin chirality¹⁶¹ $\chi = \mathbf{m}_1(\mathbf{m}_2 \times \mathbf{m}_3)$. As demonstrated in Ref.118 already the arrangement of three point-wise non-coplanar magnetic impurities leads to the generation of the spontaneous supercurrent and superconducting phase gradients $\mathbf{j}, \nabla\varphi \propto \chi$.

The anomalous phase shifts has been studied in Josephson junctions through various non-coplanar magnetic textures, including the three-layer systems^{99,106,108,110,111,113,116,162,163}, magnetic helices^{118,146} and skyrmions¹¹⁸. In most cases the magnetic systems are assumed to be metallic consisting either of strong ferromagnets or the half-metals. However, in several papers it has been shown that magnetoelectric effects can be engineered even with the help of ferromagnetic insulators^{116,163} (FI) which are currently considered as the promising platform for coupling of the superconductivity and ferromagnetism^{164–168}. Below we discuss the particular example of of such system¹⁶³.

Let us consider the system shown in Fig.7 consisting of two superconducting electrodes $S_{1,2}$ separated by a single FI interlayer acting as a spin-filtering barrier with polarization \mathbf{P} . The outer FI layers generate Zee-

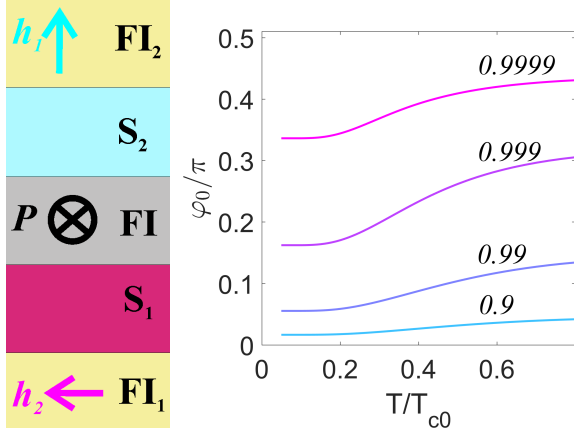


FIG. 7. (Left panel) Sketch of FI-S-FI-S-FI [FI stands for a ferromagnetic insulator] non-coplanar spin valve system with the superconducting electrodes $S_{1,2}$ having different phases $\varphi_{1,2}$. The exchange fields $\mathbf{h}_{1,2}$ in $\text{FI}_{1,2}$ form a non-coplanar system with the spin polarization of central barrier \mathbf{P} . Lengths of S layers are of the order of the superconducting coherence length to ensure well-pronounced proximity-induced exchange field in the S-layers. (Right panel) Temperature dependencies of the anomalous phase shift at $P = 0.9; 0.99; 0.999; 0.9999$ (curves from top to bottom) for $\mathbf{h}_1 \perp \mathbf{h}_2 \perp \mathbf{P}$.

man fields $\mathbf{h}_{1,2}$ in $S_{1,2}$ due to the magnetic proximity effect^{169,170}. To calculate the currents across spin-filtering barriers we use generalized Kuprianov-Lukichev boundary conditions¹⁷¹, that include spin-polarized tunnelling at the SF interfaces^{11,114,115,172}. The matrix tunnelling current from S_1 to S_2 is given by

$$\tilde{I}_{12} = [\tilde{\Gamma} \tilde{g}_1 \tilde{\Gamma}^\dagger, \tilde{g}_2], \quad (21)$$

where \tilde{g}_k for $k = 1, 2$ are the matrix Green's functions in the superconducting electrodes S_k . The spin-polarized tunnelling matrix has the form $\tilde{\Gamma} = t_+ \hat{\sigma}_0 \hat{\tau}_0 + t_- (\mathbf{m} \hat{\boldsymbol{\sigma}}) \hat{\tau}_3$, where \mathbf{m} is the direction of barrier magnetization, $t_\pm = \sqrt{(1 \pm \sqrt{1 - P^2})/2}$ and P being the spin-filter efficiency of the barrier that ranges from 0 (no polarization) to 1 (100% filtering efficiency). The matrix Green's functions are determined by the equation⁹

$$[\omega_n \tau_3 + i(\mathbf{h} \cdot \boldsymbol{\sigma}) \tau_3 + \tilde{\Delta} - \tilde{\Sigma}_s, \tilde{g}] = 0. \quad (22)$$

Here $\omega_n = (2n + 1)\pi T$ is the Matsubara frequency, $\tilde{\Delta} = \Delta \tau_1 e^{i\tau_3 \varphi}$ is the order parameter with the amplitude Δ and phase φ , \mathbf{h} is the exchange field. We include the spin-orbital (SO) scattering process which lead to the spin relaxation described by⁹ $\tilde{\Sigma}_s = (\mathbf{S} \cdot \tilde{\mathbf{g}} \mathbf{S})/8\tau_{so}$, where τ_{so} is the SO scattering time. Due to the normalization condition $\tilde{g}^2 = 1$.

The solution of Eq. (22) can be found in the form

$$g = \tau_3 [g_{03} + g_{33}(\boldsymbol{\sigma} \mathbf{h})] + \tau_1 [g_{01} + g_{31}(\boldsymbol{\sigma} \mathbf{h})] \quad (23)$$

The terms diagonal in Nambu space (τ_3) correspond to the normal correlations which determine the den-

sity of states. The off-diagonal components (τ_1) describe spin-singlet g_{01} and spin-triplet g_{31} superconducting correlations which appear as a result of the exchange splitting¹⁷³.

The CPR (7) can be calculated for the spin-valve shown in Fig.(7) using the general matrix current (21). The usual $j_0 = j_c \cos \varphi_0$ and anomalous $j_{an} = j_c \sin \varphi_0$ Josephson currents through tunnel barrier are given by

$$\frac{R_N j_0}{\pi e T} = \sum_{\omega_n} [r(g_{01}^2 + h_{1\parallel} h_{2\parallel} g_{31}^2) + (\mathbf{h}_{1\perp} \mathbf{h}_{2\perp}) g_{31}^2] \quad (24)$$

$$\frac{R_N j_{an}}{\pi e T} = \chi P \sum_{\omega_n} g_{31}^2, \quad (25)$$

where $\chi = \mathbf{P}(\mathbf{h}_1 \times \mathbf{h}_2)$ is the spin chirality, $\mathbf{h}_{i\perp}$ are the projections of \mathbf{h}_i on the plane perpendicular to \mathbf{P} .

Expressions (24, 25) show that the anomalous current j_{an} is mediated by spin-triplet component g_{31} . Physically the phase-shifting term j_{an} appears as a result of the additional phase picked up by the spin-triplet Cooper pairs when tunnelling between two superconductors with non-collinear exchange fields through the spin-polarising barrier. Therefore φ_0 Josephson effect is the directly observable signature of the spin-triplet superconducting current across the junction. For the ideal spin filter $P = 1$ Eqs. (24), (25) yield a temperature-independent phase shift of CPR $\varphi_0 = \theta_h$, where θ_h is the geometric angle between the vectors $\mathbf{h}_{1\perp}$ and $\mathbf{h}_{2\perp}$. In the general case φ_0 can be quite different, as shown in Fig.(7).

D. Direct magnetoelectric effect in Josephson junctions via spin-orbit materials

The direct magnetoelectric effect was predicted for superconducting systems in the presence of spin-orbit coupling, where it represents the generation of an equilibrium spin polarization in response to supercurrent. The spin-orbit coupling can be both of intrinsic type, that is arising due to the inversion symmetry breaking^{62,63,125,126} and of extrinsic type, that is impurity-induced^{66,67}. Physically, the effect is the same for superconductors in the presence of the spin-orbit coupling and for the Josephson junctions and can be expressed by the general equation:

$$S^a = \frac{1}{e v_F} \kappa_k^a j_{s,k} \quad (26)$$

where $j_{s,k}$ is the k -component of the supercurrent density. However, in this review we describe the effect and the used theoretical approaches focusing on the Josephson junctions. The direct magnetoelectric effect was considered both for ballistic¹²⁶ and diffusive Josephson junctions¹²⁵ via spin-orbit coupled materials.

We will focus on the case of ballistic S/NSO/S junction with Rashba-type spin-orbit coupling in the interlayer and discuss the value of the electron spin polarization

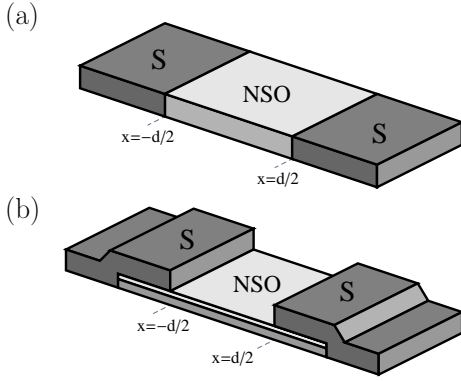


FIG. 8. Sketches of possible realizations of the S/NSO/S junction [NSO means normal metal with spin-orbit coupling]. Adopted from Ref. 126.

induced by the applied supercurrent and the theoretical approach used for solving the problem in Ref. 126. The sketch of the system under consideration is shown in Fig. 8. The S/NSO interfaces are at $x = \mp d/2$. The Hamiltonian of a singlet superconductor in the presence of an arbitrary linear in momentum spin-orbit (SO) coupling^{174,175}:

$$\hat{H} = \int d^2\mathbf{r}' \hat{\Psi}^\dagger(\mathbf{r}') \hat{H}_0(\mathbf{r}') \hat{\Psi}(\mathbf{r}') + \Delta(\mathbf{r}) \Psi_\uparrow^\dagger(\mathbf{r}) \Psi_\downarrow^\dagger(\mathbf{r}) + \Delta^*(\mathbf{r}) \Psi_\downarrow(\mathbf{r}) \Psi_\uparrow(\mathbf{r}), \quad (27)$$

$$\hat{H}_0(\mathbf{r}) = \frac{\hat{\mathbf{p}}^2}{2m} - \frac{1}{2} \hat{\mathbf{A}} \hat{\mathbf{p}} - \mu, \quad (28)$$

where $\Delta(\mathbf{r})$ is the superconducting parameter, which is nonzero only in the superconducting leads. \hat{H}_0 is the Hamiltonian of the normal metal in the presence of the spin-orbit coupling (NSO). The general linear in momentum SO is expressed by the term $\frac{1}{2} \hat{\mathbf{A}} \hat{\mathbf{p}} = \frac{1}{2} A_j^\alpha p_j \hat{\sigma}^\alpha$, where $\hat{\sigma}^\alpha$ are Pauli matrices in spin space. $\hat{\Psi} = (\Psi_\uparrow, \Psi_\downarrow)^T$, μ is the chemical potential. For particular case of the Rashba SOC $A_x^y = -A_y^x = \alpha$ and for the Dresselhaus SOC $A_x^x = -A_y^y = \beta$.

In the superconducting systems under the applied supercurrent the Cooper pairs acquire nonzero total momentum, which leads to the analogous shift of the Fermi surfaces in the momentum space, as it was discussed in the introduction for nonsuperconducting materials. But in the superconducting case the polarization is provided by the averaged polarization of triplet pairs, as it supported below by the corresponding expression of the polarization in terms of the anomalous Green's function. Therefore, the supercurrent-induced polarization is intimately connected to another manifestation of the magnetoelectric effect in superconducting systems: generation of triplet pairs under the applied electric current. Now our goal is to describe this effect in Josephson junctions.

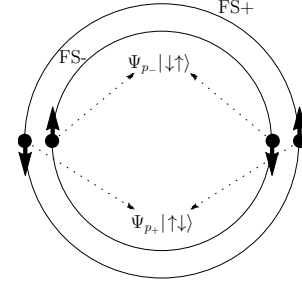


FIG. 9. Opposite-spin and opposite-momenta pairing for the Rashba material. Two spin-split Fermi-surfaces are denoted by FS_\pm .

Superconducting hybrid mesoscopic systems are often considered within the framework of the quasiclassical theory, which makes it possible to effectively solve spatially inhomogeneous problems. The SOC can be treated in the quasiclassical approximation when its characteristic energy Δ_{so} is much less than the Fermi energy ε_F . This situation is typical. However the quasiclassical consideration does not capture the magnetoelectric effects, which are of the first order with respect to the parameter $\Delta_{so}/\varepsilon_F$. In particular, it is known that the standard quasiclassical equations in the presence of SOC and in the absence of an exchange field do not provide a transformation of singlet correlations to the triplet ones^{174,175}. The physical reason for this can be immediately seen from Fig. 9. The opposite-momenta pairing occurs between the electrons of the same helical band. It is obvious that for a given momentum direction one can compose a pair $\Psi_{p+} |\uparrow\downarrow\rangle$ at one of the subbands and a pair $\Psi_{p-} |\downarrow\uparrow\rangle$ for the other subband, where p_\pm are Fermi momenta of the both helical subbands. Each of the pairs is a singlet-triplet mixture. Therefore, taking into account the fact that wave functions of the pairs differ at different Fermi surfaces $\Psi_{p+} \neq \Psi_{p-}$, we obtain a triplet admixture of the pair wave function¹⁷⁶. However, the quasiclassical approximation disregards the difference between the values of the Fermi momenta for the both helical subbands, that is $p_+ = p_-$ with the quasiclassical accuracy. In this case the singlet pairs do not accompanied by such a triplet admixture. Therefore, in order to describe the triplet correlations in SOC materials and the resulting magnetoelectric effects, a generalization of the quasiclassical theory to include the first order corrections with respect to the parameter $\Delta_{so}/\varepsilon_F$ is required. Several approaches have been reported in the literature^{98,125,126}. We focus on the approach developed in Ref. 126.

The generalized quasiclassical equation for the quasiclassical Green's function can be written as follows:

$$iv_F \nabla \check{g} + \left[\varepsilon \hat{\tau}_z + \check{\Delta}(\mathbf{r}) + \frac{1}{2} \hat{\mathbf{A}} \mathbf{p}_F, \check{g} \right] + \frac{p_y}{4v_{F,x}} [\hat{A}_x, \hat{A}_y] (\check{g} - \text{sgn} v_{F,x}) + \frac{i \hat{A}_y p_y}{2p_{F,x}} \partial_x \check{g} = 0. \quad (29)$$

The second line of Eq. (29) represents the corrections of the order of $\Delta_{so}/\varepsilon_F$ to the standard Eilenberger equation¹⁷⁷. Eq. (29) should be supplied by the normalization condition. In usual quasiclassical theory, the normalization condition is $\check{g}^2 = 1$. However, in the framework of the discussed approach, it should be modified if one would like to take into account the terms of the order of $\Delta_{so}/\varepsilon_F$. It takes the form:

$$\check{g}^2 - \frac{\hat{A}_y p_y \text{sgn} v_{F,x}}{p_{F,x} v_{F,x}} \left[\check{g} - \text{sgn} v_{F,x} \right] = 1 \quad (30)$$

Quasiclassical equations are not valid in the vicinity of interfaces, where the normal state Hamiltonian of the system changes over the atomic length scales. Therefore they should be supplied by the boundary conditions. Corrections to the boundary conditions appear even for the simplest “absolutely transparent interfaces” case when the boundary conditions take the form:

$$\check{g}^l - \check{g}^r = \pm \left\{ \text{sgn} v_{F,x} - \check{g}, \frac{\hat{A}_y p_y}{4v_{F,x} p_{F,x}} \right\}, \quad (31)$$

The signs \pm correspond to the NSO/S and S/NSO interfaces, respectively. It is seen that neglecting the right hand side of the above equation, which is of the first order in $\Delta_{so}/\varepsilon_F$, we obtain the well-known quasiclassical boundary condition at a fully transparent interface: $\check{g}^l = \check{g}^r = \check{g}$, that is just the continuity of the Green’s function. In the framework of this modified quasiclassical theory, the boundary condition is reduced to the standard continuity condition $\check{g}^l = \check{g}^r$ only for the case of equal SO coupling in both materials.

For the considered S/NSO/S junction the y -component of the triplet anomalous Green’s function in the NSO interlayer, which determines the electron polarization S_y , takes the form:

$$f_{\pm}^y = -(x \pm \frac{d}{2}) M_{\pm} \frac{p_{F,x}}{p_F} e^{2i\varepsilon x/v_{F,x}}, \quad (32)$$

$$M_{\pm} = \frac{i\alpha p_y^2 \Delta}{p_{F,x} v_{F,x}^2 p_F} e^{\mp i\chi/2 + i\varepsilon d/|v_{F,x}|}. \quad (33)$$

It is seen that the triplet correlations are of the first order with respect to the parameter $\Delta_{so}/\varepsilon_F = \alpha p_F/\varepsilon_F$. Result (32) coincides with the result of the exact calculation in terms of Gor’kov Green’s functions beyond the quasiclassical approximation¹⁷⁸ up to the first order with respect to the parameter $\Delta_{so}/\varepsilon_F$. Please note that the statement of Ref. (178) that the triplet pairing vanishes to the first order in $\Delta_{so}/\varepsilon_F$ is not correct. The correct expansion contains terms of the first order by this parameter.

Making use of the above equations it is possible to evaluate the average spin polarization:

$$\mathbf{S} = \frac{1}{2} \langle \hat{\Psi}^\dagger(\mathbf{r}, t) \hat{\boldsymbol{\sigma}} \hat{\Psi}(\mathbf{r}, t) \rangle. \quad (34)$$

The supercurrent-induced spin polarization is directly related to the triplet pairing. It can be written as¹²⁶

$$\mathbf{S} \propto \int d\varepsilon dp_y \tanh \frac{\varepsilon}{2T} \text{Re} \left[\frac{1}{g_{+,s}^R} \left(f_{+,s}^R \tilde{f}_{+,t}^R + \tilde{f}_{+,s}^R f_{+,t}^R \right) + \frac{1}{g_{-,s}^R} \left(f_{-,s}^R \tilde{f}_{-,t}^R + \tilde{f}_{-,s}^R f_{-,t}^R \right) \right]. \quad (35)$$

$g_s(f_s)$ and $g_t(f_t)$ are the singlet and triplet components of the normal (anomalous) Green’s function, which can be found from the matrix Green’s function structure:

$$\check{g} = \begin{pmatrix} g_s + \mathbf{g}_t \boldsymbol{\sigma} & f_s + \mathbf{f}_t \boldsymbol{\sigma} \\ \tilde{f}_s + \mathbf{\tilde{f}}_t \boldsymbol{\sigma} & \tilde{g}_s + \mathbf{\tilde{g}}_t \boldsymbol{\sigma} \end{pmatrix}, \quad (36)$$

where the structure in the particle-hole space is shown explicitly and the matrix structure in the spin space is encoded in the Pauli matrices $\boldsymbol{\sigma}$. The anomalous Green’s function \tilde{f} can be expressed as $\tilde{f}_{\pm}^y = -f_{\mp}^y(-\Delta, -\chi, -v_{F,x})$. The only component of the triplet anomalous Green’s function \mathbf{f} , which is not an odd function of p_y and, therefore, survives after integration over p_y , is f_y , expressed by Eq. (32). As a result, only the y -component of the spin polarization is nonzero in the Josephson junction via the Rashba SOC material, according to the qualitative consideration above. In a vector form the induced spin polarization can be represented as

$$\mathbf{S} = \kappa [\mathbf{c} \times \frac{\mathbf{j}_s}{ev_F}]. \quad (37)$$

For the considered case $\alpha p_F/2\pi T = \Delta_{so}/2\pi T \gg 1$

$$\kappa = \frac{\alpha p_F}{8\varepsilon_F}. \quad (38)$$

It is the same value as for homogeneous superconductors⁶². Whether this universal behavior holds for S/NSO/S tunnel junctions has not yet been investigated. It is worth to note here that the direct magneto-electric effect should also take place in S/NSO/S junctions with very strong SO coupling in the interlayer ($\Delta_{so} \sim \varepsilon_F$), but the described theory is not able to consider this case quantitatively. This problem can be solved on the basis of the different quasiclassical formalism, where the SO interaction is so strong that the coupling between the two helical subbands is disregarded^{88,179}.

Another technique accounting for the magnetoelectric effects is a gauge-covariant approach to establish the transport equations⁹⁸. In this approach, both the electromagnetic and spin interactions are described in terms of $U(1)$ Maxwell and $SU(2)$ Yang-Mills equations, respectively. The additional terms to the Eilenberger equation are expressed via the gauge field $\mathbf{F}_{\mu\nu} = \partial_\mu \mathbf{A}_\nu - \partial_\nu \mathbf{A}_\mu + i[\mathbf{A}_\mu, \mathbf{A}_\nu]$. In the framework of this approach the well-known Edelstein’s results for supercurrent induced spin polarization in homogeneous superconductors, which were obtained in the diffusive⁶³ and ballistic limits⁶², have been generalized for the case of arbitrary disorder strength⁶⁵.

The supercurrent-induced spin polarization in the S/NSO/S Josephson junctions has also been calculated in the diffusive limit¹²⁵. The first-order corrections in $\Delta_{so}/\varepsilon_F$ were added to the Usadel equation for the Green's functions. The triplet anomalous Green's function has been obtained in the form

$$f_t = -i \frac{\alpha\tau}{\sqrt{2}} \frac{\partial f_s}{\partial x}. \quad (39)$$

The supercurrent-induced electron spin polarization is

$$\mathbf{S} = \frac{eN_F\alpha\tau}{\sigma} [\mathbf{c} \times \mathbf{j}_s], \quad (40)$$

where σ - is the conductivity of the NSO interlayer, N_F is the density of states at the Fermi level and τ is the elastic-scattering time. The ratio $Sev_f/(j_s) \sim \alpha p_f/\varepsilon_F$ in Eq. (40) is also of the first order in $\Delta_{so}/\varepsilon_F$. In the subsequent paper¹⁸⁰ of the same group, the S/NSO/S junction under the applied voltage has also been considered. It was predicted that the spin-Hall current does not turn to zero in contrast to the stationary Josephson effect. The physical reason is that besides a direct proximity effect caused by a Cooper pair's transition into a triplet state, the spin current and polarization are also driven by a periodic electric field associated with the charge imbalance.

E. Direct magnetoelectric effect in S/TI/S junctions

As it is discussed in the previous section, the value of the supercurrent-induced electron spin polarization in Josephson junctions via SO-materials is rather small and $\propto \Delta_{so}/\varepsilon_F$. The physical reason for this is the presence of *two* helical Fermi surfaces in the material with intrinsic SOC, which contribute to the direct magnetoelectric effect in opposite directions. In contrast, the 2D Fermi surface of the conductive surface states of the 3D topological insulators (TIs) consists of the only helical Fermi surface, see Fig. 5(b). It leads to the absence of the partial compensation of the current-induced electron spin polarization produced by the helical Fermi surfaces with the opposite helicities. As a result, the current-induced spin polarization does not contain the reducing factor $\Delta_{so}/\varepsilon_F$ and takes the form:

$$\langle \mathbf{s} \rangle = -\frac{1}{2ev_F} [\mathbf{e}_z \times \mathbf{j}_s]. \quad (41)$$

Eq. (41) has been obtained, making use of the quasiclassical theory for TI-based superconducting hybrid structures (assuming no Zeeman field in the system)⁶⁸, which has already been described in Sec. II B. Eq. (41) coincides with the result for the current-induced spin polarization in normal state TI surface states¹⁸¹.

While the supercurrent-induced spin polarization in TIs has not been measured yet, the current-induced spin polarization in normal state TIs has been directly measured as a voltage on a ferromagnetic metal tunnel barrier

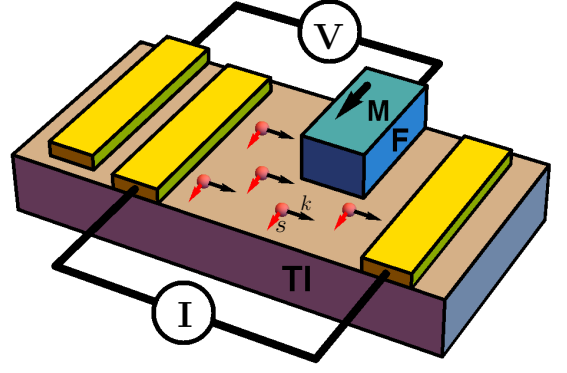


FIG. 10. Sketch of the experimental setup for the electrical measurement of the direct magnetoelectric effect at the surface of the 3D TI. If the magnetization (\mathbf{M}) of the ferromagnetic detector (F, blue) has a component along the conductivity electron polarization (red arrows), the voltage V is nonzero. If the magnetization of the detector is along the current axis, $V = 0$.

surface contact⁴². The voltage measured at the contact is proportional to the projection of the spin polarization of the TI onto the direction of the ferromagnet magnetization. An unpolarized bias current is applied between two nonmagnetic contacts, see Fig. 10. When the charge current is orthogonal to the magnetization of the ferromagnetic detector contact, the TI spin is parallel (or antiparallel) to the magnetization, and a spin-related signal is detected at the ferromagnetic contact proportional to the magnitude of the charge current. When the direction of the charge current is reversed, the measured voltage changes sign. When the contact magnetization is rotated in-plane 90° so that the charge current is parallel to the magnetization, no spin voltage is detected, because the TI spin polarization is now perpendicular to the contact magnetization.

III. MAGNETOELECTRIC EFFECTS AND MAGNETIZATION DYNAMICS

A. Direct coupling between magnetization and superconducting condensate: basic physics and equations

The discussed above direct and inverse magnetoelectric effects are of great interest for Josephson junctions with ferromagnetic interlayers because they result in the coupling between the ferromagnet magnetization and the Josephson current. This leads to several interesting ways of electrical control of magnetization and electrical detection in S/F/S junctions. The present section aims to a discussion of those effects.

First of all we formulate the basic equations and describe qualitatively the physics underlying the direct coupling between the supercurrent and the magnetization.

In the considered S/F/S junction the coupled dynamics of magnetization \mathbf{M} and Josephson phase difference χ is determined by the following closed set of equations

$$j = j_c(\mathbf{M}) \sin(\chi - \chi_0\{\mathbf{M}\}) + \frac{\dot{\chi} - \dot{\chi}_0\{\mathbf{M}\}}{2eRS}. \quad (42)$$

$$\frac{\partial \mathbf{M}}{\partial t} = -\gamma \mathbf{M} \times \mathbf{H}_{eff} + \frac{\alpha}{M} \mathbf{M} \times \frac{\partial \mathbf{M}}{\partial t} + \mathbf{T}, \quad (43)$$

Eq.(42) represents the non-equilibrium current-phase relation (CPR) generalizing resistively shunted Josephson junction (RSJ) model. The capacitive term is neglected here. This relation is written¹⁴⁹ in a gauge-invariant form amended to include the anomalous phase shift $\chi_0\{\mathbf{M}\}$ defined by SOC and magnetic texture. In contrast to the previously used gauge non-invariant formulations^{182,183} Eq.(42) describes the normal spin-galvanic effects when $j_c = 0$ such as the electromotive force and charge current generated in the ferromagnet due to the time derivative of the Berry phase^{52,54–57,184,185}. The analogous equation is also valid for a more general nonsinusoidal CPR.

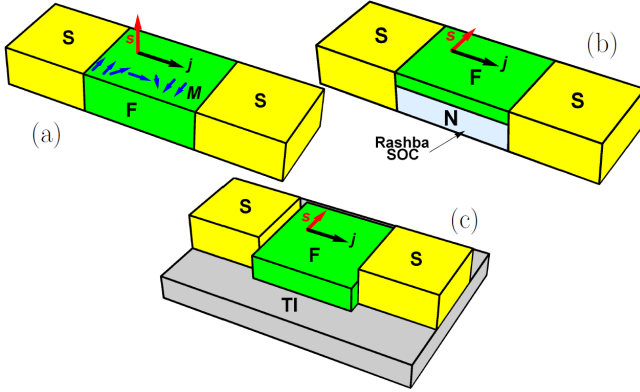


FIG. 11. Examples of Josephson junctions, where the current-induced electron polarization is possible. The direction of the spin polarization relative to the current is shown by red arrows. (a) a JJ via a spin-textured ferromagnet (F); (b) a JJ via a combined ferromagnet (F) + SOC material interlayer (N); (c) a JJ via a ferromagnet on top of a 3D topological insulator (TI). For all the cases it is assumed that the interlayer length should not exceed a few normal state coherence lengths of the interlayer material to ensure a sizeable Josephson current through the JJ.

The dynamic is described by the Landau-Lifshitz-Gilbert (LLG) equation (43), where α is the Gilbert damping constant. The polarization of the conductivity electrons, which occurs in the interlayer of the JJ due to the direct magnetoelectric effect discussed above, interacts with the ferromagnet magnetization by the exchange mechanism. Suppose this interaction is internal for the ferromagnet. In that case, it can be accounted for in the framework of the s-d model⁴⁴, which describes the exchange interaction between the conductivity electrons and localized electrons responsible for the magnetization according to $\hat{H}_{s-d} = -J \sum_i \hat{S}_i \hat{s}$, where \hat{S}_i is the

spin operator of the localized spin at site i and \hat{s} is the spin operator of the conductivity electron. The examples are interlayers made of spin-textured ferromagnets or ferromagnets with intrinsic SOC. In hybrid interlayers consisting of a ferromagnet and a nonmagnetic material with SOC or a topological insulator, see examples in Fig. 11, the spin polarization induced by the current in the nonmagnetic material (NM) due to the direct magnetoelectric effect, see Secs. II D and II E, interacts with the ferromagnet magnetization via the exchange interaction at the F/NM interface:

$$H_{int} = - \int d^2 \mathbf{r} \hat{\Psi}^\dagger(\mathbf{r}) J_{ex} \mathbf{S} \sigma \hat{\Psi}(\mathbf{r}), \quad (44)$$

where $\hat{\Psi} = (\Psi_\uparrow, \Psi_\downarrow)^T$, \mathbf{S} is the localized spin operator in the ferromagnet, J_{ex} is the interface exchange constant and the integration is performed over the 2D interface.

In both cases the torque can be represented in the form:

$$\mathbf{T} = J \mathbf{M} \times \langle \mathbf{s} \rangle. \quad (45)$$

where $\langle \mathbf{s} \rangle$ is the averaged polarization of conductivity electrons. J is the exchange constant of the s-d model or $J = J_{ex}/d_F$ for the hybrid F/HM interlayers with d_F standing for the ferromagnet thickness.

Below, the particular examples of the electrically induced magnetization dynamics in JJ via ferromagnets and the backward influence of the dynamics on the JJ are discussed.

B. Supercurrent-induced magnetization dynamics in S/F/S junctions via spin-textured ferromagnets

In the context of inhomogeneous ferromagnetic interlayers, the supercurrent-induced spin torques have been calculated theoretically in Josephson junctions through single spins^{186–188} two^{189–191}, three¹¹¹ FM layers and bulk inhomogeneous ferromagnets¹⁴⁷. The supercurrent-induced dynamics has also been studied. In particular, the supercurrent-induced magnetization switching in S/F/N/F/S JJs between parallel and antiparallel configurations has been predicted in Ref. 190. The supercurrent-induced DW motion has been studied in Ref. 147. The spin torque in these systems is commonly viewed as a spin transfer from the spin-polarized triplet supercurrent to the magnetization. However, it can also be understood in terms of the supercurrent-induced conductivity electron spin polarization. From this point of view, it can be considered in a unified manner with the supercurrent-induced torque in JJs with SOC in the interlayer. Below we illustrate this concept by the example of the supercurrent-induced DW motion in S/F/S JJs.

Let us consider an S/F/S JJ via a strong ferromagnet with the exchange energy h of the order of the Fermi energy. This model is relevant for most classical ferromagnets, including Fe, Ni, Co and permalloy. It is well-known that in this case, the opposite spin pairs decay very rapidly into the depth of the ferromagnet (on the

length scale of a few nanometers), and the Josephson current is presumably carried by equal spin pairs^{8,9}. These pairs can be generated via different mechanisms, including rotation of the pair spin at magnetic inhomogeneities and spin-flip scattering at S/F interfaces¹¹. The theory of equal-spin Josephson current via homogeneous strong ferromagnets has been developed in Refs. 113 and 192. In order to describe the Josephson current in strong inhomogeneous ferromagnets and its influence on the magnetic texture, this theory has been generalized for the case of inhomogeneous magnetization in Refs. 117 and 147.

The hamiltonian of the ferromagnetic interlayer is

$$\hat{H}(t, \mathbf{r}) = -\frac{\hat{\Pi}_{\mathbf{r}}^2}{2m_F} + (\hat{\sigma}\mathbf{h}(\mathbf{r}, t)) - i(\hat{\sigma}\hat{B}\hat{\Pi}_{\mathbf{r}}), \quad (46)$$

where $\hat{\Pi}_{\mathbf{r}} = \nabla - i(e/c)\mathbf{A}(\mathbf{r})$ and \mathbf{A} is the vector potential of the electromagnetic field. The last term in Eq. (46) is the general form of a linear in momentum spin-orbit coupling (SOC) determined by the constant tensor coefficient \hat{B} .

The quasiclassical theory is formulated in terms of the spinless quasiclassical Keldysh-Green's function $\hat{g}_{\sigma}(t_1, t_2)$ ($\sigma = \pm 1$), which is defined separately at each of the Zeeman split Fermi-surfaces for spin-up and spin-down electrons and in general depends on the spatial coordinates \mathbf{r} and the two time variables $t_{1,2}$. This theory only accounts for the equal-spin Cooper pairs residing at the same Fermi surface. In contrast, the opposite spin correlations residing at different Fermi surfaces are neglected due to their strong suppression resulting from the large Zeeman splitting of the Fermi surfaces. The Usadel equation takes the form:

$$\{\hat{\tau}_3\partial_t, \hat{g}_{\sigma}\}_t - D_{\sigma}\hat{\partial}_{\mathbf{r}}(\hat{g}_{\sigma} \circ \hat{\partial}_{\mathbf{r}}\hat{g}_{\sigma}) = 0, \quad (47)$$

where D_{σ} are the spin-dependent diffusion coefficients, in the isotropic case given by $D_{\sigma} = \tau_{\sigma}v_{\sigma}^2/3$. The spin-dependent Fermi velocities $v_{\pm} = \sqrt{2(\mu \pm h)/m_F}$ are determined on each of the spin-split Fermi surfaces with m_F being the electron mass. The time dependence appears due to the dynamical character of the problem under consideration and \circ -product is defined as $(\hat{A} \circ \hat{B})(t_1, t_2) = \int_{-\infty}^{\infty} dt \hat{A}(t_1, t) \hat{B}(t, t_2)$. The commutator of the Green's function with an arbitrary operator \hat{C} is defined as $[\hat{C}, \hat{g}]_t = \hat{C}(t_1, \mathbf{r}_1)\hat{g} - \hat{g}\hat{C}(t_2, \mathbf{r}_2)$. The anti-commutator $\{\hat{C}, \hat{g}\}_t$ is defined analogously with the plus sign. $\hat{\sigma}_i$ and $\hat{\tau}_i$ are Pauli matrices in spin and Nambu spaces, respectively. and

$$\hat{\partial}_{\mathbf{r}} = \nabla - ie[\mathbf{A}\hat{\tau}_3, \cdot]_t + i\sigma[\mathbf{Z}\hat{\tau}_3, \cdot]_t. \quad (48)$$

The spin-dependent gauge field is given by the superposition of two terms $\mathbf{Z} = \mathbf{Z}^m + \mathbf{Z}^{so}$, where $Z_i^m = -i\text{Tr}(\hat{\sigma}_z\hat{U}^{\dagger}\partial_i\hat{U})/2$ is the texture-induced part. $\hat{U} = \hat{U}(\mathbf{r}, t)$ is in general the time- and space-dependent unitary 2×2 matrix that rotates the spin quantization axis \mathbf{z} to the local frame determined by the exchange field,

so that $\mathbf{h} \parallel \mathbf{z}$. The term $Z_i^{so} = m_F(\mathbf{m}\mathbf{B}_i)$ (where $\mathbf{m} = \mathbf{M}/M$) appears due to the SOC.

Eq. (47) is a spin-scalar equation but do not describe conventional spin-singlet superconducting correlations, unlike the standard spin-scalar form of the non-stationary Usadel equation. It is only applicable for strong ferromagnets and describes equal-spin triplet correlations.

In the framework of this theory the torque Eq. (45) consists of two terms

$$\mathbf{T} = \mathbf{T}_{st} + \mathbf{T}_{so}, \quad (49)$$

$$\mathbf{T}_{st} = 2\mu_B(\tilde{\mathbf{J}}^z\nabla)\mathbf{m}, \quad (50)$$

$$\mathbf{T}_{so} = 4\mu_B m_F(\mathbf{m} \times \mathbf{B}_j)\cdot\tilde{\mathbf{J}}_j^z, \quad (51)$$

where $\mathbf{m} = \mathbf{M}/M$, $\mathbf{B}_j = (B_{xj}, B_{yj}, B_{zj})$ is a vector, which is determined by j -th coordinate component of the tensor \hat{B} and $\tilde{\mathbf{J}}^z$ is the spin current in the local frame determined by the exchange field, which is represented by difference between the Josephson current carried by spin-up and spin-down pairs. In Eqs. (49)-(51) \mathbf{T}_{st} is the supercurrent spin transfer torque¹⁹³⁻¹⁹⁵. In the considered approximation it takes the form of the adiabatic torque and does not contain a non-adiabatic torque term. \mathbf{T}_{so} is the spin-orbit torque¹⁹⁶⁻¹⁹⁸. Its particular structure strongly depends on the type of the spin-orbit coupling, realized in the system.

Eqs. (49)-(51) can be viewed in terms of the supercurrent induced spin polarization. If the Josephson current flows along the x direction, the spin polarization takes the form

$$\langle \mathbf{s}_{\perp} \rangle = -\frac{2\mu_B\tilde{J}_x^z}{JM} \left[\mathbf{m} \times \partial_x \mathbf{m} + 2m_F \mathbf{m} \times (\mathbf{m} \times \mathbf{B}_x) \right] \quad (52)$$

where only perpendicular to \mathbf{m} component of the polarization is considered. The first term is the current-induced spin polarization originated from the spin texture and is analogous to the first term in Eq. (2). The second term of Eq. (2) associated with the nonadiabatic torque does not appear here because locally spin-up and spin-down pairs are not coupled in the framework of this theory and, therefore, the pair analogue of spin-flip processes, which account for this term, is not allowed. The second term represents the current-induced polarization due to the SOC.

It was shown¹⁴⁷ that the current-induced torques, Eqs. (50) and (51) allow for the DW motion in the S/F/S junction in full analogy with the case of a non-superconducting ferromagnets. In the absence of the spin-orbit torque, the DW motion driven by the adiabatic torque only occurs if the Josephson current exceeds a threshold value $\tilde{J}_x^z > \tilde{J}_x^{z, crit}$, where $\tilde{J}_x^{z, crit}$ corresponds to the electric current density $eKd_{DW}/\hbar \sim eK_{\perp}d_{DW}/\hbar$, where K and K_{\perp} are the easy- and hard-axis anisotropy constants of the considered ferromagnet, respectively, and d_{DW} is the DW width. This estimate is in full agreement with the result obtained in Ref. 199 for nonsuperconducting ferromagnetic strips

under the action of the adiabatic torque, where it has been concluded that $j^{crit} \sim K_{\perp} d_{DW}$, while in the numerical analysis of Ref. 147 only the case $K_{\perp} \sim K$ has been investigated. Taking for estimations the material parameters of CrO_2 nanowires²⁰⁰ one can obtain that $j^{crit} \sim 10^{10} - 10^{11} A/m^2$, what is one-two orders of magnitude larger than the Josephson critical current density $j_c \sim 10^9 A/m^2$, measured in such nanowires²⁰¹. Other S/F/S devices with large critical current density use usual Co and Ni ferromagnets^{202–204}, rare earth ferromagnet Ho²⁰⁵ and half-metal manganite²⁰⁶. Recently the Josephson S/F/S junction thorough the pinned domain wall in Ni was realized²⁰⁴. In principle, it should be possible to realize the supercurrent-controlled domain wall motion in such systems.

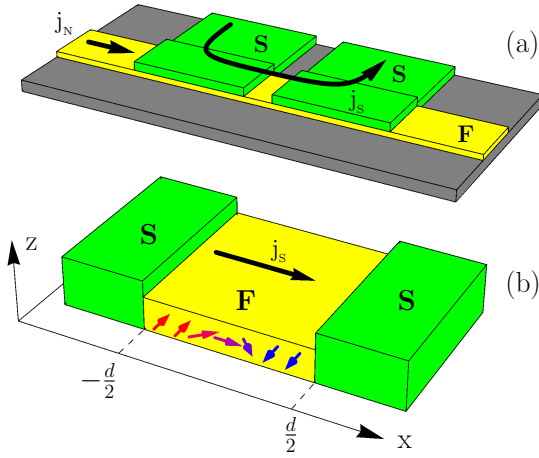


FIG. 12. (a) Sketch of the system, where the Josephson current-induced DW motion can be realized. Superconducting electrodes forming a Josephson junction are fabricated over a ferromagnetic strip. The normal current j_N flowing through the strip controls the position of the DW and can be used to move it inside the Josephson junction. (b) A simplified model of the Josephson junction region. There is a Neel-type DW in the interlayer. The Josephson supercurrent flows in the F region in x direction. Adopted from Ref. 149.

The DW motion of an unpinned DW under the action of the spin-orbit torque is possible for arbitrary small values of the applied supercurrent. For example, if we consider a Neel DW in the (x, y) -plane, see Fig. 12, and a Rashba-type spin-orbit coupling with $\mathbf{B}_x = (0, B_R, 0)$ the spin-orbit torque Eq. (51) at small applied supercurrents leads to the stationary motion of the DW with the velocity

$$v_{st} = -u \frac{\beta}{\alpha}, \quad (53)$$

where $u = 2\mu_B J_s / M$ is the characteristic velocity associated with the value of spin current $J_s = (1/2e)(J_{\uparrow} - J_{\downarrow})$ flowing through the ferromagnetic interlayer and $\beta = 2m_F B_R d_{DW}$ is the dimensionless SO coupling parameter.

C. Resistive state of the Josephson junctions in the presence of magnetization dynamics

The reciprocal effect to the torque is the appearance of a gauge spin-dependent vector potential \mathbf{Z} in the local spin basis^{174,207–213}. The gauge spin-dependent vector potential generates an anomalous phase shift. In case the magnetization depends on time, it also produces an electromotive force^{214–216}. It has been shown¹⁴⁹ that due to the presence of this electromotive force, the magnetization dynamics deprives the Josephson junctions of the nondissipative regime, i.e. they cannot support a supercurrent because of the appearance of a nonzero voltage between the leads. The voltage appears to compensate the electromotive force. This voltage that maintains the DW motion in spin-textured interlayers or precession of a homogeneous magnetization in JJs, compensating the dissipation power occurring due to Gilbert damping by the work done by a power source.

Suppose that we apply a constant electric current $I = jS$ (here S is the junction area) to the Josephson junction and consider a steady motion of the DW across the junction with a constant velocity defined by Eq. (53) under the action of the spin-orbit torque. In this case the time-averaged voltage induced at the junction can be calculated from Eq. (42) and takes the form

$$\overline{V(t)} = RS \sqrt{j^2 - j_c^2} + \frac{\pi \beta^2 u}{e \alpha d_W}, \quad (54)$$

where the first term is well-known and represents the conventional Josephson voltage appearing at $j > j_c$. The second term V_M is nonzero both at $j > j_c$ and at $j < j_c$ and leads to the fact that the Josephson junction is in the resistive state if the DW is driven by current. The corresponding IV-characteristics of the junction are shown in Fig. 13. For numerical estimates of V_M one can take $\alpha = 0.01$, $d_W = 60 nm$, $u \approx 1 m/s$, what corresponds to the maximal Josephson current density²⁰¹ through the CrO_2 nanowire $j_c \sim 10^9 A/m^2$. The dimensionless SOC constant β can vary in wide limits. Having in mind that experimentally the predictions can be realized, for example, for hybrid interlayers consisting of a ferromagnet/heavy metal bilayers, $\beta = 1 - 10$ considering that the SOC α_R ranges from 10^{-11} to $10^{-10} eV m$ at interfaces of heavy-metal systems²¹⁷. Then one can obtain $V_M|_{j=j_c}$ up to $10^{-5} - 10^{-3} V$.

The resistance of the junction at $j < j_c$ caused by the DW motion is given by

$$R_{DW} = \left(\frac{\partial V}{\partial I} \right)_{I < I_c} = \frac{\pi \gamma \beta^2 \hbar}{2e^2 S \alpha d_W M}, \quad (55)$$

It is important that according to Eq. (55) R_{DW} per unit area does not depend on the Josephson junction parameters, such as j_c and R , and is determined only by the characteristics of the magnetic subsystem. In this case, the work done by a power source is exactly equal to the energy losses in the magnetic subsystem due to the

Gilbert damping and is not spent on compensating the Joule losses in the interlayer. Indeed, at $j < j_c$ the normal current through the Josephson junction is zero despite nonzero voltage generated at the junction. It is seen directly from Eq. (42) because for $j < j_c$ it has the solution $\dot{\chi}(t) = \dot{\chi}_0(t)$. The equivalent circuit scheme of the junction is presented in the insert to Fig. 13. The voltage is compensated by the electromotive force induced in the junction by the emergent electric field $(\hbar/e)\dot{\mathbf{Z}}^{so}$.

In real setups the time of the DW motion through the junction is limited by the finite junction length: $t_{DW} \approx d/v_{st} = (\alpha/\beta)(d/u)$. Therefore, the voltage should be averaged over $t < t_{DW}$. Although experiments on the DW motion in Josephson junctions have not yet been carried out, the estimates $t_{DW} \geq 0.5(\alpha/\beta) \times 10^{-6}\text{s}$ has been obtained¹⁴⁹ for $j_c \sim 10^9\text{A/m}^2$. For other setups, which report the Josephson current carried by equal-spin triplet correlations^{202,205}, this time can be several orders of magnitude higher due to much less values of the critical current density.

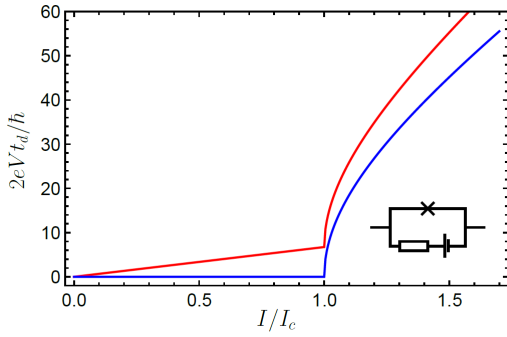


FIG. 13. IV-characteristics of the SFS junction with a DW at rest (blue) and a moving DW (red). $\beta = 1$, $\alpha = 0.1$, $eKd_W/(\pi j_c) = 5$. Data are taken from Ref. 149. Insert: the equivalent circuit scheme of the junction.

From the practical point of view, it is convenient to induce DW motion by large current pulses. For short pulses $j(t) = j\theta(t)\theta(T-t)$ with $T < t_{DW}$, the DW does not leave the junction during the impulse time. The resulting voltage signal consists of two parts of different physical origins. The first part is the conventional Josephson response with the characteristic time $t_J = 1/2eRI_c$. The other part is of purely magnetic origin and vanishes if there is no motion of the domain wall in the junction. The resulting voltage signals for $j < j_c$ are shown in Fig. 14. In this regime, the typical $V(t)$ curve consists of an initial sharp Josephson voltage impulse, a final sharp impulse of the same nature and a gradual voltage increase and decrease of purely magnetic origin, which takes the form $V(t) = -\pi\beta v(t)/ed_W$. This gradual voltage increase does not occur if the DW does not move.

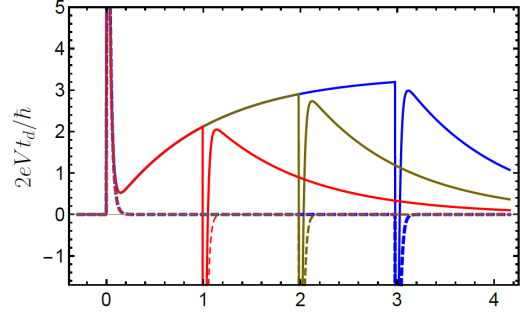


FIG. 14. $V(t)$ for rectangular current impulses. Different curves correspond to different impulse periods T ; The solid lines correspond to $\beta = 1$ (the anomalous phase due to the DW motion is nonzero) and the dashed lines are for $\beta = 0$ (the anomalous phase shift is zero). Different colors correspond to different values of a characteristic time scale t_d , where the DW velocity reaches its stationary value: (a) $j = 0.5j_c$, $T = 3t_d$ (blue), $T = 2t_d$ (yellow), $T = t_d$ (red). $\alpha = 0.1$, $eKd_W/(\pi j_c) = 5$, $t_d = 40t_J$. Data are taken from Ref. 149.

D. Electrical control of magnetization in S/F/S junctions

1. Magnetization dynamics under the applied voltage

In general, a Josephson current can induce magnetization dynamics. The coupling is described by Eq. (45) and realized via the generation of the electron spin polarization in the interlayer region, carried by triplet pairs. The pair spin should be misaligned with the ferromagnet magnetization to exert a torque on the magnetization. It can be achieved in JJs with misaligned or spin-textured ferromagnets or in the presence of the SOC.

The torque can be obtained from a direct calculation of the average electron polarization \mathbf{s}^{191} . However, there is another widely used approach for calculating the torque. Its strategy is to determine the Josephson energy of the system E_J and then find the additional contribution to the effective field $\delta\mathbf{H}_{eff}$ according to the relation $\delta\mathbf{H}_{eff} = -(1/V_F)\delta E_J/\delta\mathbf{M}$, where V_F is the ferromagnet volume^{111,148,182,183,189,190,218}. One should understand that this approach only takes into account the torque caused by the *supercurrent*. At the same time, under the applied voltage, the supercurrent via the JJ is accompanied by the normal current described by the second term in Eq. (42). The normal current also contributes to the current-induced electron polarization and, therefore, to the torque. The same thing should also be considered for problems under the applied current if the situation cannot be considered stationary, for example in the case of finite current pulses. However, for complex interlayers composed of ferromagnetic and non-ferromagnetic materials, the supercurrent and the normal current can presumably flow via the different layers. Therefore the approach based on the Josephson energy is applicable.

The example is an S/F/S JJ via a metallic ferromagnet on top of a 3D TI¹⁴⁸, where the supercurrent flows via the TI conductive surface states and the normal current flows via the ferromagnet and does not contribute to the torque.

The magnetization dynamics has been analyzed in voltage-biased JJs via single spins^{187,188}, where Josephson nutations were predicted. In addition, a possibility of obtaining supercurrent-induced magnetization switching in voltage-biased JJ, where the interlayer is composed of two misaligned ferromagnets separated by a normal spacer, has been reported¹⁹⁰. The effect is based on the generation of triplet superconducting correlations in the misaligned configuration of the ferromagnet magnetizations. The pair spin polarization of these triplet correlations is not aligned with the magnetizations of the layers exerting a torque on the free layer. The magnetization dynamics has also been considered for the interlayer with three misaligned ferromagnets, two of which are fixed in misaligned configurations²¹⁹. It has been demonstrated that the magnetic system exhibits a range of different behaviors, from simple harmonic oscillations to fractional-frequency periodic behavior and chaotic motion depending on the ratio between the Josephson frequency $\omega_J = 2eV$ and the characteristic frequency of the magnetic system.

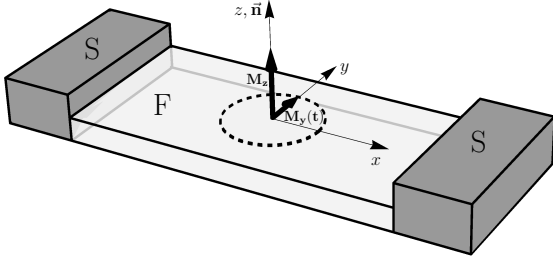


FIG. 15. Sketch of the Josephson junction via an z -easy axis ferromagnet with SOC. Redrawn after Ref. 182. The voltage-induced magnetization dynamics at $\Gamma \ll 1$ is shown.

Magnetization dynamics has also been studied in S/F/S Josephson junctions in the presence of the Rashba SOC inside the F interlayer¹⁸². The sketch of the considered setup is presented in Fig. 15. The ferromagnet has been assumed to be an easy-axis type with the easy axis along the z -direction. It was obtained that in the low-frequency regime $\hbar\omega_J \ll T_c$ the Josephson current can cause rich dynamics of the magnetization. The influence of the Josephson subsystem on the magnetic subsystem is controlled by the parameter $\Gamma = rE_J/E_M$, where E_J is the Josephson energy, E_M is the energy of the easy-axis magnetic anisotropy and $r \propto (\Delta_{so}/\varepsilon_F)d$ - is the parameter characterising the SOC strength and the magnitude of the anomalous phase shift, see Sec. II A. In the "weak coupling regime" $\Gamma \ll 1$, the magnetic moment precesses around the z -axis with the Josephson frequency ω_J . In the limit of the strong coupling $\Gamma \gg 1$, the solution of

the LLG equation yields

$$\begin{aligned} m_y &\approx 0, \\ m_x(t) &= \sin\left[\frac{\Gamma}{\omega}(1 - \cos \omega_J t)\right], \\ m_z(t) &= \cos\left[\frac{\Gamma}{\omega}(1 - \cos \omega_J t)\right], \end{aligned} \quad (56)$$

where $\omega = \omega_J/\omega_F$ is the ratio of the Josephson frequency to the ferromagnetic resonance one. It is seen that in this regime, the magnetic moment precesses around the y -axis, which is the direction of the pseudo magnetic Rashba field induced by the current. If $\Gamma/\omega > \pi/2$, the full magnetization reversal occurs in the system. For general coupling regimes, the magnetic dynamics was found to be complicated and strongly nonharmonic.

2. Electrical control of the magnetization easy axis

It has been demonstrated that in S/F/S JJs with SOC in the interlayer, the stable position of the ferromagnet easy axis can be dynamically reoriented under the applied voltage. The system in which such a feature was first studied is called the Kapitza pendulum. Particularly, in a pendulum with a vibrating point of suspension, the external sinusoidal force can invert the stability position of the pendulum²²⁰. In Ref. 221 it was predicted that the S/F/S JJ with SOC exhibits the analogous behavior: the unstable fixed point, which does not coincide with the equilibrium ferromagnet easy-axis, can become dynamically stable under the applied voltage. It was found that if the equilibrium easy axis of the magnet is the z -axis (the sketch of the considered system is shown in Fig. 15), then under the applied voltage, the new stability point is in the (z, y) -plane. The angle Θ between the stability direction and the z -axis is determined by

$$\sin \Theta = \frac{-1 + \sqrt{1 + 4\beta^2}}{2\beta}, \quad (57)$$

where $\beta = \Gamma^2 r \alpha / 2\omega(1 + \alpha^2)$. Eq. (57) determines two dynamical stability points, as it is shown in Fig. 16 instead of the equilibrium stability points $m_z = \pm 1$. The physical origin of the phenomenon is clear: in the presence of the Josephson current, the magnetic moment is influenced not only by the magnetic anisotropy field, but also by the pseudo magnetic Rashba field aligned with the y -axis. In the limit $\Gamma \gg 1$, the dynamical easy axis lies along the y -direction. The full time evolution of the y -component of the magnetization is shown in Fig. 17 for different values of the coupling between the magnetic and Josephson subsystems.

Another interesting effect related to the electrical control of the ferromagnet easy axis is the easy axis splitting in S/F/S JJs on top of the 3D TI¹⁴⁸. The qualitative difference of this system from the case of the S/F/S JJ with the SOC in the interlayer is that in 3D TI-based JJs the critical current demonstrates strong dependence

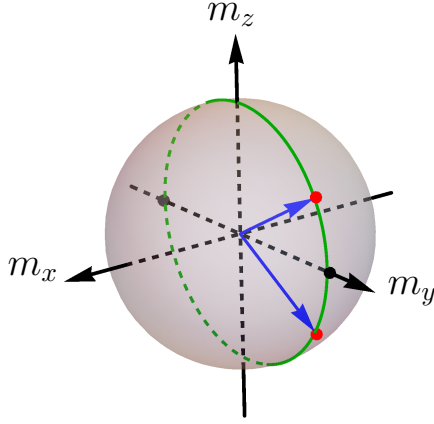


FIG. 16. Dynamical stability points (red circles) of the ferromagnet easy axis for the S/F/S JJ with the Rashba SOC in the interlayer. Redrawn after Ref. 221.

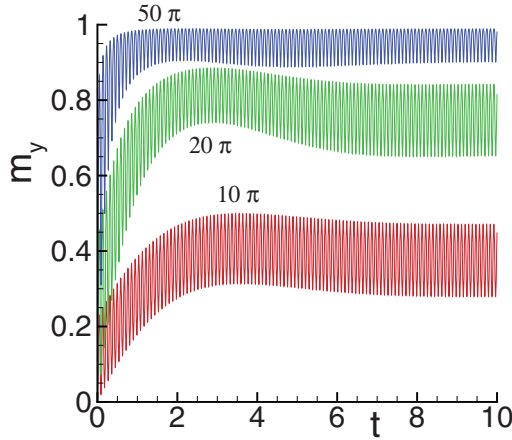


FIG. 17. Dynamical evolution of m_y for the voltage-biased S/F/S JJ with the Rashba SOC in the interlayer. Different colors represent the data corresponding to different values of the parameter Γ/r . The numerical data and picture are provided by I.Rahmonov.

on the x -component of magnetization. At the same time in S/F/S JJ with the SOC it has been considered as independent on the magnetization direction. The dependence and its physical origin were discussed in Sec. II B. The suppression of the critical current as a function of $m_x \equiv M_x/M_s$ has been discussed in Ref. 150 and is presented in Fig. 18. For estimates we take $d = 50\text{nm}$, $v_F = 10^5\text{m/s}$ and $T_c = 10\text{K}$, what corresponds to the parameters of $\text{Nb}/\text{Bi}_2\text{Te}_3/\text{Nb}$ Josephson junctions²²². In this case $\xi_N = v_F/2\pi T_c \approx 12\text{nm}$. $j_c(m_x)$ for $T_c = 1.8\text{K}$ has also been plotted, what corresponds to the Josephson junctions with *Al* leads.

Now let us assume that the ferromagnetic interlayer of the JJ has an easy axis along the y -direction. The dependence of the anomalous phase shift on m_y Eq. (19) re-

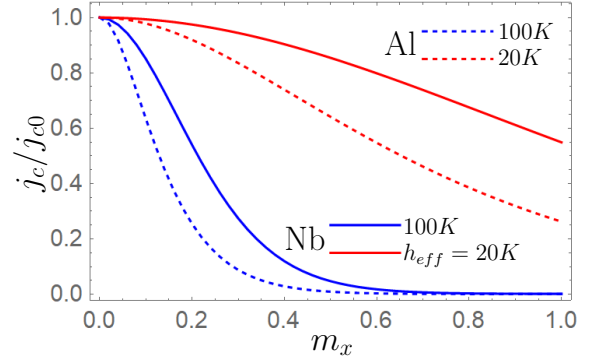


FIG. 18. Results of the numerical calculation of the critical current of the S/F/S JJ on top of the 3D TI as a function of m_x . The parameters are chosen to be relevant for a JJ with Nb superconducting leads (solid lines) and Al leads (dashed lines). The value of the effective exchange field is $h_{eff} = 20\text{K}$ for red lines. In this case, the suppression of the critical by m_x is not very strong. For comparison the blue lines represent the critical current at $h_{eff} = 100\text{K}$. It is seen that in this case it is strongly suppressed. j_c is normalized to $j_{c0} \equiv j_c(m_x = 0)$. Data are taken from Ref. 150.

sults in the additional contribution to the y -component of the effective magnetic field $\delta H_{eff,y} = -(1/V_F)\delta E_J/\delta m_y$, where $E_J = \Phi_0(j_c/2\pi)[1 - \cos(\chi - \chi_0)]$ with j_c and χ_0 determined by Eqs. (18) and (19). The effective magnetic field is added to the magnetic anisotropy field and does not cause the magnetization dynamics if the magnetization is along the easy axis. At the same time the dependence of the critical current on m_x leads to nonzero $H_{eff,x} = A m_x$ at small m_x . This means that the easy y -axis can become unstable in a voltage-driven or current-driven junction, while this axis is always stable if the critical current does not depend on magnetization direction. Moreover, there is no difference for the system between $\pm m_x$ -components of the magnetization. This leads to the fact that in the driven system an easy the axis does not reorient, keeping two stable magnetizations directions, as it was already obtained earlier, but splits. As a result, *four stable* directions of magnetization appear. This splitting effect can be realized in a range of the parameter A values, which can be achieved experimentally according to the estimates of Ref. 148.

Fig. 19 demonstrate the corresponding four stability points (red arrows). The dynamically stable easy axes are in the (x, y) -plane, therefore if the magnetization direction is parametrized as $\mathbf{m} = (\sin \Theta \cos \Phi, \cos \Theta, \sin \Theta \sin \Phi)$, the stable points correspond to $\Phi = 0, \pi$. Red circles shown them at the vector fields, which demonstrate the time evolution of the magnetization starting from an arbitrary initial magnetization position. Panel (a) corresponds to the small value of the parameter A when the easy-axis is not split yet. Panels (b)-(c) are in the parameter range where the splitting occurs, and for panel (d), the A value already exceeds the upper boundary of the range. In this case, the easy

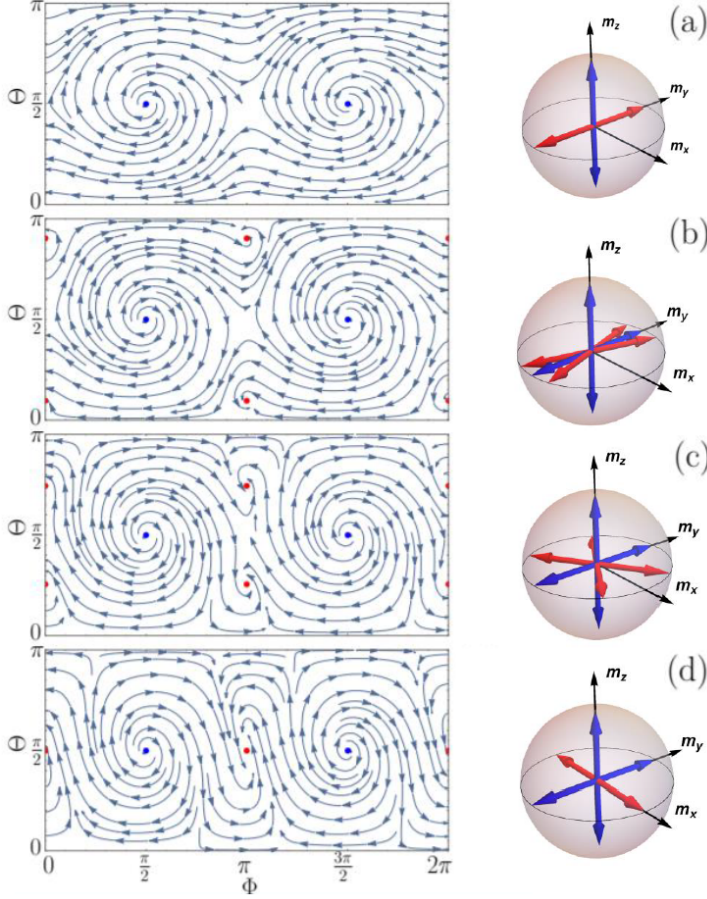


FIG. 19. Dynamical easy axis positions for the ferromagnet in the interlayer of the S/F/S JJ on top of the 3D TI are shown in the right column by the red arrows. The corresponding vector fields demonstrating the time evolution of the magnetization are represented in the left column. The stable points are shown by red circled, see text. Different panels corresponds to different values of A . Data are taken from Ref. 148.

axis is reoriented to the x -direction.

3. Magnetization reversal by electric current pulses. Cryogenic memory elements.

Another intriguing effect related to the electrical control of the magnetization in S/F/S JJs is the ferromagnet magnetization reversal by the Josephson current pulses. One of the key challenges towards developing ultra-low-power computers is the fabrication of a reliable and scalable cryogenic memory architecture. Superconductor-ferromagnet-superconductor (S-F-S) junctions are promising structures suggested for such memories^{142,143,223–233}. The magnetization reversal by the electric current pulses discussed here has also been suggested as one of the possible realizations of the JJ-

based cryogenic memory elements.

The magnetization reversal by current pulses has been originally discussed in Ref. 183 for the S/F/S Josephson junction with the Rashba SOC in the interlayer. The magnetization dynamics in the system shown in Fig. 15 has been considered in the regime of applied electric current pulses. The torque acting on the magnetization has been calculated via contribution to the effective magnetic field, produced by the supercurrent $\delta \mathbf{H}_{eff} = -(1/V_F)\delta E_J/\delta \mathbf{M}$. The possibility of the moment reversal has been demonstrated. The possibility depends strongly on the pulse amplitude and duration, as well as on the value of the SOC parameter r and the coupling strength between the magnetic and Josephson subsystems Γ . The ideas suggested in Ref. 183 have been developed in several subsequent papers. In particular, a periodicity in the appearance of intervals of the reversal of the magnetic moment under the variation of the spin-orbit coupling r , Gilbert damping parameter, and the coupling parameter Γ ²³⁴ has been predicted. An example of the corresponding periodic patterns is represented in Fig. 20. Furthermore, an analytical criterion of the most efficient reversal for the easy-axis magnet has been formulated²³⁵. The criterion allows for optimization of the pulse parameters.

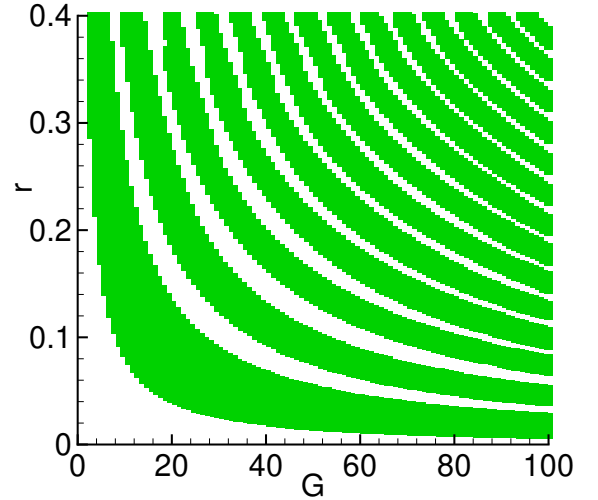


FIG. 20. Periodicity of reversal intervals in the plane (G, r) , where $G = \Gamma/r$. The numerical data and picture are provided by I.Rahmonov.

In Ref. 218 the idea to exploit the S/F/S JJ with the Rashba SOC as a cryogenic memory element has been investigated. The two memory states are encoded in the direction of the out-of-plane magnetization and the current pulses switch between them. The robustness of the current-induced magnetization reversal against thermal fluctuations has been explored^{218,236}. It has also been suggested²¹⁸ that the readout of the memory state can be nondestructively performed by direct measurement of the magnetization state through a dc SQUID inductively coupled to the junction.

The magnetization reversal by the electric current pulses has also been investigated for the 3D TI-based S/F/S JJs¹⁵¹. The advantage of this system is the very strong value of the SOC parameter r provided by the spin-momentum locking in the TI surface states, what allows to use low-current pulses for the reversal of the magnetization. The full spin-orbit torque containing the contributions both from the supercurrent and the normal current can be found in terms of the current-induced polarization of the surface states conductivity electrons Eq. (41) and takes the form

$$\mathbf{N} = \frac{J_{ex}}{d_F} \mathbf{M} \times \langle \mathbf{s} \rangle = -\frac{\gamma \hbar T I j}{e M v_F d_F} [\mathbf{m} \times \mathbf{e}_y]. \quad (58)$$

Whether there will be a reversal of the magnetic moment under the action of a given current pulse - depends strongly on the amplitude and duration of the pulse. It is illustrated by numerical data represented in Fig. 21. This diagram shows regions where the reversal occurs/does not occur in the (dt, A_s) -plane, where dt is the current pulse duration, and A_s is its amplitude. It is seen that the regions where the reversal occurs (colored) and does not occur (white) are separated by striped regions, where the behavior of the system is very difficult to predict. Therefore, the result of the operation (yes/no reversal) is very sensitive to the pulse parameters. It was reported that the widths of the uncertainty regions depend on the magnetic anisotropy of the ferromagnet. In Ref. 151 the magnetic anisotropy field in the ferromagnet was chosen as follows:

$$\mathbf{H}_{eff} = -\frac{K}{M} m_z \mathbf{e}_z + \frac{K_u}{M} m_x \mathbf{e}_x, \quad (59)$$

where K and K_u are the hard axis and the easy axis anisotropy constants, respectively. Therefore, an easy-plane anisotropy was considered in addition to the easy axis anisotropy, investigated earlier. This situation corresponds to the experimental data reported for YIG thin films²³⁷. The parameter $k = K/K_u$ can describe the ratio of the hard and easy-axis anisotropy parameters. The nonzero value of this parameter results in the appearance of the uncertainty regions in the reversal diagrams, Fig. 21. These regions grow with an increase of k and disappear at $k \rightarrow 0$.

In addition, it has been suggested in Ref. 151 to exploit the voltage induced at the junction due to the magnetization dynamics for electrical detection of the magnetization reversal. To detect the reversal $\mathbf{m} = \mathbf{e}_x \rightarrow -\mathbf{e}_x$ it is efficient to measure the transverse voltage generated between the additional leads, as it is shown in Fig. 22. This voltage is measured in the open circuit geometry when the electric current between the additional transverse electrodes is zero. In this case the solution of Eq. (42) takes the form $\dot{\chi} = \dot{\chi}_0$. Then the voltage generated between the additional electrodes due to magnetization dynamics is determined by the dynamics of m_x and can be written as follows¹⁵⁰:

$$V_t = \hbar T I_x d / e v_F. \quad (60)$$

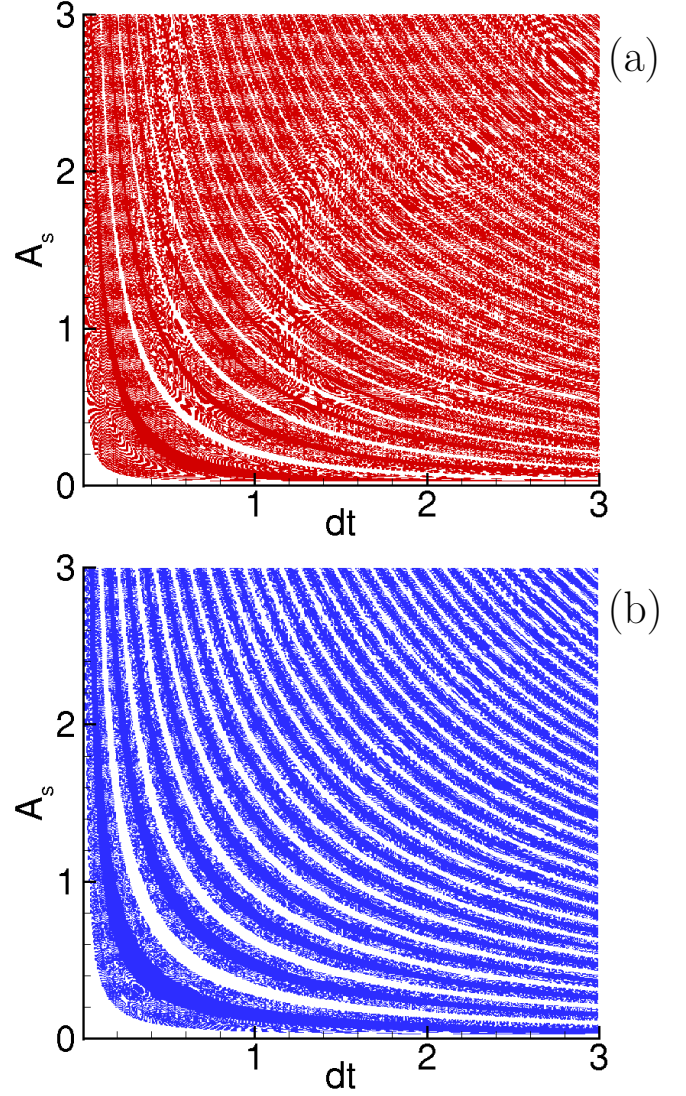


FIG. 21. Numerically calculated yes/no reversal diagram in the (dt, A_s) -plane, where dt is the current pulse duration and A_s is its amplitude, normalized to the value of the critical current at $T = 0$ and $m_x = 0$. dt is measured in units of $M/\gamma K_u$. The regions, where the reversal occurs are colored and where it does not occur are white. They are separated by the white/colored striped regions, which represent an "uncertainty" regime and discussed in the text. (a) $k = 10$, (b) $k = 1$. Data are taken from Ref. 151.

This voltage is the same both for superconducting additional electrodes and for nonsuperconducting electrodes and is only determined by the electromotive force. If the magnetization dynamics is caused by the pulse of electric current applied in the x -direction, then

$$\int V_t(t) dt = r \frac{\hbar}{e} \frac{\Delta m_x}{2}, \quad (61)$$

where Δm_x is the full change of m_x caused by the pulse. If the magnetization reversal $\mathbf{m} = \mathbf{e}_x \rightarrow -\mathbf{e}_x$ occurred,

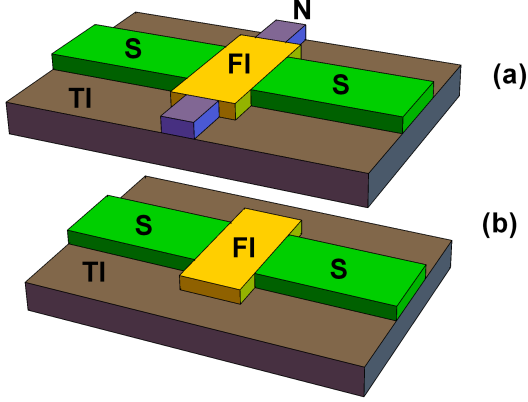


FIG. 22. (a) Sketch of the superconductor/ferromagnetic insulator/superconductor (S/FI/S) JJ on top of the 3D topological insulator (TI) with additional normal (N) electrodes, which are used for the electrical detection of $\mathbf{m} = \mathbf{e}_x \rightarrow -\mathbf{e}_x$ reversal in comparison to (b) the basic S/FI/S JJ. Taken from Ref. 151.

then $\Delta m_x = -2$, otherwise it is zero. Therefore, the integrated over time value of the voltage between the additional electrodes can be used as a criterion of the magnetization reversal.

IV. TRIPLET CORRELATIONS GENERATED BY THE MOVING CONDENSATE

Another type of magnetoelectric effect, specific for superconducting systems, is the generation of triplet $S = 1$ Cooper pairs by the condensate motion. It is well-established that the nonzero momentum of moving superconducting condensate is a pair-breaking factor. The reason is that it makes the momenta of two paired electrons to be not exactly opposite, and such a finite-momentum pairing has less binding energy. This fundamental mechanism called the orbital depairing effect exists in any superconducting system and leads to the suppression of superconductivity by the magnetic field or by the supercurrent²³⁸.

A. Triplets induced by the static Meissner currents

In Ref. 239 it has been demonstrated that in superconductor/ferromagnet hybrids with interfacial SOC controllable condensate motion can *induce* superconducting correlations. More specifically, it was predicted that the condensate motion provides effective manipulation of the odd-frequency spin-triplet pairing states²⁴⁰ which have attracted continual interest for several decades^{9,107,241–262}. It has been suggested

that this mechanism should generate equal-spin triplet Cooper pairs in currently available experimental setups with SOC^{263–270}. In the context of superconductor/ferromagnet hybrid structures these correlations are known as long-range triplets (LRT) because they can penetrate at large distances into the ferromagnetic material^{9,106,110,112,173,192,201–203,205,206,271–276}. Consequently, in S/F/S JJs the magnetic field can in fact stimulate Josephson current by generating long-range equal-spin odd-frequency triplet correlations.

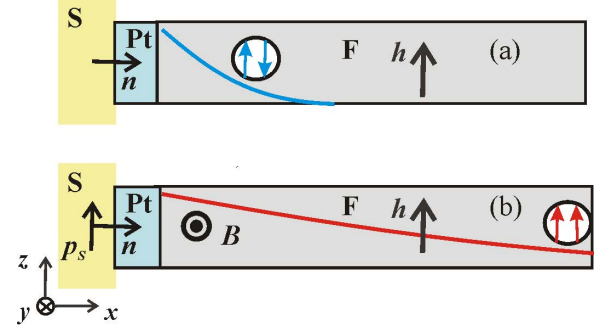


FIG. 23. Schematic picture of the simplest system, where the LRTs are generated by the moving condensate: a diffusive superconductor/ferromagnet junction with Rashba SOC at the S/F interface induced by the thin heavy metal Pt layer. (a) In the absence of the moving condensate, only short-range superconducting correlations are present. (b) The condensate motion along the exchange field direction is induced, for example, by the magnetic field through the Meissner effect. The interplay of condensate momentum \mathbf{p}_s , SOC and exchange field \mathbf{h} leads to the generation of long-range s-wave spin-triplet component. Taken from Ref. 239.

The sketch of the basic structure is shown in Fig. 23. Without the supercurrent, LRT are absent in the generic S/F structures such as shown in Fig.23(a). Here the exchange field $\mathbf{h} \parallel \mathbf{z}$ produces only short-range triplets (SRT) with $S_z = 0$, shown schematically by the blue arrows, which decay at a short length of the order $\xi_F \sim 1$ nm in usual ferromagnets. It has been demonstrated^{174,175} that, in principle, the SOC in combination with the exchange field can induce LRTs in diffusive systems. However, pure Rashba or Dresselhaus SO coupling does not induce the LRTs in a transversal geometry with an in-plane magnetization¹⁷⁴. It is this situation that is the most common experimental setup and is depicted in Fig. 23. The generation of LRT with $S_z = \pm 1$ shown schematically by red arrows in Fig.23(b) can be achieved by inducing the superconducting condensate momentum \mathbf{p}_s satisfying the condition $\mathbf{h} \times (\mathbf{n} \times \mathbf{p}_s) \neq 0$. The required condensate motion can be achieved, for example, by applying the external magnetic field along the y -direction, which causes the Meissner currents along the z -direction.

The qualitative physics of the effect can be described as follows. The general structure of anomalous function describing the pairing in a spin-triplet channel can be

parameterized as $(\hat{\sigma} \cdot \mathbf{d})$, where $\hat{\sigma}$ is the vector of Pauli matrices. The role of $\mathbf{h} \parallel \mathbf{z}$ is to generate $S_z = 0$ spin triplet correlations with $\mathbf{d}_{SRT} \propto \mathbf{h}$. The role of SOC $\hat{H}_{soc} = \alpha[\mathbf{n} \times \mathbf{p}]$ is to convert them to $S_z = \pm 1$ correlations due to the momentum-dependent spin rotation by the SOC. The resulting p -wave spin vector is $\mathbf{d}_{pw} = F_{pw}(\omega)\mathbf{h} \times (\mathbf{n} \times \mathbf{p})$ with the amplitude $F_{pw}(\omega)$ which is an even function of the Matsubara frequency ω . Such momentum-odd correlations are greatly suppressed in diffusive systems due to the efficient impurity-induced momentum averaging.

The externally induced superflow $\mathbf{p}_s \neq 0$ induces Doppler shift of the quasiparticle energy levels^{277,278} $\mathbf{v}_F \cdot \mathbf{p}_s$. It results in the suppression of pairing on one part of Fermi surface, namely for electrons with momentum $\mathbf{p} \parallel \mathbf{p}_s$. In the simplest case of homogeneous system this leads to the shift of imaginary frequencies so that the amplitude of triplet correlations is given by $F_{pw}(\omega - i\mathbf{v}_F \cdot \mathbf{p}_s) \approx F_{pw}(\omega) - i(\mathbf{v}_F \cdot \mathbf{p}_s)\partial_\omega F_{pw}$. This modification of the pairing amplitude results in the additional component of the spin vector $\delta\mathbf{d} = -i\partial_\omega F_{pw}(\mathbf{v}_F \cdot \mathbf{p}_s)\mathbf{h} \times (\mathbf{n} \times \mathbf{p})$. The s-wave component $\mathbf{d}_{sw} = \langle \delta\mathbf{d} \rangle_p$ is given by $\mathbf{d}_{sw} = (2/3i)E_F(\partial_\omega F_{pw})\mathbf{h} \times (\mathbf{n} \times \mathbf{p}_s)$.

By the order of magnitude $|\mathbf{d}_{pw}| \sim \hbar v_F \alpha / \Delta^2 \gg v_F \alpha / E_F$. Then the typical amplitude of the s-wave correlations is $|\mathbf{d}_{sw}| \sim (p_s \xi) \hbar v_F \alpha / \Delta^2$ where ξ is the coherence length. It means that the magnitude of this magnetoelectric effect can be considerably larger than that of the effects discussed before because the magnitude of the electron spin polarization and current-induced triplet correlations due to the Rashba SOC is governed by the parameter $v_F \alpha / E_F$, see Sec. IID.

Technically the triplet correlations can be calculated on the basis of the quasiclassical Usadel equation²³⁹. If the Rashba SOC is only present at the S/F interfaces, the (SOC+supercurrent)-induced SRT-LRT conversion can be described by the effective boundary condition at the S/F interface, which in the framework of the linearized with respect to the anomalous Green's function approach takes the form²³⁹:

$$n_x \nabla_x \hat{\mathbf{f}}_{LRT} = 4i\tilde{\alpha}\tilde{\tau}_3 \hat{\mathbf{f}}_{SRT} \times (\mathbf{p}_s \times \mathbf{n}) \quad (62)$$

where the surface SOC strength $\tilde{\alpha} = \int dx \alpha(x)$. The solution of the linearized Usadel equations for the LRT anomalous Green's function

$$\frac{D}{2} \nabla_x^2 \hat{\mathbf{f}}_{LRT} = |\omega| \hat{\mathbf{f}}_{LRT} \quad (63)$$

supplemented by the boundary condition (62) gives the LRT anomalous Green's function, which in the $\xi_F \ll d_F \ll \xi_N$ takes the form:

$$\hat{\mathbf{f}}_{LRT} \propto \frac{\gamma \xi_F^2 \tilde{\alpha}}{d_F \omega} \frac{\Delta}{\sqrt{\Delta^2 + \omega^2}} \mathbf{h} \times (\mathbf{n} \times \mathbf{p}_s), \quad (64)$$

where $\xi_F = \sqrt{D/\hbar}$ is the coherence length of the SRTs in the ferromagnet and γ is the S/F interface

transparency^{9,171}. The amplitude of long-range spin-triplets is proportional to the condensate momentum \mathbf{p}_s . If it is generated by the external magnetic field through the Meissner effect, then $p_s \propto B$.

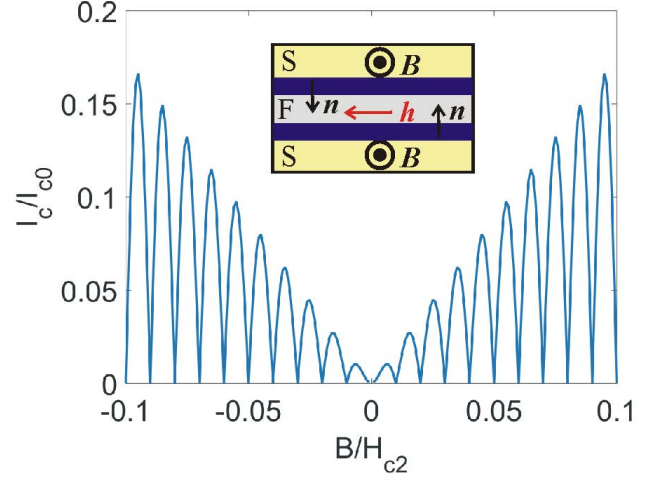


FIG. 24. Interference patterns of the critical current $I_c(\Phi)$ for the magnetic-field induced Josephson effect through the magnetic and SOC interlayers as shown in inset. The results are calculated in Ref. 239 and the figure is adopted from the same paper.

If now two S/F interfaces with Rashba SOC are combined into the S/F/S JJ, the amplitude of critical current grows as $I_c \propto B^2$ for a small external magnetic field, when the total flux through the junction area $\Phi = 2\lambda_L L B$ is small $\Phi \ll \Phi_0$. Here L is the length of the junction. For larger fields, one needs to take into account phase variation along the junction which leads to the usual factor $(L \sin \phi)/\phi$ in the critical current, where $\phi = 2\pi\Phi/\Phi_0$. It results in $I_c \propto B$ envelope dependence of the critical current shown in Fig. 24. This growth is bounded from above by the depairing effects. The $I_c(B)$ pattern in Fig. 24 drastically differs from the ones observed previously in non-ferromagnetic Josephson junctions with SOC^{121,279} and ferromagnetic ones without SOC²⁸⁰. This behaviour can be considered as the fingerprint of the LRT produced by the moving condensate in the presence of SOC.

B. Dynamic triplets induced by alternating electric fields

The moving condensate can be also induced by the alternating electric field $\mathbf{E}(t)$, which is described by the time-dependent vector potential $\mathbf{E} = -(1/c)\partial_t \mathbf{A}$. It produces an oscillating condensate motion with the momentum $\mathbf{p}_s = -(2e/c)\mathbf{A}(t)$. It has been demonstrated in Ref. 281 that in the S/F/S Josephson junction sketched in Fig. 25 with Rashba SOC at the S/F interfaces this oscillating condensate motion produces triplet correla-

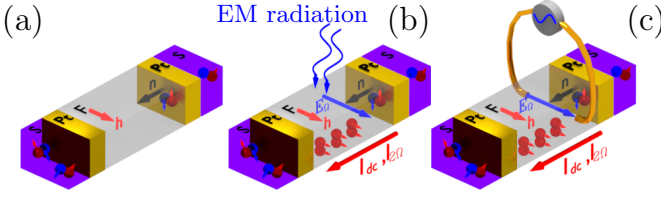


FIG. 25. S/F/S junction with Rashba SOC at the interfaces induced by the thin layer of heavy metal Pt. (a) Only short-range superconducting correlations are present shown by the blue and red spheres with opposite arrows. Therefore, if the interlayer length is of the order of several normal state coherence lengths, the Josephson current through the junction is strongly suppressed. (b,c) Generation of long-range triplet (LRT) correlations due to the irradiation of the setup with electromagnetic wave (b) and by applying the ac current source (c) both producing the electric field $\mathbf{E}(t) = \mathbf{E}_0 e^{i\Omega t}$ in the ferromagnetic interlayer. The LRT are shown schematically by the red spheres with co-directed arrows corresponding to the spin states aligned with the exchange field \mathbf{h} . They sustain the Josephson current. Adopted from Ref. 281.

tions with the energy and time-dependent spin vector constructed as follows

$$\mathbf{d}(\varepsilon, t) = \int dt' K_d(\varepsilon, t - t') (\mathbf{E}(t') \times \mathbf{n}) \times \mathbf{h}. \quad (65)$$

The scalar kernel $K_d(\varepsilon, t - t')$ is determined in the framework of a particular microscopic model.

The triplets are long-range and result in the controllable appearance of the Josephson effect in the setups shown in Fig. 25 under irradiation or by applying an ac current source. This mechanism can help to achieve switching rates in the terahertz and even the visible light frequency domains. If the applied electric field has zero time-average value, the time-average value of the dynamic triplets also vanishes. In spite of this fact, they result in nonzero dc component of the Josephson current via the JJ. For the case of a harmonic electromagnetic wave, the following current-phase relation has been obtained:

$$I(\chi, t) = [I_{dc}^c + I_{2\Omega}^c \cos(2\Omega t)] \sin \chi. \quad (66)$$

Both the dc and double-frequency critical current amplitudes are determined by the alternating electric field $I_{dc}^c \propto E_\Omega E_{-\Omega}$ and $I_{2\Omega}^c \propto E_\Omega^2$. By the order of magnitude $I_{dc}^c, I_{2\Omega}^c \sim I_0$, where

$$I_0 = -\sigma_F S (\Delta / e d_F) (2\tilde{\alpha} \gamma \xi_F / \pi)^2 (\Delta / T)^2 P / P_c \quad (67)$$

where S is the junction area, $P = c|E_\Omega|^2$ is the radiation power, $P_c = (c\hbar/e^2)\hbar\Omega^2/\xi_S^2$ is the radiation power needed to speed up the Cooper pairs to the depairing velocity. In Ref. 281 it has been estimated that $I_0/(P/P_c)^2 \sim 10^{-1} - 10^{-3}$ A for typical parameters of JJs with ferromagnetic interlayers and taking $\tilde{\alpha} \sim 0.1 - 1^{255,262,282-284}$. Assuming $\xi_S \approx 30$ one can estimate $P_c \approx 10(\Omega/GHz)^2$

W/m². Therefore such a JJ is quite sensitive to the radio-frequency and microwave irradiation. For example, a cell phone at one meter distance generates microwave radiation with $\Omega \approx 3 - 4$ GHz and $P \sim P_c$, which induces rather large currents $I_0 \sim 10^{-1} - 10^{-3}$ A. At the same time the frequency rise strongly suppresses the power sensitivity. For the frequency of the cosmic background radiation $P_c \approx 10^6$ W/m² so that the power density $P = 10^{-5}$ W/m² induces rather small critical current $I_0 \sim 10^{-12} - 10^{-15}$ A. However, even THz and visible light radiation sources can induce large critical current. For example, a THz radiation with power 1 mW/mm² yields $I_0 \sim 10^{-5} - 10^{-7}$ A. Laser beam of the frequency about $\Omega \sim 10^6$ GHz carrying the power 1 mW focused into the spot of 1 μm^2 size induces the critical current $I_0 \sim 10^{-6} - 10^{-8}$ A which is well within the measurable limits.

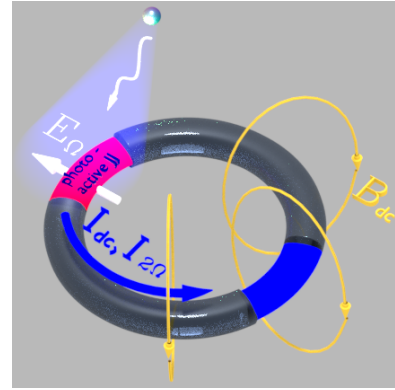


FIG. 26. Sketch of the photo-magnetic SQUID. The device consists of the photo-active Josephson junction (red weak link) and a π -JJ (blue weak link). Electric field $\mathbf{E}_0 e^{i\Omega t}$ coming from the radiation source switches on both dc I_{dc} and $I_{2\Omega} e^{2i\Omega t}$ components of the circulating current. The dc component produces spontaneous magnetic field \mathbf{B}_{dc} . Adopted from Ref. 281.

The LRT Josephson effect, induced by electromagnetic radiation, also provides an interesting possibility to create photo-magnetic devices based on the superconducting loops with the weak links formed by the radiation-controlled JJ, as it is sketched in Fig. 26. In the absence of external irradiation there are no currents in the loop. Radiation switches on the photo-active JJ. Then gradually increasing the radiation power, it has been found that the zero-current state becomes unstable under the following condition

$$I_{dc}^c > \frac{\Phi_0}{2\pi} \frac{\omega_0 \omega_p}{\sqrt{\omega_0^2 + \omega_p^2}} \quad (68)$$

where $\omega_p = \sqrt{2\pi I_\pi^c / C \Phi_0}$ is the plasma frequency corresponding to the π -JJ. Eq. (68) has been obtained under the condition $\Omega \ll \omega_0$, where $\omega_0 = 1/\sqrt{LC}$ is the eigen frequency of the superconducting loop, in order to avoid parametric effects due to the time-dependent cur-

rent amplitude of the photo-assisted JJ. In case of the typical values $\omega_p = \omega_0 \sim 10$ GHz the threshold value in the r.h.s. of Eq. (68) about 10^{-6} A. Once the condition (68) is satisfied the SQUID switches to the state with spontaneous dc current I_{dc} and constant magnetic field B_{dc} . The photo-induced magnetic flux magnitude was estimated as $\sim 10^{-2}\Phi_0$.

One can also obtain the photo-magnetic response without any threshold for the incoming power, provided the second branch of the SQUID contains the Josephson anomalous phase junction. Such photo-magnetic element generates dc current $I_{dc} \approx I_{dc}^c \cos \varphi_0$ and the corresponding magnetic field B_{dc} being exposed to any arbitrary small radiation power.

V. CONCLUSIONS

In this review, we have discussed the fundamental aspects and characteristic features of the magnetoelectric effects, which were reported in the literature on JJs. The main focus of the review is on the manifestations of the direct and inverse magnetoelectric effects in various types of Josephson systems. The coupling of the magnetization in JJs with ferromagnetic interlayers to the Josephson current via the magnetoelectric effects and perspectives of this coupling are also discussed.

To summarize, the direct magnetoelectric effect, that is, the current-induced spin polarization of the conductivity electrons, can arise in JJs via SOC materials, via topological insulators and also via spin-textured ferromagnets, which mathematically in the local spin basis can also be considered as materials with SOC. The effect is a driving force of the spin torques acting on the ferromagnet inside the JJ and, therefore, is of key importance for the electrical control of the magnetization. The inverse magnetoelectric effect in JJs takes the form of the anomalous ground state phase shift and has been re-

ported for JJs via spin-textured ferromagnets, multilayered ferromagnetic systems, homogeneous ferromagnets with SOC and combined interlayers consisting of topological insulators or materials with SOC and ferromagnets. The effect accounts for the back action of the magnetization dynamics on the Josephson subsystem, making the JJ be in the resistive state in the presence of the magnetization dynamics of any origin. Another manifestation of the magnetoelectric effects in JJs is the generation of long-range triplet pairs in S/F/S JJs by the moving condensate, which allows for controllable and low-dissipative manipulation by the critical current of the JJ.

Although by now progress has been most pronounced on the theoretical understanding of the magnetoelectric effects in JJs, the experimental activity has in the past few years started to catch up. In particular, a number of experiments confirmed the anomalous ground state phase shift in JJs via SOC materials and TIs under the applied Zeeman field. There is also a growing activity in the field of spin pumping experiments in superconducting hybrids and, in particular, JJs^{268,285,286}, where some interesting results concerning the influence of the superconducting subsystem on the ferromagnetic resonance are obtained. Nevertheless, there remains a plethora of interesting physics to investigate, and we hope that the most valuable experiments in the near future will directly verify the role of magnetoelectric effects in S/F/S JJs thus opening a way to applications in low-dissipative spintronics.

ACKNOWLEDGMENTS

The authors thank I. Rahmonov for sharing numerical data and figures. The work was supported by RSF project No. 18-72-10135. I.V.B. also acknowledges the financial support by the Foundation for the Advancement of Theoretical Physics and Mathematics “BASIS”.

-
- ¹ B.D. Josephson, “Possible new effects in superconductive tunnelling,” *Physics Letters* **1**, 251–253 (1962).
 - ² B. D. Josephson, “Coupled superconductors,” *Rev. Mod. Phys.* **36**, 216–220 (1964).
 - ³ B.D. Josephson, “Supercurrents through barriers,” *Advances in Physics* **14**, 419–451 (1965).
 - ⁴ A. A. Golubov, M. Yu. Kupriyanov, and E. Il’ichev, “The current-phase relation in josephson junctions,” *Rev. Mod. Phys.* **76**, 411–469 (2004).
 - ⁵ K. K. Likharev and V. K. Semenov, “Rsfq logic/memory family: a new josephson-junction technology for subterahertz-clock-frequency digital systems,” *IEEE Transactions on Applied Superconductivity* **1**, 3–28 (1991).
 - ⁶ Edited by H. Weinstock and Richard W. Ralston, *The New Superconducting Electronics* (Springer, Netherlands, 1993).
 - ⁷ Igor I. Soloviev, Andrey E. Schegolev, Nikolay V. Klenov, Sergey V. Bakurskiy, Mikhail Yu. Kupriyanov, Maxim V.

- Tereshonok, Anton V. Shadrin, Vasily S. Stolyarov, and Alexander A. Golubov, “Adiabatic superconducting artificial neural network: Basic cells,” *Journal of Applied Physics* **124**, 152113 (2018).
- ⁸ A. I. Buzdin, “Proximity effects in superconductor-ferromagnet heterostructures,” *Rev. Mod. Phys.* **77**, 935–976 (2005).
- ⁹ F. S. Bergeret, A. F. Volkov, and K. B. Efetov, “Odd triplet superconductivity and related phenomena in superconductor-ferromagnet structures,” *Rev. Mod. Phys.* **77**, 1321–1373 (2005).
- ¹⁰ Jacob Linder and Jason W. A. Robinson, “Superconducting spintronics,” *Nature Physics* **11**, 307–315 (2015).
- ¹¹ Matthias Eschrig, “Spin-polarized supercurrents for spintronics: a review of current progress,” *Reports on Progress in Physics* **78**, 104501 (2015).
- ¹² Sasikanth Manipatruni, Dmitri E. Nikonov, Chia-Ching Lin, Tanay A. Gosavi, Huichu Liu, Bhagwati Prasad, Yen-

- Lin Huang, Everton Bonturim, Ramamoorthy Ramesh, and Ian A. Young, "Scalable energy-efficient magnetoelectric spin-orbit logic," *Nature* **565**, 35–42 (2019).
- ¹³ T.H. O'Dell, *The electrodynamics of magneto-electric media* (North-Holland, Amsterdam, 1970).
 - ¹⁴ L.D. Landau and E.M. Lifshitz, *Electrodynamics of continuous media* (Second Revised Ed., Pergamon, Oxford, 1984).
 - ¹⁵ Manfred Fiebig, "Revival of the magnetoelectric effect," *Journal of Physics D: Applied Physics* **38**, R123–R152 (2005).
 - ¹⁶ Manfred Fiebig, Thomas Lottermoser, Dennis Meier, and Morgan Trassin, "The evolution of multiferroics," *Nature Reviews Materials* **1**, 16046 (2016).
 - ¹⁷ Nicola A. Spaldin, "Multiferroics: Past, present, and future," *MRS Bulletin* **42**, 385–390 (2017).
 - ¹⁸ M.I. Dyakonov and V.I. Perel, "Possibility of orienting electron spins with current," *JETP Letters* **13**, 467 (1971).
 - ¹⁹ M.I. Dyakonov and V.I. Perel, "Current-induced spin orientation of electrons in semiconductors," *Physics Letters A* **35**, 459 – 460 (1971).
 - ²⁰ J.-N. Chazalviel, "Spin-dependent hall effect in semiconductors," *Phys. Rev. B* **11**, 3918–3934 (1975).
 - ²¹ J. E. Hirsch, "Spin hall effect," *Phys. Rev. Lett.* **83**, 1834–1837 (1999).
 - ²² E. G. Mishchenko, A. V. Shytov, and B. I. Halperin, "Spin current and polarization in impure two-dimensional electron systems with spin-orbit coupling," *Phys. Rev. Lett.* **93**, 226602 (2004).
 - ²³ Y. K. Kato, R. C. Myers, A. C. Gossard, and D. D. Awschalom, "Current-induced spin polarization in strained semiconductors," *Phys. Rev. Lett.* **93**, 176601 (2004).
 - ²⁴ Y. K. Kato, R. C. Myers, A. C. Gossard, and D. D. Awschalom, "Observation of the spin hall effect in semiconductors," *Science* **306**, 1910–1913 (2004).
 - ²⁵ J. Wunderlich, B. Kaestner, J. Sinova, and T. Jungwirth, "Experimental observation of the spin-hall effect in a two-dimensional spin-orbit coupled semiconductor system," *Phys. Rev. Lett.* **94**, 047204 (2005).
 - ²⁶ Roberto Raimondi, Cosimo Gorini, Peter Schwab, and Michael Dzierzawa, "Quasiclassical approach to the spin hall effect in the two-dimensional electron gas," *Phys. Rev. B* **74**, 035340 (2006).
 - ²⁷ R. Raimondi, P. Schwab, C. Gorini, and G. Vignale, "Spin-orbit interaction in a two-dimensional electron gas: A su(2) formulation," *Annalen der Physik* **524** (2012), <https://doi.org/10.1002/andp.201100253>.
 - ²⁸ S. Valenzuela and M. Tinkham, "Direct electronic measurement of the spin hall effect," *Nature* **442**, 176–179 (2006).
 - ²⁹ M. Morota, Y. Niimi, K. Ohnishi, D. H. Wei, T. Tanaka, H. Kontani, T. Kimura, and Y. Otani, "Indication of intrinsic spin hall effect in 4d and 5d transition metals," *Phys. Rev. B* **83**, 174405 (2011).
 - ³⁰ Miren Isasa, Estitxu Villamor, Luis E. Hueso, Martin Gradhand, and Fèlix Casanova, "Temperature dependence of spin diffusion length and spin hall angle in au and pt," *Phys. Rev. B* **91**, 024402 (2015).
 - ³¹ A. G. Aronov and Yu. B. Lyanda-Geller, "Nuclear electric resonance and orientation of carrier spins by an electric field," *JETP Letters* **50**, 431 (1989).
 - ³² V.M. Edelstein, "Spin polarization of conduction electrons induced by electric current in two-dimensional asymmetric electron systems," *Solid State Communications* **73**, 233 – 235 (1990).
 - ³³ A. Yu. Silov, P. A. Blajnov, J. H. Wolter, R. Hey, K. H. Ploog, and N. S. Averkiev, "Current-induced spin polarization at a single heterojunction," *Applied Physics Letters* **85**, 5929–5931 (2004).
 - ³⁴ G. Dresselhaus, "Spin-orbit coupling effects in zinc blende structures," *Phys. Rev.* **100**, 580–586 (1955).
 - ³⁵ E. Rashba, "Properties of semiconductors with an extremum loop. i. cyclotron and combinational resonance in a magnetic field perpendicular to the plane of the loop," *Sov. Phys.-Solid State* **2**, 1109 (1960).
 - ³⁶ F.T. Vas'ko, "Spin splitting in the spectrum of two-dimensional electrons due to the surface potential," *P. Zh. Eksp. Teor. Fiz.* **30**, 574 (1979).
 - ³⁷ Y.A. Bychkov and E.I. Rashba, "Properties of a 2d electron gas with lifted spectral degeneracy," *P. Zh. Eksp. Teor. Fiz.* **39**, 66 (1984).
 - ³⁸ S. LaShell, B. A. McDougall, and E. Jensen, "Spin splitting of an au(111) surface state band observed with angle resolved photoelectron spectroscopy," *Phys. Rev. Lett.* **77**, 3419–3422 (1996).
 - ³⁹ A. A. Burkov and D. G. Hawthorn, "Spin and charge transport on the surface of a topological insulator," *Phys. Rev. Lett.* **105**, 066802 (2010).
 - ⁴⁰ Dimitrie Culcer, E. H. Hwang, Tudor D. Stanescu, and S. Das Sarma, "Two-dimensional surface charge transport in topological insulators," *Phys. Rev. B* **82**, 155457 (2010).
 - ⁴¹ Oleg V. Yazyev, Joel E. Moore, and Steven G. Louie, "Spin polarization and transport of surface states in the topological insulators Bi_2Se_3 and Bi_2Te_3 from first principles," *Phys. Rev. Lett.* **105**, 266806 (2010).
 - ⁴² C. H. Li, O. M. J. van 't Erve, J. T. Robinson, Y. Liu, L. Li, and B. T. Jonker, "Electrical detection of charge-current-induced spin polarization due to spin-momentum locking in Bi_2Se_3 ," *Nature Nanotech* **9**, 218 (2014).
 - ⁴³ C. H. Li, Y. Y. van 't Erve, O. M. J. Li, L. Li, and B. T. Jonker, "Electrical detection of the helical spin texture in a p-type topological insulator Sb_2Te_3 ," *Sci. Rep.* **6**, 29533 (2016).
 - ⁴⁴ Edited by Evgeny Y. Tsymbal and Igor Zutic, *Handbook of spin transport and magnetism* (CRC Press, Boca Raton, 2012).
 - ⁴⁵ Ka Shen, G. Vignale, and R. Raimondi, "Microscopic theory of the inverse edelstein effect," *Phys. Rev. Lett.* **112**, 096601 (2014).
 - ⁴⁶ S. D. Ganichev, E. L. Ivchenko, V. V. Bel'kov, S. A. Tarasenko, M. Sollinger, D. Weiss, W. Wegscheider, and W. Prettl, "Spin-galvanic effect," *Nature* **417**, 153–156 (2002).
 - ⁴⁷ J. C. Rojas Sánchez, L. Vila, G. Desfonds, S. Gambarelli, J. P. Attané, J. M. De Teresa, C. Magén, and A. Fert, "Spin-to-charge conversion using rashba coupling at the interface between non-magnetic materials," *Nature Communications* **4**, 2944 (2013).
 - ⁴⁸ J.-C. Rojas-Sánchez, S. Oyarzún, Y. Fu, A. Marty, C. Vergnaud, S. Gambarelli, L. Vila, M. Jamet, Y. Ohtsubo, A. Taleb-Ibrahimi, P. Le Fèvre, F. Bertran, N. Reyren, J.-M. George, and A. Fert, "Spin to charge conversion at room temperature by spin pumping into a new type of topological insulator: α -sn films," *Phys. Rev. Lett.* **116**, 096602 (2016).

- ⁴⁹ S. Zhang and A. Fert, “Conversion between spin and charge currents with topological insulators,” *Phys. Rev. B* **94**, 184423 (2016).
- ⁵⁰ Ady Stern, “Berry’s phase, motive forces, and mesoscopic conductivity,” *Phys. Rev. Lett.* **68**, 1022–1025 (1992).
- ⁵¹ Michael Stone, “Magnus force on skyrmions in ferromagnets and quantum hall systems,” *Phys. Rev. B* **53**, 16573–16578 (1996).
- ⁵² G.E. Volovik, *J. Phys. C* **20**, L83 (1987).
- ⁵³ L. Berger, “Possible existence of a josephson effect in ferromagnets,” *Phys. Rev. B* **33**, 1572–1578 (1986).
- ⁵⁴ S. E. Barnes and S. Maekawa, “Generalization of faraday’s law to include nonconservative spin forces,” *Phys. Rev. Lett.* **98**, 246601 (2007).
- ⁵⁵ R. A. Duine, “Spin pumping by a field-driven domain wall,” *Phys. Rev. B* **77**, 014409 (2008).
- ⁵⁶ Wayne M. Saslow, “Spin pumping of current in non-uniform conducting magnets,” *Phys. Rev. B* **76**, 184434 (2007).
- ⁵⁷ Yaroslav Tserkovnyak and Matthew Mecklenburg, “Electron transport driven by nonequilibrium magnetic textures,” *Phys. Rev. B* **77**, 134407 (2008).
- ⁵⁸ Shufeng Zhang and Steven S.-L. Zhang, “Generalization of the landau-lifshitz-gilbert equation for conducting ferromagnets,” *Phys. Rev. Lett.* **102**, 086601 (2009).
- ⁵⁹ Shengyuan A. Yang, Geoffrey S. D. Beach, Carl Knutson, Di Xiao, Qian Niu, Maxim Tsoi, and James L. Erskine, “Universal electromotive force induced by domain wall motion,” *Phys. Rev. Lett.* **102**, 067201 (2009).
- ⁶⁰ Shengyuan A. Yang, Geoffrey S. D. Beach, Carl Knutson, Di Xiao, Zhenyu Zhang, Maxim Tsoi, Qian Niu, A. H. MacDonald, and James L. Erskine, “Topological electromotive force from domain-wall dynamics in a ferromagnet,” *Phys. Rev. B* **82**, 054410 (2010).
- ⁶¹ S. E. Barnes, J. Ieda, and S. Maekawa, “Magnetic memory and current amplification devices using moving domain walls,” *Applied Physics Letters* **89**, 122507 (2006).
- ⁶² Victor M. Edelstein, “Magnetoelectric effect in polar superconductors,” *Phys. Rev. Lett.* **75**, 2004–2007 (1995).
- ⁶³ Victor M. Edelstein, “Magnetoelectric effect in dirty superconductors with broken mirror symmetry,” *Phys. Rev. B* **72**, 172501 (2005).
- ⁶⁴ Cristina Sanz-Fernández, Juan Borge, Ilya V. Tokatly, and F. Sebastián Bergeret, “Nonlocal magnetoelectric effects in diffusive conductors with spatially inhomogeneous spin-orbit coupling,” *Phys. Rev. B* **100**, 195406 (2019).
- ⁶⁵ Stefan Ilić, Ilya V. Tokatly, and F. Sebastián Bergeret, “Unified description of spin transport, weak antilocalization, and triplet superconductivity in systems with spin-orbit coupling,” *Phys. Rev. B* **102**, 235430 (2020).
- ⁶⁶ F. Sebastian Bergeret and Ilya V. Tokatly, “Manifestation of extrinsic spin hall effect in superconducting structures: Nondissipative magnetoelectric effects,” *Phys. Rev. B* **94**, 180502 (2016).
- ⁶⁷ P. Virtanen, F. S. Bergeret, and I. V. Tokatly, “Magnetoelectric effects in superconductors due to spin-orbit scattering: Nonlinear σ -model description,” *Phys. Rev. B* **104**, 064515 (2021).
- ⁶⁸ I. V. Bobkova, A. M. Bobkov, Alexander A. Zyuzin, and Mohammad Alidoust, “Magnetoelectrics in disordered topological insulator josephson junctions,” *Phys. Rev. B* **94**, 134506 (2016).
- ⁶⁹ I. V. Bobkova and A. M. Bobkov, “Electrically controllable spin filtering based on superconducting helical states,” *Phys. Rev. B* **96**, 224505 (2017).
- ⁷⁰ D. S. Rabinovich, I. V. Bobkova, A. M. Bobkov, and M. A. Silaev, “Magnetoelectric effects in superconductor/ferromagnet bilayers,” *Phys. Rev. B* **99**, 214501 (2019).
- ⁷¹ Hao Meng, A. V. Samokhvalov, and A. I. Buzdin, “Nonuniform superconductivity and josephson effect in a conical ferromagnet,” *Phys. Rev. B* **99**, 024503 (2019).
- ⁷² S. K. Yip, “Two-dimensional superconductivity with strong spin-orbit interaction,” *Phys. Rev. B* **65**, 144508 (2002).
- ⁷³ I. V. Bobkova and Yu. S. Barash, “Effects of spin-orbit interaction on superconductor-ferromagnet heterostructures: Spontaneous electric and spin surface currents,” *Journal of Experimental and Theoretical Physics Letters* **80**, 494–499 (2004).
- ⁷⁴ Sergey S. Pershoguba, Kristofer Björnson, Annica M. Black-Schaffer, and Alexander V. Balatsky, “Currents induced by magnetic impurities in superconductors with spin-orbit coupling,” *Phys. Rev. Lett.* **115**, 116602 (2015).
- ⁷⁵ A. G. Mal’shukov, “Nonlocal effect of a varying in-space zeeman field on supercurrent and helix state in a spin-orbit-coupled s -wave superconductor,” *Phys. Rev. B* **93**, 054511 (2016).
- ⁷⁶ S. Mironov and A. Buzdin, “Spontaneous currents in superconducting systems with strong spin-orbit coupling,” *Phys. Rev. Lett.* **118**, 077001 (2017).
- ⁷⁷ A. G. Mal’shukov, “Spontaneous generation of vortices by a nonuniform zeeman field in a two-dimensional rashba-coupled superconductor,” *Phys. Rev. B* **102**, 144503 (2020).
- ⁷⁸ A. G. Mal’shukov, “Supercurrent vortices and majorana zero modes induced by an in-plane zeeman field on the surface of a three-dimensional topological insulator,” *Phys. Rev. B* **101**, 134514 (2020).
- ⁷⁹ Peter Fulde and Richard A. Ferrell, “Superconductivity in a strong spin-exchange field,” *Phys. Rev.* **135**, A550–A563 (1964).
- ⁸⁰ A.I. Larkin and Yu.N. Ovchinnikov, “Nonuniform state of superconductors,” *Sov. Phys. JETP* **20**, 762 (1965).
- ⁸¹ S. Mironov, A. Mel’nikov, and A. Buzdin, “Vanishing meissner effect as a hallmark of in-plane fulde-ferrell-larkin-ovchinnikov instability in superconductor-ferromagnet layered systems,” *Phys. Rev. Lett.* **109**, 237002 (2012).
- ⁸² S. V. Mironov, D. Yu. Vodolazov, Y. Yerin, A. V. Samokhvalov, A. S. Mel’nikov, and A. Buzdin, “Temperature controlled fulde-ferrell-larkin-ovchinnikov instability in superconductor-ferromagnet hybrids,” *Phys. Rev. Lett.* **121**, 077002 (2018).
- ⁸³ V.M. Edelstein, “Characteristics of the cooper pairing in two-dimensional noncentrosymmetric electron systems,” *Sov. Phys. JETP* **68**, 1244 (1989).
- ⁸⁴ Victor Barzykin and Lev P. Gor’kov, “Inhomogeneous stripe phase revisited for surface superconductivity,” *Phys. Rev. Lett.* **89**, 227002 (2002).
- ⁸⁵ K. V. Samokhin, “Magnetic properties of superconductors with strong spin-orbit coupling,” *Phys. Rev. B* **70**, 104521 (2004).
- ⁸⁶ R. P. Kaur, D. F. Agterberg, and M. Sigrist, “Helical vortex phase in the noncentrosymmetric CePt_3Si ,” *Phys. Rev. Lett.* **94**, 137002 (2005).
- ⁸⁷ Olga Dimitrova and M. V. Feigel’man, “Theory of a two-dimensional superconductor with broken inversion sym-

- metry,” *Phys. Rev. B* **76**, 014522 (2007).
- ⁸⁸ Manuel Houzet and Julia S. Meyer, “Quasiclassical theory of disordered rashba superconductors,” *Phys. Rev. B* **92**, 014509 (2015).
 - ⁸⁹ I. V. Krive, L. Y. Gorelik, R. I. Shekhter, and M. Jonson, “Chiral symmetry breaking and the josephson current in a ballistic superconductor–quantum wire–superconductor junction,” *Low Temperature Physics* **30**, 398–404 (2004).
 - ⁹⁰ Konstantin N. Nesterov, Manuel Houzet, and Julia S. Meyer, “Anomalous josephson effect in semiconducting nanowires as a signature of the topologically nontrivial phase,” *Phys. Rev. B* **93**, 174502 (2016).
 - ⁹¹ A. A. Reynoso, Gonzalo Usaj, C. A. Balseiro, D. Feinberg, and M. Avignon, “Anomalous josephson current in junctions with spin polarizing quantum point contacts,” *Phys. Rev. Lett.* **101**, 107001 (2008).
 - ⁹² A. Buzdin, “Direct coupling between magnetism and superconducting current in the josephson φ_0 junction,” *Phys. Rev. Lett.* **101**, 107005 (2008).
 - ⁹³ A. Zazunov, R. Egger, T. Jonckheere, and T. Martin, “Anomalous josephson current through a spin-orbit coupled quantum dot,” *Phys. Rev. Lett.* **103**, 147004 (2009).
 - ⁹⁴ Aldo Brunetti, Alex Zazunov, Arijit Kundu, and Reinhold Egger, “Anomalous josephson current, incipient time-reversal symmetry breaking, and majorana bound states in interacting multilevel dots,” *Phys. Rev. B* **88**, 144515 (2013).
 - ⁹⁵ Tomohiro Yokoyama, Mikio Eto, and Yuli V. Nazarov, “Anomalous josephson effect induced by spin-orbit interaction and zeeman effect in semiconductor nanowires,” *Phys. Rev. B* **89**, 195407 (2014).
 - ⁹⁶ Bergeret, F. S. and Tokatly, I. V., “Theory of diffusive josephson junctions in the presence of spin-orbit coupling,” *EPL* **110**, 57005 (2015).
 - ⁹⁷ G. Campagnano, P. Lucignano, D. Giuliano, and A. Tagliacozzo, “Spin–orbit coupling and anomalous josephson effect in nanowires,” *Journal of Physics: Condensed Matter* **27**, 205301 (2015).
 - ⁹⁸ Fran çois Konschelle, Ilya V. Tokatly, and F. Sebastián Bergeret, “Theory of the spin-galvanic effect and the anomalous phase shift φ_0 in superconductors and josephson junctions with intrinsic spin-orbit coupling,” *Phys. Rev. B* **92**, 125443 (2015).
 - ⁹⁹ Dushko Kuzmanovski, Jacob Linder, and Annica Black-Schaffer, “Quantum ground state control in superconductor-silicene structures: $0-\pi$ transitions, φ_0 -junctions, and majorana bound states,” *Phys. Rev. B* **94**, 180505 (2016).
 - ¹⁰⁰ A. G. Mal’shukov, Severin Sadjina, and Arne Brataas, “Inverse spin hall effect in superconductor/normal-metal/superconductor josephson junctions,” *Phys. Rev. B* **81**, 060502 (2010).
 - ¹⁰¹ Yukio Tanaka, Takehito Yokoyama, and Naoto Nagaosa, “Manipulation of the majorana fermion, andreev reflection, and josephson current on topological insulators,” *Phys. Rev. Lett.* **103**, 107002 (2009).
 - ¹⁰² Jacob Linder, Yukio Tanaka, Takehito Yokoyama, Asle Sudbø, and Naoto Nagaosa, “Interplay between superconductivity and ferromagnetism on a topological insulator,” *Phys. Rev. B* **81**, 184525 (2010).
 - ¹⁰³ Fabrizio Dolcini, Manuel Houzet, and Julia S. Meyer, “Topological josephson φ_0 junctions,” *Phys. Rev. B* **92**, 035428 (2015).
 - ¹⁰⁴ Alexander Zyuzin, Mohammad Alidoust, and Daniel Loss, “Josephson junction through a disordered topological insulator with helical magnetization,” *Phys. Rev. B* **93**, 214502 (2016).
 - ¹⁰⁵ Bo Lu, Keiji Yada, A. A. Golubov, and Yukio Tanaka, “Anomalous josephson effect in d -wave superconductor junctions on a topological insulator surface,” *Phys. Rev. B* **92**, 100503 (2015).
 - ¹⁰⁶ V. Braude and Yu. V. Nazarov, “Fully developed triplet proximity effect,” *Phys. Rev. Lett.* **98**, 077003 (2007).
 - ¹⁰⁷ Yasuhiro Asano, Yuki Sawa, Yukio Tanaka, and Alexander A. Golubov, “Odd-frequency pairs and josephson current through a strong ferromagnet,” *Phys. Rev. B* **76**, 224525 (2007).
 - ¹⁰⁸ Jun-Feng Liu and K. S. Chan, “Anomalous josephson current through a ferromagnetic trilayer junction,” *Phys. Rev. B* **82**, 184533 (2010).
 - ¹⁰⁹ Mohammad Alidoust and Jacob Linder, “ φ -state and inverted fraunhofer pattern in nonaligned josephson junctions,” *Phys. Rev. B* **87**, 060503 (2013).
 - ¹¹⁰ S. Mironov and A. Buzdin, “Triplet proximity effect in superconducting heterostructures with a half-metallic layer,” *Phys. Rev. B* **92**, 184506 (2015).
 - ¹¹¹ Iryna Kulagina and Jacob Linder, “Spin supercurrent, magnetization dynamics, and φ -state in spin-textured josephson junctions,” *Phys. Rev. B* **90**, 054504 (2014).
 - ¹¹² Matthias Eschrig and Tomas Löfwander, “Triplet supercurrents in clean and disordered half-metallic ferromagnets,” *Nature Physics* **4**, 138–143 (2008).
 - ¹¹³ R. Grein, M. Eschrig, G. Metalidis, and Gerd Schön, “Spin-dependent cooper pair phase and pure spin supercurrents in strongly polarized ferromagnets,” *Phys. Rev. Lett.* **102**, 227005 (2009).
 - ¹¹⁴ Andreas Moor, Anatoly F. Volkov, and Konstantin B. Efetov, “Chirality and spin transformation of triplet cooper pairs upon interaction with singlet condensate,” *Phys. Rev. B* **92**, 214510 (2015).
 - ¹¹⁵ Andreas Moor, Anatoly F. Volkov, and Konstantin B. Efetov, “Nematic versus ferromagnetic spin filtering of triplet cooper pairs in superconducting spintronics,” *Phys. Rev. B* **92**, 180506 (2015).
 - ¹¹⁶ M. A. Silaev, I. V. Tokatly, and F. S. Bergeret, “Anomalous current in diffusive ferromagnetic josephson junctions,” *Phys. Rev. B* **95**, 184508 (2017).
 - ¹¹⁷ I. V. Bobkova, A. M. Bobkov, and M. A. Silaev, “Gauge theory of the long-range proximity effect and spontaneous currents in superconducting heterostructures with strong ferromagnets,” *Phys. Rev. B* **96**, 094506 (2017).
 - ¹¹⁸ D. S. Rabinovich, I. V. Bobkova, A. M. Bobkov, and M. A. Silaev, “Chirality selective spin interactions mediated by the moving superconducting condensate,” *Phys. Rev. B* **98**, 184511 (2018).
 - ¹¹⁹ William Mayer, Matthieu C. Dartiaillh, Joseph Yuan, Kaushini S. Wickramasinghe, Enrico Rossi, and Javad Shabani, “Gate controlled anomalous phase shift in al/inas josephson junctions,” *Nature Communications* **11**, 212 (2020).
 - ¹²⁰ D. B. Szombati, S. Nadj-Perge, D. Car, S. R. Plissard, E. P. A. M. Bakkers, and L. P. Kouwenhoven, “Josephson ϕ_0 -junction in nanowire quantum dots,” *Nature Physics* **12**, 568–572 (2016).
 - ¹²¹ Alexandre Assouline, Cheryl Feuillet-Palma, Nicolas Bergeal, Tianzhen Zhang, Alireza Mottaghizadeh, Alexandre Zimmers, Emmanuel Lhuillier, Mahmoud Ed-drie, Paola Atkinson, Marco Aprili, and Hervé Aubin,

- “Spin-orbit induced phase-shift in Bi_2Se_3 josephson junctions,” *Nature Communications* **10**, 126 (2019).
- ¹²² Anil Murani, Alik Kasumov, Shamashis Sengupta, Yu A. Kasumov, V. T. Volkov, I. I. Khodos, F. Brisset, Raphaëlle Delagrè, Alexei Chepelianskii, Richard Deblock, Hélène Bouchiat, and Sophie Guéron, “Ballistic edge states in bismuth nanowires revealed by squid interferometry,” *Nature Communications* **8**, 15941 (2017).
 - ¹²³ G. A. Bobkov, I. V. Bobkova, and A. M. Bobkov, “Long-range interaction of magnetic moments in a coupled system of superconductor-ferromagnet-superconductor josephson junctions with anomalous ground-state phase shift,” *Phys. Rev. B* **105**, 024513 (2022).
 - ¹²⁴ Yu. M. Shukrinov, “Anomalous josephson effect,” *Phys. Usp.* **accepted**, DOI: **10.3367/UFNe.2020.11.038894** (accepted, DOI: 10.3367/UFNe.2020.11.038894), 10.3367/UFNe.2020.11.038894.
 - ¹²⁵ A. G. Mal’shukov and C. S. Chu, “Spin hall effect in a josephson contact,” *Phys. Rev. B* **78**, 104503 (2008).
 - ¹²⁶ I. V. Bobkova and A. M. Bobkov, “Quasiclassical theory of magnetoelectric effects in superconducting heterostructures in the presence of spin-orbit coupling,” *Phys. Rev. B* **95**, 184518 (2017).
 - ¹²⁷ A. G. Mal’shukov, “Supercurrent generation by spin injection in an *s*-wave superconductor-rashba metal bilayer,” *Phys. Rev. B* **95**, 064517 (2017).
 - ¹²⁸ Camilla Espedal, Peter Lange, Severin Sadjina, A. G. Mal’shukov, and Arne Brataas, “Spin hall effect and spin swapping in diffusive superconductors,” *Phys. Rev. B* **95**, 054509 (2017).
 - ¹²⁹ Saburo Takahashi and Sadamichi Maekawa, “Spin current in metals and superconductors,” *Journal of the Physical Society of Japan* **77**, 031009 (2008).
 - ¹³⁰ Alexandre I. Buzdin, L. N. Bulaevskii, and S. V. Panyukov, “Critical-current oscillations as a function of the exchange field and thickness of the ferromagnetic metal (*f*) in an sfs josephson junction,” *JETP Lett.* **35**, 147 (1982).
 - ¹³¹ V. V. Ryazanov, V. A. Oboznov, A. Yu. Rusanov, A. V. Veretennikov, A. A. Golubov, and J. Aarts, “Coupling of two superconductors through a ferromagnet: Evidence for a π junction,” *Physical Review Letters* **86**, 2427 (2001).
 - ¹³² V. A. Oboznov, V. V. Bol’ginov, A. K. Feofanov, V. V. Ryazanov, and A. I. Buzdin, “Thickness dependence of the josephson ground states of superconductor-ferromagnet-superconductor junctions,” *Physical Review Letters* **96**, 197003 (2006).
 - ¹³³ J. J. A. Baselmans, A. F. Morpurgo, B. J. Van Wees, and T. M. Klapwijk, “Reversing the direction of the supercurrent in a controllable josephson junction,” *Nature* **397**, 43–45 (1999).
 - ¹³⁴ Tatiana E. Golikova, Michael J. Wolf, Detlef Beckmann, Grigory A. Penzyakov, Igor E. Batov, Irina V. Bobkova, Alexander M. Bobkov, and Valery V. Ryazanov, “Controllable supercurrent in mesoscopic superconductor-normal metal-ferromagnet crosslike josephson structures,” *Supercond. Sci. Technol.* **34**, 095001 (2021).
 - ¹³⁵ Dale J Van Harlingen, “Phase-sensitive tests of the symmetry of the pairing state in the high-temperature superconductors—evidence for $d_{x^2-y^2}$ symmetry,” *Reviews of Modern Physics* **67**, 515 (1995).
 - ¹³⁶ Hans Hilgenkamp, Henk-Jan H Smilde, Dave H. A. Blank, Guus Rijnders, Horst Rogalla, John R Kirtley, Chang C Tsuei, *et al.*, “Ordering and manipulation of the magnetic moments in large-scale superconducting π -loop arrays,” *Nature* **422**, 50–53 (2003).
 - ¹³⁷ Jorden A. Van Dam, Yuli V. Nazarov, Erik P. A. M. Bakkers, Silvano De Franceschi, and Leo P. Kouwenhoven, “Supercurrent reversal in quantum dots,” *Nature* **442**, 667–670 (2006).
 - ¹³⁸ J.-P. Cleuziou, Wolfgang Wernsdorfer, V. Bouchiat, Thierry Ondarçuhu, and Marc Monthieux, “Carbon nanotube superconducting quantum interference device,” *Nature nanotechnology* **1**, 53–59 (2006).
 - ¹³⁹ F. Vischi, M. Carrega, E. Strambini, S. D’Ambrosio, F. S. Bergeret, Yu. V. Nazarov, and F. Giazotto, “Coherent transport properties of a three-terminal hybrid superconducting interferometer,” *Physical Review B* **95**, 054504 (2017).
 - ¹⁴⁰ Esin Terzioglu and MR Beasley, “Complementary josephson junction devices and circuits: A possible new approach to superconducting electronics,” *IEEE Transactions on applied superconductivity* **8**, 48–53 (1998).
 - ¹⁴¹ A. V. Ustinov and V. K. Kaplunenko, “Rapid single-flux quantum logic using π -shifters,” *Journal of Applied Physics* **94**, 5405–5407 (2003).
 - ¹⁴² A. K. Feofanov, V. A. Oboznov, V. V. Bol’ginov, J. Lisenfeld, S. Poletto, V. V. Ryazanov, A. N. Rossolenko, M. Khabipov, D. Balashov, A. B. Zorin, P. N. Dmitriev, V. P. Koshelets, and A. V. Ustinov, “Implementation of superconductor/ferromagnet/ superconductor π -shifters in superconducting digital and quantum circuits,” *Nature Physics* **6**, 593–597 (2010).
 - ¹⁴³ E. C. Gingrich, Bethany M. Niedzielski, Joseph A. Glick, Yixing Wang, D. L. Miller, Reza Loloee, W. P. Pratt Jr, and Norman O. Birge, “Controllable $0-\pi$ josephson junctions containing a ferromagnetic spin valve,” *Nature Physics* **12**, 564–567 (2016).
 - ¹⁴⁴ I. V. Tokatly, “Usadel equation in the presence of intrinsic spin-orbit coupling: A unified theory of magnetoelectric effects in normal and superconducting systems,” *Physical Review B* **96**, 060502 (2017).
 - ¹⁴⁵ Chunli Huang, Ilya V. Tokatly, and F. Sebastian Bergeret, “Extrinsic spin-charge coupling in diffusive superconducting systems,” *Physical Review B* **98**, 144515 (2018).
 - ¹⁴⁶ I. V. Bobkova, A. M. Bobkov, and M. A. Silaev, “Gauge theory of the long-range proximity effect and spontaneous currents in superconducting heterostructures with strong ferromagnets,” *Phys. Rev. B* **96**, 094506 (2017).
 - ¹⁴⁷ I. V. Bobkova, A. M. Bobkov, and M. A. Silaev, “Spin torques and magnetic texture dynamics driven by the supercurrent in superconductor/ferromagnet structures,” *Phys. Rev. B* **98**, 014521 (2018).
 - ¹⁴⁸ M. Nashaat, I. V. Bobkova, A. M. Bobkov, Yu. M. Shukrinov, I. R. Rahmonov, and K. Sengupta, “Electrical control of magnetization in superconductor/ferromagnet/superconductor junctions on a three-dimensional topological insulator,” *Phys. Rev. B* **100**, 054506 (2019).
 - ¹⁴⁹ D. S. Rabinovich, I. V. Bobkova, A. M. Bobkov, and M. A. Silaev, “Resistive state of superconductor-ferromagnet-superconductor josephson junctions in the presence of moving domain walls,” *Phys. Rev. Lett.* **123**, 207001 (2019).
 - ¹⁵⁰ D. S. Rabinovich, I. V. Bobkova, and A. M. Bobkov, “Electrical response of superconductor/ferromagnet/topological-

- insulator/superconductor junctions to magnetic texture dynamics,” *Phys. Rev. B* **101**, 054517 (2020).
- ¹⁵¹ I. V. Bobkova, A. M. Bobkov, I. R. Rahmonov, A. A. Mazanik, K. Sengupta, and Yu. M. Shukrinov, “Magnetization reversal in superconductor/insulating ferromagnet/superconductor josephson junctions on a three-dimensional topological insulator,” *Phys. Rev. B* **102**, 134505 (2020).
 - ¹⁵² Hao Meng, Yajie Ren, Javier E. Villegas, and A. I. Buzdin, “Josephson current through a ferromagnetic bilayer: Beyond the quasiclassical approximation,” *Physical Review B* **100**, 224514 (2019).
 - ¹⁵³ Elia Strambini, Andrea Iorio, Ofelia Durante, Roberta Citro, Cristina Sanz-Fernández, Claudio Guarcello, Ilya V Tokatly, Alessandro Braggio, Mirko Rocci, Nadia Ligato, *et al.*, “A josephson phase battery,” *Nature Nanotechnology* **15**, 656–660 (2020).
 - ¹⁵⁴ Zilong Jiang, Ferhat Katmis, Chi Tang, Peng Wei, Jagadeesh S. Moodera, and Jing Shi, “A comparative transport study of Bi_2Se_3 and Bi_2Se_3 /yttrium iron garnet,” *Applied Physics Letters* **104**, 222409 (2014).
 - ¹⁵⁵ Peng Wei, Ferhat Katmis, Badih A. Assaf, Hadar Steinberg, Pablo Jarillo-Herrero, Donald Heiman, and Jagadeesh S. Moodera, “Exchange-coupling-induced symmetry breaking in topological insulators,” *Phys. Rev. Lett.* **110**, 186807 (2013).
 - ¹⁵⁶ Zilong Jiang, Cui-Zu Chang, Chi Tang, Peng Wei, Jagadeesh S. Moodera, and Jing Shi, “Independent tuning of electronic properties and induced ferromagnetism in topological insulators with heterostructure approach,” *Nano Letters* **15**, 5835–5840 (2015), pMID: 26288309.
 - ¹⁵⁷ Zilong Jiang, Cui-Zu Chang, Chi Tang, Jian-Guo Zheng, Jagadeesh S. Moodera, and Jing Shi, “Structural and proximity-induced ferromagnetic properties of topological insulator-magnetic insulator heterostructures,” *AIP Advances* **6**, 055809 (2016).
 - ¹⁵⁸ Henning G. Hugdal, Jacob Linder, and Sol H. Jacobsen, “Quasiclassical theory for the superconducting proximity effect in dirac materials,” *Phys. Rev. B* **95**, 235403 (2017).
 - ¹⁵⁹ A. G. Mal’shukov, “Long-range effect of a zeeman field on the electric current through the helical metal-superconductor interface in an andreev interferometer,” *Phys. Rev. B* **97**, 064515 (2018).
 - ¹⁶⁰ A. G. Mal’shukov, “Fraunhofer oscillations of the critical current at a varying zeeman field in a spin-orbit coupled josephson junction,” *Phys. Rev. B* **102**, 134509 (2020).
 - ¹⁶¹ Gen Tatara, “Effective gauge field theory of spintronics,” *Physica E: Low-dimensional Systems and Nanostructures* **106**, 208–238 (2019).
 - ¹⁶² I. Margaritis, V. Paltoglou, and N. Flytzanis, “Zero phase difference supercurrent in ferromagnetic josephson junctions,” *Journal of Physics: Condensed Matter* **22**, 445701 (2010).
 - ¹⁶³ M. A. Silaev, “ θ_0 thermal josephson junction,” *Physical Review B* **96**, 064519 (2017).
 - ¹⁶⁴ Yu Liu, Saulius Vaitiekėnas, Sara Martí-Sánchez, Christian Koch, Sean Hart, Zheng Cui, Thomas Kanne, Sabir A Khan, Rawa Tanta, Shivendra Upadhyay, *et al.*, “Semiconductor–ferromagnetic insulator–superconductor nanowires: stray field and exchange field,” *Nano letters* **20**, 456–462 (2019).
 - ¹⁶⁵ S. Vaitiekėnas, Y. Liu, P. Krogstrup, and C. M. Marcus, “Zero-bias peaks at zero magnetic field in ferromagnetic hybrid nanowires,” *Nature Physics* **17**, 43–47 (2021).
 - ¹⁶⁶ E. Strambini, V. N. Golovach, G. De Simoni, J. S. Moodera, F. S. Bergeret, and F. Giazotto, “Revealing the magnetic proximity effect in eus/al bilayers through superconducting tunneling spectroscopy,” *Physical Review Materials* **1**, 054402 (2017).
 - ¹⁶⁷ Mikel Rouco, Subrata Chakraborty, Faluke Aikebaier, Vitaly N Golovach, Elia Strambini, Jagadeesh S Moodera, Francesco Giazotto, Tero T Heikkilä, and F Sebastian Bergeret, “Charge transport through spin-polarized tunnel junction between two spin-split superconductors,” *Physical Review B* **100**, 184501 (2019).
 - ¹⁶⁸ Tero T Heikkilä, Mikhail Silaev, Pauli Virtanen, and F Sebastian Bergeret, “Thermal, electric and spin transport in superconductor/ferromagnetic-insulator structures,” *Progress in Surface Science* **94**, 100540 (2019).
 - ¹⁶⁹ T. Tokuyasu, J. A. Sauls, and D. Rainer, “Proximity effect of a ferromagnetic insulator in contact with a superconductor,” *Phys. Rev. B* **38**, 8823–8833 (1988).
 - ¹⁷⁰ A. Millis, D. Rainer, and J. A. Sauls, “Quasiclassical theory of superconductivity near magnetically active interfaces,” *Phys. Rev. B* **38**, 4504 (1988).
 - ¹⁷¹ M. Yu. Kuprianov and V.F. Lukichev, “Influence of boundary transparency on the critical current of dirty SS’S structures,” *Sov. Phys. JETP* **67**, 1163 (1988).
 - ¹⁷² F. S. Bergeret, Alvise Verso, and Anatoly F. Volkov, “Electronic transport through ferromagnetic and superconducting junctions with spin-filter tunneling barriers,” *Phys. Rev. B* **86**, 214516 (2012).
 - ¹⁷³ F. S. Bergeret, A. F. Volkov, and K. B. Efetov, “Long-range proximity effects in superconductor-ferromagnet structures,” *Phys. Rev. Lett.* **86**, 4096–4099 (2001).
 - ¹⁷⁴ F. S. Bergeret and I. V. Tokatly, “Singlet-triplet conversion and the long-range proximity effect in superconductor-ferromagnet structures with generic spin dependent fields,” *Phys. Rev. Lett.* **110**, 117003 (2013).
 - ¹⁷⁵ F. S. Bergeret and I. V. Tokatly, “Spin-orbit coupling as a source of long-range triplet proximity effect in superconductor-ferromagnet hybrid structures,” *Phys. Rev. B* **89**, 134517 (2014).
 - ¹⁷⁶ Lev P. Gor’kov and Emmanuel I. Rashba, “Superconducting 2d system with lifted spin degeneracy: Mixed singlet-triplet state,” *Phys. Rev. Lett.* **87**, 037004 (2001).
 - ¹⁷⁷ Gert Eilenberger, “Transformation of gorkov’s equation for type ii superconductors into transport-like equations,” *Zeitschrift für Physik A Hadrons and nuclei* **214**, 195–213 (1968).
 - ¹⁷⁸ Christopher R. Reeg and Dmitrii L. Maslov, “Proximity-induced triplet superconductivity in rashba materials,” *Phys. Rev. B* **92**, 134512 (2015).
 - ¹⁷⁹ D. F. Agterberg and R. P. Kaur, “Magnetic-field-induced helical and stripe phases in rashba superconductors,” *Phys. Rev. B* **75**, 064511 (2007).
 - ¹⁸⁰ A. G. Mal’shukov and C. S. Chu, “Spin-hall current and spin polarization in an electrically biased sns josephson junction,” *Phys. Rev. B* **84**, 054520 (2011).
 - ¹⁸¹ Y. Shiomi, K. Nomura, Y. Kajiwar, K. Eto, M. Novak, Kouji Segawa, Yoichi Ando, and E. Saitoh, “Spin-electricity conversion induced by spin injection into topological insulators,” *Phys. Rev. Lett.* **113**, 196601 (2014).
 - ¹⁸² F. Konschelle and A. Buzdin, “Magnetic moment manipulation by a josephson current,” *Phys. Rev. Lett.* **102**, 017001 (2009).
 - ¹⁸³ Yu. M. Shukrinov, I. R. Rahmonov, K. Sengupta, and A. Buzdin, “Magnetization reversal by superconducting

- current in φ josephson junctions,” *Applied Physics Letters* **110**, 182407 (2017).
- ¹⁸⁴ T. Schulz, R. Ritz, A. Bauer, M. Halder, M. Wagner, C. Franz, C. Pfleiderer, K. Everschor, M. Garst, and A. Rosch, “Emergent electrodynamics of skyrmions in a chiral magnet,” *Nature Physics* **8**, 301–304 (2012).
- ¹⁸⁵ Naoto Nagaosa and Yoshinori Tokura, “Topological properties and dynamics of magnetic skyrmions,” *Nature Nanotechnology* **8**, 899–911 (2013).
- ¹⁸⁶ C. Holmqvist, W. Belzig, and M. Fogelström, “Nonequilibrium charge and spin transport in superconducting-ferromagnetic-superconducting point contacts,” *Philosophical Transactions of the Royal Society A: Mathematical, Physical and Engineering Sciences* **376**, 20150229 (2018).
- ¹⁸⁷ Zohar Nussinov, Alexander Shnirman, Daniel P. Arovas, Alexander V. Balatsky, and Jian Xin Zhu, “Spin and spin-wave dynamics in josephson junctions,” *Phys. Rev. B* **71**, 214520 (2005).
- ¹⁸⁸ Jian-Xin Zhu, Z. Nussinov, A. Shnirman, and A. V. Balatsky, “Novel spin dynamics in a josephson junction,” *Phys. Rev. Lett.* **92**, 107001 (2004).
- ¹⁸⁹ Xavier Waintal and Piet W. Brouwer, “Magnetic exchange interaction induced by a josephson current,” *Phys. Rev. B* **65**, 054407 (2002).
- ¹⁹⁰ Jacob Linder and Takehito Yokoyama, “Supercurrent-induced magnetization dynamics in a josephson junction with two misaligned ferromagnetic layers,” *Phys. Rev. B* **83**, 012501 (2011).
- ¹⁹¹ Klaus Halterman and Mohammad Alidoust, “Josephson currents and spin-transfer torques in ballistic SFSFS nanojunctions,” *Superconductor Science and Technology* **29**, 055007 (2016).
- ¹⁹² M. Eschrig, J. Kopu, J. C. Cuevas, and Gerd Schön, “Theory of half-metal/superconductor heterostructures,” *Phys. Rev. Lett.* **90**, 137003 (2003).
- ¹⁹³ L. Berger, “Emission of spin waves by a magnetic multilayer traversed by a current,” *Phys. Rev. B* **54**, 9353–9358 (1996).
- ¹⁹⁴ J.C. Slonczewski, “Current-driven excitation of magnetic multilayers,” *Journal of Magnetism and Magnetic Materials* **159**, L1–L7 (1996).
- ¹⁹⁵ D.C. Ralph and M.D. Stiles, “Spin transfer torques,” *Journal of Magnetism and Magnetic Materials* **320**, 1190–1216 (2008).
- ¹⁹⁶ Ioan Mihai Miron, Gilles Gaudin, Stéphane Auffret, Bernard Rodmacq, Alain Schuhl, Stefania Pizzini, Jan Vogel, and Pietro Gambardella, “Current-driven spin torque induced by the rashba effect in a ferromagnetic metal layer,” *Nature Materials* **9**, 230–234 (2010).
- ¹⁹⁷ Pietro Gambardella and Ioan Mihai Miron, “Current-induced spin-orbit torques,” *Philosophical Transactions of the Royal Society A: Mathematical, Physical and Engineering Sciences* **369**, 3175–3197 (2011).
- ¹⁹⁸ A. Manchon and S. Zhang, “Theory of nonequilibrium intrinsic spin torque in a single nanomagnet,” *Phys. Rev. B* **78**, 212405 (2008).
- ¹⁹⁹ Gen Tatara and Hiroshi Kohno, “Theory of current-driven domain wall motion: Spin transfer versus momentum transfer,” *Phys. Rev. Lett.* **92**, 086601 (2004).
- ²⁰⁰ Xiaojing Zou and Gang Xiao, “Magnetic domain configurations of epitaxial chromium dioxide (cro₂) nanostructures,” *Applied Physics Letters* **91**, 113512 (2007).
- ²⁰¹ Amrita Singh, Charlotte Jansen, Kaveh Lahabi, and Jan Aarts, “High-quality cro₂ nanowires for dissipation-less spintronics,” *Phys. Rev. X* **6**, 041012 (2016).
- ²⁰² Trupti S. Khaire, Mazin A. Khasawneh, W. P. Pratt, and Norman O. Birge, “Observation of spin-triplet superconductivity in co-based josephson junctions,” *Phys. Rev. Lett.* **104**, 137002 (2010).
- ²⁰³ J. W. A. Robinson, Gábor B. Halász, A. I. Buzdin, and M. G. Blamire, “Enhanced supercurrents in josephson junctions containing nonparallel ferromagnetic domains,” *Phys. Rev. Lett.* **104**, 207001 (2010).
- ²⁰⁴ Ekta Bhatia, Anand Srivastava, James Devine-Stoneman, Nadia A Stelmashenko, Zoe H Barber, Jason WA Robinson, and Kartik Senapati, “Nanoscale domain wall engineered spin-triplet josephson junctions and squid,” *Nano Letters* **21**, 3092–3097 (2021).
- ²⁰⁵ J. W. A. Robinson, J. D. S. Witt, and M. G. Blamire, “Controlled injection of spin-triplet supercurrents into a strong ferromagnet,” *Science* **329**, 59–61 (2010).
- ²⁰⁶ A. Srivastava, L. A. B. Olde Olthof, A. Di Bernardo, S. Komori, M. Amado, C. Palomares-Garcia, M. Alidoust, K. Halterman, M. G. Blamire, and J. W. A. Robinson, “Magnetization control and transfer of spin-polarized cooper pairs into a half-metal manganite,” *Phys. Rev. Applied* **8**, 044008 (2017).
- ²⁰⁷ Jürg Fröhlich and Urban M. Studer, “Gauge invariance and current algebra in nonrelativistic many-body theory,” *Rev. Mod. Phys.* **65**, 733–802 (1993).
- ²⁰⁸ A. Rebei and O. Heinonen, “Spin currents in the rashba model in the presence of nonuniform fields,” *Phys. Rev. B* **73**, 153306 (2006).
- ²⁰⁹ Pei-Qing Jin and You-Quan Li, “Generalized kubo formula for spin transport: A theory of linear response to non-abelian fields,” *Phys. Rev. B* **74**, 085315 (2006).
- ²¹⁰ B. Andrei Bernevig, J. Orenstein, and Shou-Cheng Zhang, “Exact su(2) symmetry and persistent spin helix in a spin-orbit coupled system,” *Phys. Rev. Lett.* **97**, 236601 (2006).
- ²¹¹ Naomichi Hatano, Ryōen Shirasaki, and Hiroaki Nakamura, “Non-abelian gauge field theory of the spin-orbit interaction and a perfect spin filter,” *Phys. Rev. A* **75**, 032107 (2007).
- ²¹² B.W.A. Leurs, Z. Nazario, D.I. Santiago, and J. Zaanen, “Non-abelian hydrodynamics and the flow of spin in spin-orbit coupled substances,” *Annals of Physics* **323**, 907–945 (2008).
- ²¹³ I. V. Tokatly, “Equilibrium spin currents: Non-abelian gauge invariance and color diamagnetism in condensed matter,” *Phys. Rev. Lett.* **101**, 106601 (2008).
- ²¹⁴ Kyoung-Whan Kim, Jung-Hwan Moon, Kyung-Jin Lee, and Hyun-Woo Lee, “Prediction of giant spin motive force due to rashba spin-orbit coupling,” *Phys. Rev. Lett.* **108**, 217202 (2012).
- ²¹⁵ Gen Tatara, Noriyuki Nakabayashi, and Kyung-Jin Lee, “Spin motive force induced by rashba interaction in the strong *sd* coupling regime,” *Phys. Rev. B* **87**, 054403 (2013).
- ²¹⁶ Yuta Yamane, Jun’ichi Ieda, and Sadamichi Maekawa, “Spinmotive force with static and uniform magnetization induced by a time-varying electric field,” *Phys. Rev. B* **88**, 014430 (2013).
- ²¹⁷ Christian R. Ast, Jürgen Henk, Arthur Ernst, Luca Moreschini, Mihaela C. Falub, Daniela Pacilé, Patrick Bruno, Klaus Kern, and Marco Grioni, “Giant spin splitting through surface alloying,” *Phys. Rev. Lett.* **98**,

- 186807 (2007).
- 218 C. Guarcello and F.S. Bergeret, “Cryogenic memory element based on an anomalous josephson junction,” *Phys. Rev. Applied* **13**, 034012 (2020).
 - 219 V. Braude and Ya. M. Blanter, “Triplet josephson effect with magnetic feedback in a superconductor-ferromagnet heterostructure,” *Phys. Rev. Lett.* **100**, 207001 (2008).
 - 220 P.L. Kapitza, “Dynamic stability of the pendulum with vibrating suspension point,” *Sov. Phys. JETP* **21**, 588 (1951).
 - 221 Yu. M. Shukrinov, A. Mazanik, I. R. Rahmonov, A. E. Botha, and A. Buzdin, “Re-orientation of the easy axis in φ_0 -junction,” *EPL (Europhysics Letters)* **122**, 37001 (2018).
 - 222 M. Veldhorst, M. Snelder, M. Hoek, T. Gang, V. K. Guduru, X. L. Wang, U. Zeitler, W. G. van der Wiel, A. A. Golubov, H. Hilgenkamp, and A. Brinkman, “Josephson supercurrent through a topological insulator surface state,” *Nature Materials* **11**, 417–421 (2012).
 - 223 Valery V. Ryazanov, Vitaly V. Bol’ginov, Danila S. Sobanin, Igor V. Vernik, Sergey K. Tolpygo, Alan M. Kadin, and Oleg A. Mukhanov, “Magnetic josephson junction technology for digital and memory applications,” *Physics Procedia* **36**, 35–41 (2012), superconductivity centennial conference 2011.
 - 224 Burm Baek, William H. Rippard, Samuel P. Benz, Stephen E. Russek, and Paul D. Dresselhaus, “Hybrid superconducting-magnetic memory device using competing order parameters,” *Nature Communications* **5**, 3888 (2014).
 - 225 T. Golod, A. Iovan, and V. M. Krasnov, “Single abrikosov vortices as quantized information bits,” *Nature Communications* **6**, 8628 (2015).
 - 226 Bethany M. Niedzielski, T. J. Bertus, Joseph A. Glick, R. Loloee, W. P. Pratt, and Norman O. Birge, “Spin-valve josephson junctions for cryogenic memory,” *Phys. Rev. B* **97**, 024517 (2018).
 - 227 I. M. Dayton, T. Sage, E. C. Gingrich, M. G. Loving, T. F. Ambrose, N. P. Siwak, S. Keebaugh, C. Kirby, D. L. Miller, A. Y. Herr, Q. P. Herr, and O. Naaman, “Experimental demonstration of a josephson magnetic memory cell with a programmable π -junction,” *IEEE Magnetics Letters* **9**, 1–5 (2018).
 - 228 Giorgio De Simoni, Elia Strambini, Jagadeesh S. Moodera, F. Sebastian Bergeret, and Francesco Giazotto, “Toward the absolute spin-valve effect in superconducting tunnel junctions,” *Nano Letters* **18**, 6369–6374 (2018).
 - 229 R. de Andrés Prada, T. Golod, O. M. Kapran, E. A. Borodianskyi, Ch. Bernhard, and V. M. Krasnov, “Memory-functionality superconductor/ferromagnet/superconductor junctions based on the high- T_c cuprate superconductors $\text{YBa}_2\text{Cu}_3\text{O}_{7-x}$ and the colossal magnetoresistive manganite ferromagnets $\text{La}_{2/3}\text{X}_{1/3}\text{MnO}_{3+\delta}$ ($\text{X} = \text{Ca}, \text{Sr}$),” *Phys. Rev. B* **99**, 214510 (2019).
 - 230 V. V. Bol’ginov, V. S. Stolyarov, D. S. Sobanin, A. L. Karpovich, and V. V. Ryazanov, “Magnetic switches based on nb-pdfe-nb josephson junctions with a magnetically soft ferromagnetic interlayer,” *JETP Letters* **95**, 366–371 (2012).
 - 231 Timofei I. Larkin, Vitaly V. Bol’ginov, Vasily S. Stolyarov, Valery V. Ryazanov, Igor V. Vernik, Sergey K. Tolpygo, and Oleg A. Mukhanov, “Ferromagnetic josephson switching device with high characteristic voltage,” *Applied Physics Letters* **100**, 222601 (2012).
 - 232 S. V. Bakurskiy, N. V. Klenov, I. I. Soloviev, V. V. Bol’ginov, V. V. Ryazanov, I. V. Vernik, O. A. Mukhanov, M. Yu. Kupriyanov, and A. A. Golubov, “Theoretical model of superconducting spintronic sisfs devices,” *Applied Physics Letters* **102**, 192603 (2013).
 - 233 S. V. Bakurskiy, N. V. Klenov, I. I. Soloviev, N. G. Pugach, M. Yu. Kupriyanov, and A. A. Golubov, “Protected $0-\pi$ states in sisfs junctions for josephson memory and logic,” *Applied Physics Letters* **113**, 082602 (2018).
 - 234 P. Kh Atanasova, S. A. Panayotova, I. R. Rahmonov, Yu. M. Shukrinov, E. V. Zemlyanaya, and M. V. Bashashin, “Periodicity in the appearance of intervals of the reversal of the magnetic moment of a φ_0 josephson junction,” *JETP Letters* **110**, 722–726 (2019).
 - 235 A.A. Mazanik, I.R. Rahmonov, A.E. Botha, and Yu.M. Shukrinov, “Analytical criteria for magnetization reversal in a φ_0 josephson junction,” *Phys. Rev. Applied* **14**, 014003 (2020).
 - 236 C. Guarcello and F.S. Bergeret, “Thermal noise effects on the magnetization switching of a ferromagnetic anomalous josephson junction,” *Chaos, Solitons, Fractals* **142**, 110384 (2021).
 - 237 J. Mendil, M. Trassin, Q. Bu, J. Schaab, M. Baumgartner, C. Murer, P. T. Dao, J. Vijayakumar, D. Bracher, C. Bouillet, C. A. F. Vaz, M. Fiebig, and P. Gambardella, “Magnetic properties and domain structure of ultrathin yttrium iron garnet/Pt bilayers,” *Phys. Rev. Materials* **3**, 034403 (2019).
 - 238 Michael Tinkham, *Introduction to superconductivity* (Courier Corporation, 1996).
 - 239 M. A. Silaev, I. V. Bobkova, and A. M. Bobkov, “Odd triplet superconductivity induced by a moving condensate,” *Phys. Rev. B* **102**, 100507 (2020).
 - 240 V.L. Berezinskii, “New model of the anisotropic phase of superfluid He_3 ,” *JETP Letters* **20**, 287 (1974).
 - 241 D. Belitz and T. R. Kirkpatrick, “Even-parity spin-triplet superconductivity in disordered electronic systems,” *Phys. Rev. B* **46**, 8393–8408 (1992).
 - 242 D. Belitz and T. R. Kirkpatrick, “Properties of spin-triplet, even-parity superconductors,” *Phys. Rev. B* **60**, 3485–3498 (1999).
 - 243 Alexander Balatsky and Elihu Abrahams, “New class of singlet superconductors which break the time reversal and parity,” *Phys. Rev. B* **45**, 13125–13128 (1992).
 - 244 Elihu Abrahams, Alexander Balatsky, D. J. Scalapino, and J. R. Schrieffer, “Properties of odd-gap superconductors,” *Phys. Rev. B* **52**, 1271–1278 (1995).
 - 245 P. Coleman, E. Miranda, and A. Tsvelik, “Odd-frequency pairing in the kondo lattice,” *Phys. Rev. B* **49**, 8955–8982 (1994).
 - 246 A. F. Volkov, F. S. Bergeret, and K. B. Efetov, “Odd triplet superconductivity in superconductor-ferromagnet multilayered structures,” *Phys. Rev. Lett.* **90**, 117006 (2003).
 - 247 Ya. V. Fominov, Y. Tanaka, Y. Asano, and M. Eschrig, “Odd-frequency superconducting states with different types of meissner response: Problem of coexistence,” *Phys. Rev. B* **91**, 144514 (2015).
 - 248 Jacob Linder and Alexander V. Balatsky, “Odd-frequency superconductivity,” *Rev. Mod. Phys.* **91**, 045005 (2019).
 - 249 Annica M. Black-Schaffer and Alexander V. Balatsky, “Odd-frequency superconducting pairing in topological insulators,” *Phys. Rev. B* **86**, 144506 (2012).

- 250 Annica M. Black-Schaffer and Alexander V. Balatsky, “Odd-frequency superconducting pairing in multiband superconductors,” *Phys. Rev. B* **88**, 104514 (2013).
- 251 A. Di Bernardo, S. Diesch, Y. Gu, J. Linder, G. Divitini, C. Ducati, E. Scheer, M. G. Blamire, and J. W. A. Robinson, “Signature of magnetic-dependent gapless odd frequency states at superconductor/ferromagnet interfaces,” *Nature Communications* **6**, 8053 (2015).
- 252 L. Komendová and A. M. Black-Schaffer, “Odd-frequency superconductivity in Sr_2RuO_4 measured by kerr rotation,” *Phys. Rev. Lett.* **119**, 087001 (2017).
- 253 Jorge Cayao and Annica M. Black-Schaffer, “Odd-frequency superconducting pairing and subgap density of states at the edge of a two-dimensional topological insulator without magnetism,” *Phys. Rev. B* **96**, 155426 (2017).
- 254 Christopher Triola and Annica M. Black-Schaffer, “Odd-frequency pairing and kerr effect in the heavy-fermion superconductor Upt_3 ,” *Phys. Rev. B* **97**, 064505 (2018).
- 255 Jorge Cayao and Annica M. Black-Schaffer, “Odd-frequency superconducting pairing in junctions with rashba spin-orbit coupling,” *Phys. Rev. B* **98**, 075425 (2018).
- 256 Paramita Dutta and Annica M. Black-Schaffer, “Signature of odd-frequency equal-spin triplet pairing in the josephson current on the surface of weyl nodal loop semimetals,” *Phys. Rev. B* **100**, 104511 (2019).
- 257 P. O. Sukhachov, Vladimir Juričić, and A. V. Balatsky, “Odd-frequency berezinskii superconductivity in dirac semimetals,” *Phys. Rev. B* **100**, 180502 (2019).
- 258 Mohammad Alidoust, Alexander Zyuzin, and Klaus Halterman, “Pure odd-frequency superconductivity at the cores of proximity vortices,” *Phys. Rev. B* **95**, 045115 (2017).
- 259 Y. Tanaka, Y. Tanuma, and A. A. Golubov, “Odd-frequency pairing in normal-metal/superconductor junctions,” *Phys. Rev. B* **76**, 054522 (2007).
- 260 Yasuhiro Asano and Yukio Tanaka, “Majorana fermions and odd-frequency cooper pairs in a normal-metal nanowire proximity-coupled to a topological superconductor,” *Phys. Rev. B* **87**, 104513 (2013).
- 261 Takehito Yokoyama, Yukio Tanaka, and Alexander A. Golubov, “Theory of pairing symmetry inside the abrikosov vortex core,” *Phys. Rev. B* **78**, 012508 (2008).
- 262 N. Banerjee, J. A. Ouassou, Y. Zhu, N. A. Stelmashenko, J. Linder, and M. G. Blamire, “Controlling the superconducting transition by spin-orbit coupling,” *Phys. Rev. B* **97**, 184521 (2018).
- 263 Nathan Satchell and Norman O. Birge, “Supercurrent in ferromagnetic josephson junctions with heavy metal interlayers,” *Phys. Rev. B* **97**, 214509 (2018).
- 264 Nathan Satchell, Reza Loloee, and Norman O. Birge, “Supercurrent in ferromagnetic josephson junctions with heavy-metal interlayers. ii. canted magnetization,” *Phys. Rev. B* **99**, 174519 (2019).
- 265 Kun-Rok Jeon, Xavier Montiel, Sachio Komori, Chiara Ciccarelli, James Haigh, Hidekazu Kurebayashi, Lesley F. Cohen, Alex K. Chan, Kilian D. Stenning, Chang-Min Lee, Mark G. Blamire, and Jason W. A. Robinson, “Tunable pure spin supercurrents and the demonstration of their gateability in a spin-wave device,” *Phys. Rev. X* **10**, 031020 (2020).
- 266 Kun-Rok Jeon, Chiara Ciccarelli, Hidekazu Kurebayashi, Lesley F. Cohen, Sachio Komori, Jason W. A. Robinson, and Mark G. Blamire, “Abrikosov vortex nucleation and its detrimental effect on superconducting spin pumping in $\text{Pt}/\text{Nb}/\text{Ni}_{80}\text{Fe}_{20}/\text{Nb}/\text{Pt}$ proximity structures,” *Phys. Rev. B* **99**, 144503 (2019).
- 267 Kun-Rok Jeon, Chiara Ciccarelli, Hidekazu Kurebayashi, Lesley F. Cohen, Xavier Montiel, Matthias Eschrig, Sachio Komori, Jason W. A. Robinson, and Mark G. Blamire, “Exchange-field enhancement of superconducting spin pumping,” *Phys. Rev. B* **99**, 024507 (2019).
- 268 Kun-Rok Jeon, Chiara Ciccarelli, Hidekazu Kurebayashi, Lesley F. Cohen, Xavier Montiel, Matthias Eschrig, Thomas Wagner, Sachio Komori, Anand Srivastava, Jason W.A. Robinson, and Mark G. Blamire, “Effect of meissner screening and trapped magnetic flux on magnetization dynamics in thick $\text{Nb}/\text{Ni}_{80}\text{Fe}_{20}/\text{Nb}$ trilayers,” *Phys. Rev. Applied* **11**, 014061 (2019).
- 269 Kun-Rok Jeon, Chiara Ciccarelli, Andrew J. Ferguson, Hidekazu Kurebayashi, Lesley F. Cohen, Xavier Montiel, Matthias Eschrig, Jason W. A. Robinson, and Mark G. Blamire, “Enhanced spin pumping into superconductors provides evidence for superconducting pure spin currents,” *Nature Materials* **17**, 499–503 (2018).
- 270 A. M. Petrzhik, K. Y. Constantinian, G. A. Ovsyannikov, A. V. Zaitsev, A. V. Shadrin, A. S. Grishin, Yu. V. Kisilinski, G. Cristiani, and G. Logvenov, “Superconducting current and low-energy states in a mesa-heterostructure interlayered with a strontium iridate film with strong spin-orbit interaction,” *Phys. Rev. B* **100**, 024501 (2019).
- 271 F. S. Bergeret, A. F. Volkov, and K. B. Efetov, “Enhancement of the josephson current by an exchange field in superconductor-ferromagnet structures,” *Phys. Rev. Lett.* **86**, 3140–3143 (2001).
- 272 M. Houzet and A. I. Buzdin, “Long range triplet josephson effect through a ferromagnetic trilayer,” *Phys. Rev. B* **76**, 060504 (2007).
- 273 R. S. Keizer, S. T. B. Goennenwein, T. M. Klapwijk, G. Miao, G. Xiao, and A. Gupta, “A spin triplet supercurrent through the half-metallic ferromagnet CrO_2 ,” *Nature* **439**, 825–827 (2006).
- 274 Ya. V. Fominov, A. F. Volkov, and K. B. Efetov, “Josephson effect due to the long-range odd-frequency triplet superconductivity in SFS junctions with néel domain walls,” *Phys. Rev. B* **75**, 104509 (2007).
- 275 Klaus Halterman and Mohammad Alidoust, “Half-metallic superconducting triplet spin valve,” *Phys. Rev. B* **94**, 064503 (2016).
- 276 Mohammad Alidoust and Klaus Halterman, “Half-metallic superconducting triplet spin multivalves,” *Phys. Rev. B* **97**, 064517 (2018).
- 277 A. Kohen, Th. Proslier, T. Cren, Y. Noat, W. Sacks, H. Berger, and D. Roditchev, “Probing the superfluid velocity with a superconducting tip: The doppler shift effect,” *Phys. Rev. Lett.* **97**, 027001 (2006).
- 278 W. V. Budzinski, M. P. Garfunkel, and R. W. Markley, “Magnetic field dependence of the surface resistance of pure and impure superconducting aluminum at photon energies near the energy gap,” *Phys. Rev. B* **7**, 1001–1016 (1973).
- 279 H. J. Suominen, J. Danon, M. Kjaergaard, K. Flensberg, J. Shabani, C. J. Palmstrøm, F. Nichele, and C. M. Marcus, “Anomalous fraunhofer interference in epitaxial superconductor-semiconductor josephson junctions,” *Phys. Rev. B* **95**, 035307 (2017).
- 280 M. Kemmler, M. Weides, M. Weiler, M. Opel, S. T. B. Goennenwein, A. S. Vasenko, A. A. Golubov, H. Kohl-

- edt, D. Koelle, R. Kleiner, and E. Goldobin, “Magnetic interference patterns in $0-\pi$ superconductor/insulator/ferromagnet/superconductor josephson junctions: Effects of asymmetry between 0 and π regions,” *Phys. Rev. B* **81**, 054522 (2010).
- ²⁸¹ I. V. Bobkova, A. M. Bobkov, and M. A. Silaev, “Dynamic spin-triplet order induced by alternating electric fields in superconductor-ferromagnet-superconductor josephson junctions,” *Phys. Rev. Lett.* **127**, 147701 (2021).
- ²⁸² Shun-Tsung Lo, Shih-Wei Lin, Yi-Ting Wang, Sheng-Di Lin, and C-T Liang, “Spin-orbit-coupled superconductivity,” *Scientific reports* **4**, 5438 (2014).
- ²⁸³ Christian R. Ast, Jürgen Henk, Arthur Ernst, Luca Moreschini, Mihaela C. Falub, Daniela Pacilé, Patrick Bruno, Klaus Kern, and Marco Gioni, “Giant spin splitting through surface alloying,” *Physical Review Letters* **98**, 186807 (2007).
- ²⁸⁴ Christopher Triola, Driss M. Badiane, Alexander V. Balatsky, and E. Rossi, “General conditions for proximity-induced odd-frequency superconductivity in two-dimensional electronic systems,” *Physical Review Letters* **116**, 257001 (2016).
- ²⁸⁵ L. L. Li, Y. L. Zhao, X. X. Zhang, and Y. Sun, “Possible evidence for spin-transfer torque induced by spin-triplet supercurrents,” *Chin. Phys. Lett.* **35**, 077401 (2018).
- ²⁸⁶ I.A. Golovchanskiy, N.N. Abramov, V.S. Stolyarov, V.I. Chichkov, M. Silaev, I.V. Shchetinin, A.A. Golubov, V.V. Ryazanov, A.V. Ustinov, and M.Yu. Kupriyanov, “Magnetization dynamics in proximity-coupled superconductor-ferromagnet-superconductor multilayers,” *Phys. Rev. Applied* **14**, 024086 (2020).